CONTRACTOR REPORT

SAND87-8180
UC-62a
Unlimited Release

Development of the Stressed Membrane Heliostat

Solar Kinetics, Inc.
Dallas, Texas

Prepared by Sandia National Laboratories, Albuquerque, New Mexico 87185 and Livermore, California 94550 for the United States Department of Energy under Contract 91-8808A.

Printed April 1987

Issued by Sandia National Laboratories, operated for the United States Department of Energy by Sandia Corporation.

Printed in the United States of America
Available from
National Technical Information Service
5285 Port Royal Road
Springfield, VA 22161

NTIS price codes
Printed copy: A09
Microfiche copy: A01

SOLAR THERMAL TECHNOLOGY
FOREWORD

The research described in this report was conducted within the U.S. Department of Energy's Solar Thermal Technology Program. This program directs efforts to incorporate technically proven and economically competitive solar thermal options into our nation's energy supply. These efforts are carried out through a network of national laboratories that work with industry.

In a solar thermal system, mirrors or lenses focus sunlight onto a receiver where a working fluid absorbs the solar energy as heat. The system then converts the energy into electricity or uses it as process heat. There are two kinds of solar thermal systems: central receiver systems and distributed receiver systems. A central receiver system uses a field of heliostats (two-axis tracking mirrors) to focus the sun's radiant energy onto a receiver mounted on a tower. A distributed receiver system uses three types of optical arrangements--parabolic troughs, parabolic dishes, and hemispherical bowls--to focus sunlight onto either a line or point receiver. Distributed receivers may either stand alone or be grouped.

This report presents the results of stressed membrane heliostat development performed by Solar Kinetics Inc.

UC-62a

SAND87-8180
Unlimited Release
Printed April 1987

DEVELOPMENT OF THE STRESSED MEMBRANE HELIOSTAT

Solar Kinetics, Inc.
Dallas, Texas

Prepared for:
Sandia National Laboratories
Under Contract #91-8808A

ABSTRACT

The stressed membrane reflective assembly offers a unique and innovative approach to heliostat design and fabrication. The concept is simple: two circular membranes or diaphragms are attached at their perimeter to a ring. The plenum formed by the membranes and ring is evacuated to privide focus. Stiffness is provided through membrane tension; the ring prevents collapse of the structure.

The stressed membrane design provides for a substantial cost and weight reduction over conventional structures. The first generation of stressed membrane design provides more than a twenty percent cost reduction (from $71 to $55 per square meter) over second generation glass/metal concentrators of similar size. Weight reduction is achieved through the unique fashion in which the concentrator carries its load.

The stressed membrane concentrator offers many benefits including lower weight, lower cost and simplicity. Our analysis indicates these benefits are gained without impairing performance.

PREFACE

This report was provided to Sandia National Laboratories, Livermore, California under contract 91-8808A, in September 1986. The study was performed by Solar Kinetics, Incorporated and the results were presented at a final review held in Livermore.

We would like to recognize the assistance provided by several individuals outside of our own organization. In particular, C. L. Mavis (Sandia) for guiding the study and providing input on several issues, and L. M. Murphy (SERI) for timely development of the structural analysis of a highly integrated structure.

CONTENTS

		Page No.
PREFACE		
1.0	INTRODUCTION	1- 1
	1.1 Recommended Follow on Activities	1- 4
	1.2 Balance of Heliostat	1- 6
	1.3 Component Relationships	1- 8
2.0	DESIGN BASIS	2- 1
	2.1 Pressure Profiles	2- 2
	2.2 Dynamic Response	2- 5
3.0	MIRROR MODULE	3- 1
	3.1 Attachment	3- 3
	3.2 Materials	3- 5
	3.3 Ring	3- 9
	3.4 Membrane	3-14
	3.5 Tension	3-15
	3.6 Supports	3-17
	3.7 Manufacturing Techniques	3-19
4.0	SUPPORT STRUCTURE DESIGN	4- 1
	4.1 Design Considerations	4- 1
	4.2 Loads	4- 1
	4.3 Materials	4- 1
	4.4 Components	4- 2
	4.5 Support Structure Weight	4- 8
5.0	CONTROLS	5- 1
	5.1 Response	5- 1
	5.2 Transducer Accuracy	5- 3
	5.3 Prime Mover	5- 6
	5.4 Convexity	5- 7
	5.5 Mounting	5-11
	5.6 Miscellaneous Control Elements	5-11
6.0	INTRODUCTION TO MANUFACTURING AND COST	6- 1
7.0	CENTRAL MANUFACTURING FACILITY	7- 1
	7.1 Introduction	7- 1
	7.2 Production Rates	7- 1
	7.3 Degree of Automation	7- 1

7.4 Production Description 7- 3
7.5 Plant Description 7-13
7.6 Labor 7-13
7.7 Equipment Requirements 7-16

8.0 TRANSPORTATION 8- 1

8.1 Trailer Loading 8- 1

9.0 SITE MANUFACTURING FACILITY 9- 1

9.1 Site Schedules 9- 1
9.2 Production Areas and Plant Layout 9- 1
9.3 Site Production Description 9- 2
9.4 Installation 9-11
9.5 Production Time Table 9-14
9.6 Labor Requirements 9-15

10.0 HELIOSTAT MAINTENANCE 10- 1

10.1 Scheduled Maintenance 10- 1
10.2 Unscheduled Maintenance 10- 1

11.0 COSTS 11- 1

11.1 Introduction 11- 1
11.2 Capital Costs 11- 1
11.3 Manufacturing Costs 11- 7
11.4 Transportation Cost 11-12
11.5 Other Business Costs 11-12
11.6 Balance of Heliostat Costs 11-13
11.7 Cost Summary 11-15
11.8 Cost Versus Total Production 11-15
11.9 Cost Versus Production Rate 11-20
11.10 Operation and Maintenance Costs 11-20

12.0 INTRODUCTION TO PROTOTYPE DESIGN 12- 1

13.0 PHASE I TESTING 13- 1

13.1 Material Processing 13- 1
13.2 Weld Tests 13- 3
13.3 Tensioning Method 13- 6
13.4 Surface Measurements 13-10
13.5 Ring Buckling 13-20
13.6 Control Testing 13-22

14.0 TEST AND EVALUATION 14- 1

14.1 Similitude 14- 1
14.2 Beam Quality and Surface Error 14- 2

14.3 Dynamic Response 14- 3
14.4 Focus Controls 14- 3

15.0 PROTOTYPE FABRICATION 15- 1

15.1 Membranes 15- 1
15.2 Ring 15- 6
15.3 Support 15- 8
15.4 Controls 15-12
15.5 Site Assembly 15-14

16.0 CONCLUSION 16- 1

REFERENCES 16- 3

ILLUSTRATIONS

Figure No.		Page No.
1.1	Schematic Representation of Reflector Assembly	1- 2
1.2	Major Design Conclusion	1- 3
1.3	Cost versus Size	1- 7
2.1	Assumed Wind Profile for Support Design	2- 4
2.2	Types of Error	2- 6
3.1	Mirror Module	3- 2
3.2	Error versus Wind Speeds	3- 4
3.3	Membrane Material Cost	3- 7
3.4	Membrane Material Cost	3- 8
3.5	Sensitivity of Ring Gage Selection	3-10
3.6	Mirror Module Weight versus Tension	3-12
3.7	Error versus Tension	3-13
3.8	Error, Weight versus Number of Supports	3-18
4.1	Primary/Secondary Attachment in Truss	4- 3
4.2	Truss/Hub Attachment	4- 5
4.3	Truss/Hinge Attachment	4- 6
4.4	Hub Assembly	4- 7
4.5	Truss Strapping	4- 9
5.1	Weight versus Focal Length	5- 2
5.2	Power versus Wind Speed	5- 8
5.3	Convex Radius versus Time, No Wind	5- 9
5.4	Convex Radius versus time, 27 mph Wind	5-10
5.5	Actuator Assembly	5-12
7.1	CMF Production Flow	7- 4

7.2	Membrane Fabrication - Coil Line	7- 5
7.3	Membrane Fabrication - Welding Station	7- 6
7.4	Truss Fabrication - Coil Line	7- 8
7.5	Truss Fabrication - Weld Station	7-10
7.6	Hub Production	7-12
7.7	CMF Layout	7-14
9.1	SMF Layout	9- 3
9.2	Site Manufacturing Facility	9- 5
9.3	Ring Production	9- 6
9.4	LVDT Mount	9- 9
9.5	Membrane Transfer	9-10
9.6	Truss Strapping Attachment	9-12
9.7	Installation	9-13
13.1	Weld Joint Distortion	13- 4
13.2	Joint Preparation	13- 5
13.3	Membrane Tensioning - Edge Roll	13- 7
13.4	Membrane Tensioning - Inflatable Tube	13- 8
13.5	Tension versus Tube Pressure	13- 9
13.6	Phase I Test Set-Up	13-11
13.7	Surface Error - Case 1	13-12
13.8	Surface Error - Case 2	13-13
13.9	Surface Error - Case 3	13-14
13.10	Surface Error - Case 4	13-15
13.11	Surface Error - Case 5	13-16
13.12	Surface Error - Case 6	13-17
13.13	Membrane Seam and Support Positions	13-18
13.14	Error versus Radius	13-19

13.15	Error - Seam Detail, Case 5	13-21
13.16	Natural Frequency versus Tension	13-23
15.1	Membrane at Weld Station - No Vacuum	15- 4
15.2	Membrane at Weld Station - Vacuum	15- 5
15.3	Ring - Measuring Planarity	15- 9
15.4	Frame Assembly	15-15
15.5	Membrane on Assembly Platen	15-16
15.6	Membrane Vacuum Chucked	15-17
15.7	Membrane to Ring Weld Detail	15-19
15.8	Mechanical Deformation of Ring Flange	15-20
15.9	Completed Assembly	15-21
15.10	Reflected Image	15-22

TABLES

Table No.		Page No.
4.1	Support Assembly Weight	4-10
7.1	Production Rates	7- 2
7.2	CMF Space Allocations	7-15
7.3	CMF Labor Requirements	7-17
7.4	CMF Equipment List	7-18
8.1	Transportation	8- 3
9.1	Work Stations	9- 4
10.1	Reliability of Field Replacable Components	10- 2
11.1	CMF Equipment Costs	11- 2
11.2	SMF Equipment Costs	11- 5
11.3	Direct Material Costs	11- 8
11.4	Depreciation	11-11
11.5	Balance of Heliostat Costs	11-16
11.6	Cost by Components of Required Revenue	11-17
11.7	Cost by Cost Breakdown Structure	11-18
11.8	Cost by Location	11-19
11.9	Cost for Variable Production Rates	11-21
11.10	Annual Field Operation and Maintenance Costs	11-24
15.1	Membrane Similitude	15- 2
15.2	Ring Similitude	15- 7
15.3	Support Similitude	15-10
15.4	Control Similitude	15-13

SECTION 1.0

INTRODUCTION

The stressed membrane reflector assembly is a unique concept directed towards reducing the cost of a heliostat. The system achieves cost reduction by its innovative approach in resisting and distributing loads. Conceptual descriptions and designs have been developed by several organizations (e.g., Ref. 1 and Ref. 2). The Solar Kinetics stressed membrane reflector assembly was designed under contract to Sandia; some design features outlined in the report are similar to those proposed in referenced documents, and others represent significant departures.

Figure 1.1 presents a schematic overview of the reflector assembly. The mirror module is a 150 square meter aperture, monolithic assembly composed of a tensioned membrane welded to a toroidal ring at the circumference. Membrane tension is provided by a combination of mechanical deformation of the ring flanges after membrane attachment and an inflatable tube. A fan penetrates the rear membrane to provide a pressure source. If the plenum is evacuated, the front membrane will focus; if pressurized, the membranes will de-focus. The module is mounted on six, centilever, radial arms. These arms terminate at a circular hub drive mount.

Figure 1.2 presents many of the characteristics developed in this report. Size was essentially determined by Balance of Heliostat (BOH) costs, that is, the drive, pedestal, installation, and all other components not directly associated with the reflector assembly. It is certainly possible for the stressed membrane concept to be expanded to larger apertures. We elected to select the largest area heliostat for which drive cost goals were available.

Aluminum was selected for the mirror module due to cost. The primary requirements for membrane materials are to support tension, provide good corrosion resistance, and allow handling without localized yield. Carbon steel was eliminated on the basis of corrosion protection cost. Aluminum at ten mils and austenetic stainless at three mils showed roughly similar costs.

The ring is loaded in compression by the membrane. Because the membrane enhances the stability of the system, ring design is based upon yield rather than buckling in spite of the fact that it is a long, slender column. Consequently, ring cross-sectional area requirements are based upon area and yield strength; they are not based upon bending stiffness. A direct comparison of stainless to aluminum rings indicated substantial savings in the aluminum ring. We elected to keep identical materials in the membrane and ring to take advantage of a fixed connection.

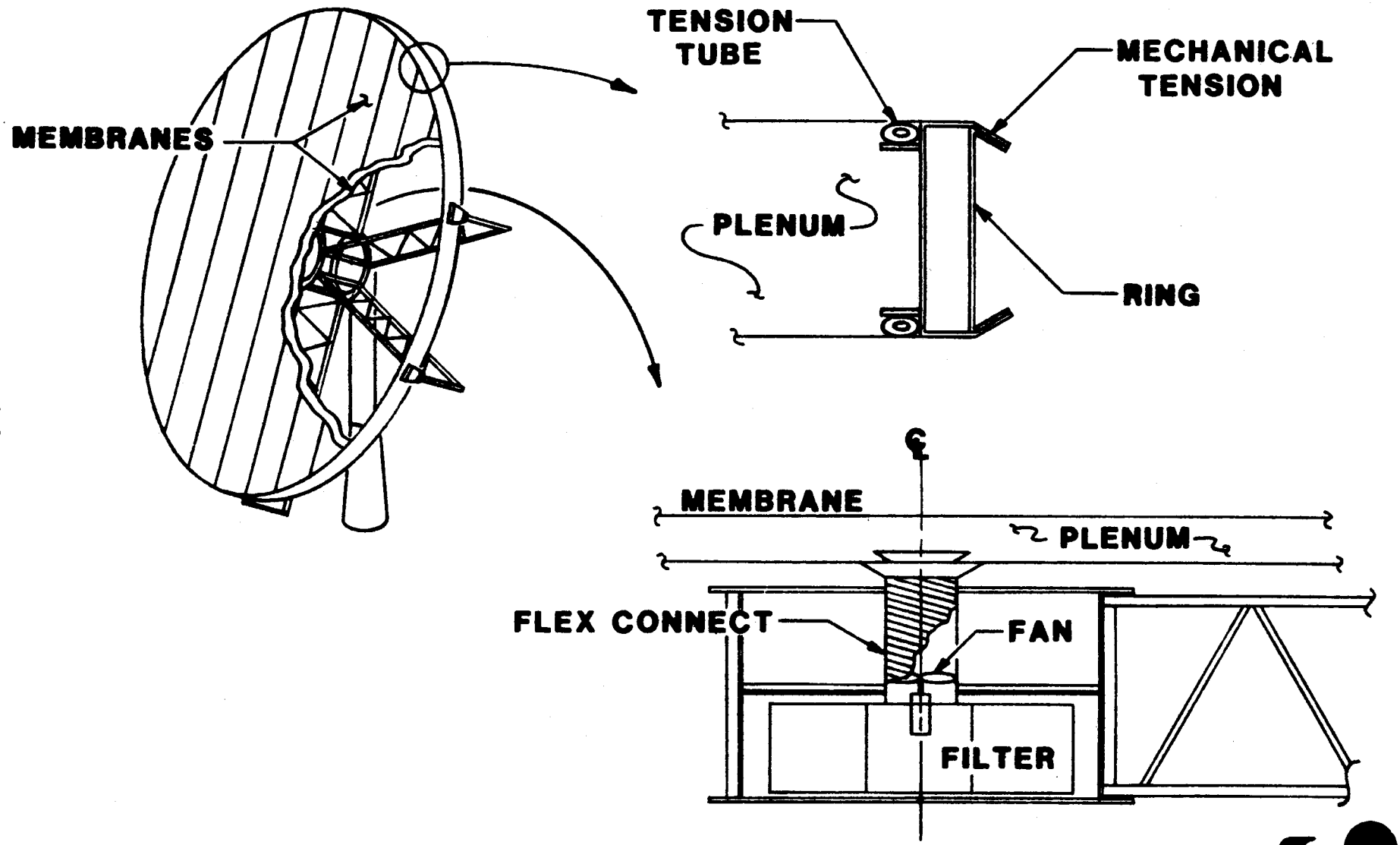

FIG. 1 SCHEMATIC REPRESENTATION OF REFLECTOR ASSEMBLY

SOLAR KINETICS INC.

• APERTURE	150 SQ METERS
• MEMBRANE	0.010" ALUMINUM 60 LB/IN TENSION
• RING	0.090" x 3" x 12" RECT TUBE ALUMINUM
• SUPPORTS	SIX STEEL TRUSS SUPPORTS
• ATTACHMENT	RADIAL/CIRCUMFERENTIAL FIX
• DESIGN BASIS	STRESS SENSITIVE AT 50 MPH
• COST	$55.26/m^2

FIG. 1.2 MAJOR DESIGN CHARACTERISTICS

The truss supports, on the other hand, are dominated by stiffness requirements. Steel was chosen as the best structural material for bending. Six supports proved to be the lowest cost approach for a concentrated load drive structure.

Different portions of the structure were critical under different loadings. In general, however, the heliostat is most severely loaded in the fifty mile per hour wind speed in a "non-stow" worst orientation. The ninety mile per hour stow wind speeds were not substantially different, however, and did control the design of a few elements.

We determined that the installed cost of a complete stressed membrane heliostat would be $55.26 per square meter of aperture in the first year of a 50000 unit production volume scenario.

The following report is essentially developed in three seperate sections. The first, Design, reviews the methodology and conclusions developed by Solar Kinetics Inc. (SKI) in the analysis of a stressed membrane reflector assembly. The second, Manufacturing and Costs, summarizes the fabrication process, facility requirements, and cost breakdowns. The last section, Prototype, reflects the testing and construction experience gained by SKI during the fabrication of the first fifty square meter stressed membrane reflector assembly for central receivers.

The contract did provide for some constraints on the commercial and prototype efforts. First, the membrane reflective polymer material was not of primary interest and polymer development was specifically excluded. The drive/pedestal portion of the heliostat was also not of primary interest, and second generation "glass to metal" components from the drive down were used for cost development. In fact, the prototype stressed membrane reflector assembly was modified slightly to mount on an existing ARCO drive/pedestal.

1.1 RECOMMENDED FOLLOW-ON ACTIVITIES

The reflector assembly installed at the Central Receiver Test Facilty (CRTF) was the first relatively large stressed membrane mirror module fabricated. There were no "practice-runs" or trials built elsewhere. Consequently, a substantial amount of fabrication techniques and information was developed. The existing prototype is successful. Based upon preliminary evaluation, we would estimate that ninety-five percent of the optical surface is an accurate contour. The remaining five percent could be gained with another unit.

We would recommend that several follow-on efforts be conducted to provide for further reductions in cost, improvements in performance, and additional confidence amongst the industry in an innovative solution:

1. Additional stressed membranes of similar size to improve fabrication techniques and further reduce material thickness.

2. A full scale stressed membrane design to demonstrate all structural and optical properties.

3. Further development of size optimizations.

4. Exploration of alternate support and drive concepts suitable for a new concentrator design.

5. Development of cleaning strategies appropriate to polymeric and membrane surfaces.

As a "one-of-a-kind" test article, there is always a slight bit of conservatism applied to the design. Some additional weight and cost reductions could be applied to the prototype and commercial assembly through further optimization of the basic design. These areas might include alternate load profiles to reduce structural weight, less concern over handling constraints to reduce membrane weight, uniform tension distribution without the cost of an inflatable tube, and possible further increases in aperture per heliostat.

The existing prototype represents an effort to scale the commercial design in order that it might be connected to an existing second generation heliostat drive/pedestal. To take advantage of the stressed membranes' unique applicability to large aperture heliostats, the concept should be demonstrated at full scale. This demonstration could potentially alleviate concerns over dynamic issues that are related to size (e.g. vortex shedding, structural natural frequency). The demonstration would also provide additional feedback on the design effort to continue the cost reduction efforts.

The pilot plant demonstrations at Barstow have clearly demonstrated the advantages of clean reflective surfaces. The stressed membrane concentrator, particularly its polymer reflective surface, cannot be subjected to the same type of wash cycle developed for glass/metal heliostats. Polymers, in their current state of development, will not tolerate agitation as the wiping will scratch the acrylic surface. There is also some concern over direct contact with a membrane causing physical damage. Consequently, we feel that some follow-on efforts should be directed towards washing techniques.

It is quite likely that some alternate means of support would provide for further cost reductions in the stressed membrane heliostat. The mirror module does exhibit a unique property; that is, the transfer of all loads to its periphery. A drive/support

structure could conceivably be designed that took advantage of this transfer. If bending and/or stability concerns could be avoided, such a support system could offer savings over centralized designs.

Another approach to reduction in support requirements is to reduce the apparent loads. The existing set of components is largely designed based upon stress in the "50 mph any orientation" condition, though the 90 mph stow position is very close and, in fact, dominates the design of portions of the support assembly. Consequently, we believe that only marginal gains are available through wind avoidance feathering schemes unless stow loadings can also be reduced.

The stressed membrane reflector assembly offers a means to substantially reduce central receiver concentrator cost. We believe that significant reductions in cost can continue to occur through further optimization efforts. We also feel that development of full size reflectors and operation of stressed membrane assemblies will reduce concern over an innovative design with substantial promise.

1.2 BALANCE OF HELIOSTAT

Balance of Heliostat (BOH) is defined as all components required for a heliostat excluding the reflector assembly. This category includes the drive, pedestal, foundations, tracking controls, field wiring, and other miscellaneous items. The approach to this reflector assembly design was to adopt a second generation pedestal and drive. The unit selected for this design is documented in Ref. 3. This drive/pedestal was used for interface design because the ball screw elevation drive provided a convenient termination point for a concentrated drive load. Alternate second generation drives could be selected to mate with the stressed membrane without significant impact upon design or cost.

BOH costs were developed from Ref. 4 which addressed expense for different sized apertures. Cost as a function of heliostat size developed into a critical issue. The size of the reflector assembly was only weakly linked to cost; a strong relationship between size and cost exists for BOH components.

Figure 1.3 summarizes the results of BOH costs for different aperture sizes. Our estimates of these costs for the 150 square meter reflector assembly is also shown.* Although this effort was devoted to reflector assembly design, it is quite clear that large aperture designs provide significant economies due to BOH costs.

* BOH costs, adjusted for inflation, and projections of large aperture costs, are developed in the cost section of this document.

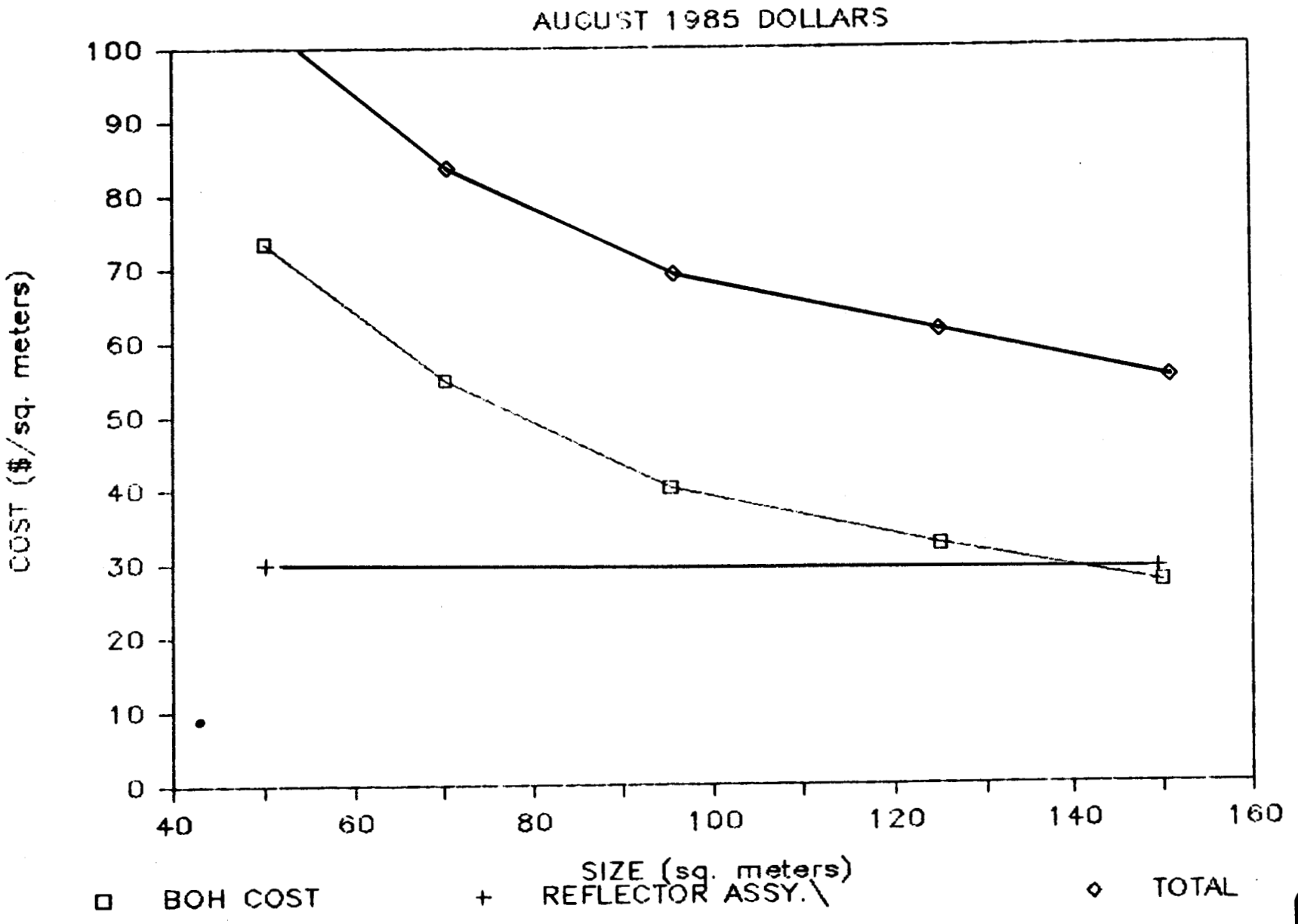

FIG. 1.3 COST VS. SIZE

It is clear that 150 square meters is not necessarily an "optimum" design size for the heliostat. The aperture was selected as the largest area for which cost projections on balance of heliostat components were available. It is likely that larger areas are practical, particularly with regard to the mirror module. There are some caveats placed on extrapolations of cost at large apertures:

1. Performance issues related to size, such as off-axis astigmatism, were specifically not addressed in this document. The reader is referred to Ref. 5 on these issues.

2. The centralized pedestal/drive assembly adopted for this design study suffers from a support structure that deflects by the cube of radius while aperture increases by the square.

3. Dynamic issues, both the response and load excitation frequencies, change with radius. At this time it is not clear if dynamic issues will limit size.

Further optimization work in this area may provide additional cost advantages.

1.3 COMPONENT RELATIONSHIPS

Each component of the stressed membrane reflector assembly has an impact upon the remaining parts. It is the very nature of a structurally efficient shape to be reliant upon the assembly of all parts, rather than several discrete components to provide load resistance. The major divisions presented below: design basis, mirror module, support structure, and focal control are for the convenience of description. It was impossible to completely divorce components from one another, optimize separately, and combine the parts.

SECTION 2.0

DESIGN BASIS

Development of the stressed membrane reflector assembly was based on criteria established by contract, including: production volume, performance goals, survival requirements, operational life, and safety. Some of these criteria are repeated below. The design requirements are in Reference 6.

A. Manufacturing volume design basis was 50000 units per year.

B. Performance requirements over normal ambient temperature ranges with the sun at or above 0.26 rad (15°) elevation were divided into no wind and 12 m/s (27 mph) wind conditions.

   1. No wind with gravity.
      a. Pointing accuracy 1.5 mrad standard deviation per gimbal axis.
      b. Ninety percent of reflected energy in theoretical beam shape plus 1.4 mrad fringe.

   2. 27 mph wind, no gravity - 1.2 mrad standard deviation in mirror normal axis with no gravity.

   3. 27 mph wind, with gravity.
      a. 3.6 mrad rms slope error over entire surface in worst orientation.
      b. Operate when subjected to oscillatory wind loads.

C. Survival Requirements.

   1. Maintain structural integrity at 22 m/s (50 mph) wind in any orientation.

   2. Maintain structural integrity at 40 m/s (90 mph) wind in stow position. Maximum angle of attack is six degrees.

   3. Withstand oscillatory wind loads.

   4. Survive 19 mm (1.0 in) diameter, 0.9 specific gravity hail impacting at 20 m/s (75 ft/s).

D. Design and material selection is based upon a 30 year life.

E. With beam control strategy, the heliostat must defocus on command to 3% of initial flux value in 120 seconds. A special requirement in the body of the contract required the pressure control unit to have the capability of changing from

any operational focal length to a convex radius in five seconds. A desire to achieve convexity on loss of communication or power was indicated. A convex radius of 1200 ft was also defined as reasonable. Convexity must be accomplished and maintained over the entire range of operational wind speeds and the 22 m/s (50 mph) any orientation case.

The requirements summarized above reflect the most important criteria in the design. The application of these requirements require amplification in some instances; consequently, they are explained here.

2.1 PRESSURE PROFILES

Structural analysis of the reflector assembly based upon wind loading requires several assumptions. Loading is influenced by site conditions, aerodynamic shape of the body and the relative position of the heliostat to obstructions (e.g. the position of heliostat in the field array). The expense and error of a reflector assembly is strongly related to the amount and distribution of material resisting that wind load. Consequently, the assumption of wind induced pressure profiles has a substantial impact upon the cost/performance tradeoff and the fundamental selection of structural shapes required to resist load and minimize error.

The design wind speeds summarized in Section 2.0 occur at a reference height of 10m (30 ft). To determine the "effective" wind velocity for the reflector assembly, a one seventh power law relationship was used with the center line of the collector representing the "effective" height. Ground effects were ignored. For ground spacings of ten percent or greater of the characteristic dimension, this assumption is accurate within approximately three percent [Ref. 7].

Wind velocity imposes a load upon the structure by virtue of dynamic pressure. The first order analysis assumes that pressure is uniform, and the magnitude of the distribution is proportional to projected area. The result of this first order analysis applied to the ring/membrane only indicated that error due to wind and gravity was most significant at 60 degrees (0 degrees is stow, 90 degrees is facing the horizon). Stress reached a maximum at 80 degrees in the 22 m/s (50 mph) condition.
The development of stress and error in response to uniform loads is treated more rigorously in Section 3.0. It is addressed here primarily to indicate the relative impact of loads upon ring stress and the magnitude of error in response to steady wind

loads. The membrane pretension induces a normal compressive stress in the ring, and it is this compression that dominates the stress state. Wind loads induce only fifteen percent of the ring stress. The error at lower wind speeds was less than 0.3 mrad because the design of the ring was stress limited. Consequently, further development of the load assumptions does not appear to be warranted.

The stress and error of the support assembly, on the other hand, is entirely dominated by wind load conditions. It is appropriate to consider some alternate wind pressure profiles. Sources of non-uniformity include unbalanced gusts, velocity gradients and ground effects, but result primarily from the tendency of the mirror module to behave as an airfoil at low angles of attack. Obviously, there is no one correct profile; the shape could best be described by a complex, time dependent function.

The worst case pressure profile assumed was a velocity of 1.5 times normal velocity striking only half of the front surface (Figure 2.1). This approach to wind design has been taken before [Ref. 13]. The profile also generates moment coefficients that are virtually identical (within 4%) to the wind tunnel results in second generation detail design reports [Ref. 14].

The next step was to determine the reactions of the six trusses from such a load. By orienting the pressure profile on the mirror module, a condition of symmetry about one axis was obtained. Summing forces in the Z axis and moments about the Y axis yield additional static equations. It was necessary to determine the strain energy of the reflective assembly when deflected.

The total stored potential energy of the system results from out of plane deflections of the ring and deflections of the trusses. The spring constant for out of plane deflections of the ring was determined by computer modeling. Truss spring constants for tip deflections were determined by iteration for allowable slope errors. An analytical procedure was developed that iterated on the minimum potential energy of the system to solve the equilibrium reactions of the six trusses.

The hinges connecting the mirror module to the support structure prevent two of the trusses from resisting loads parallel to the plane of the membrane. For structural development this load was assumed to be equally divided among the remaining four trusses. Coefficients for moments about the optical axis were taken from Reference 14. This load was equally divided among all six trusses.

Once the end loads of all six trusses were determined, a finite element model was constructed to examine stresses and deflections. Element dimensions were adjusted in subsequent runs to achieve an optimized structure for the given loading conditions.

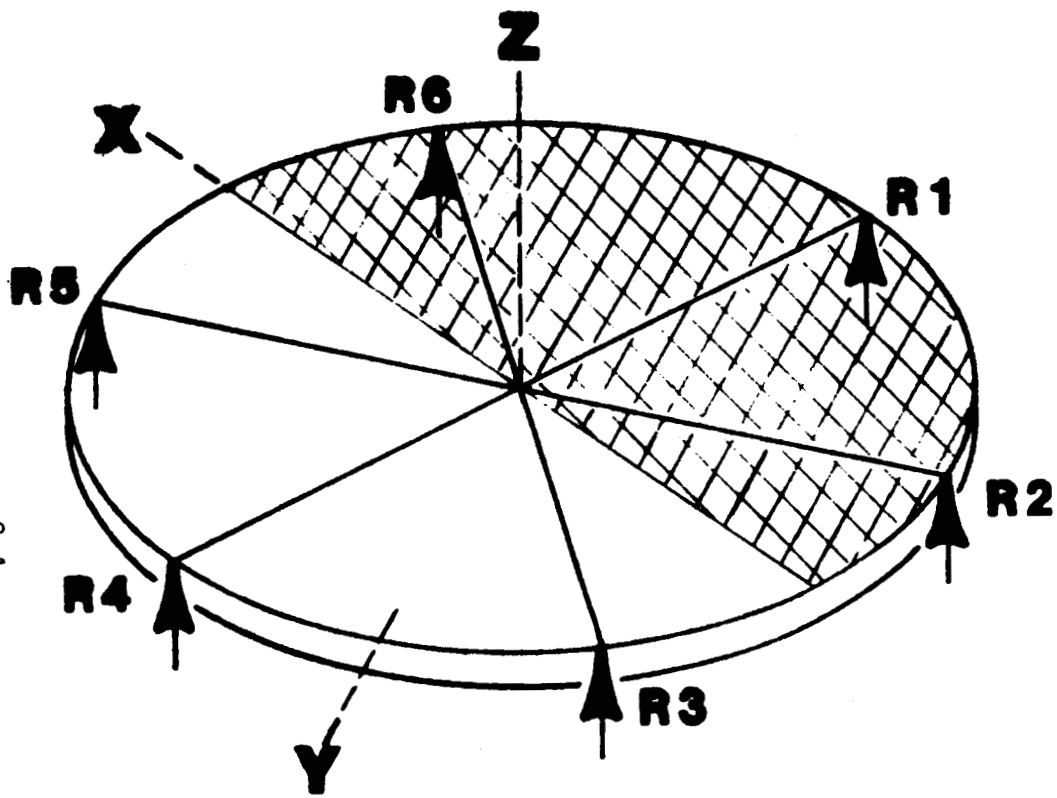

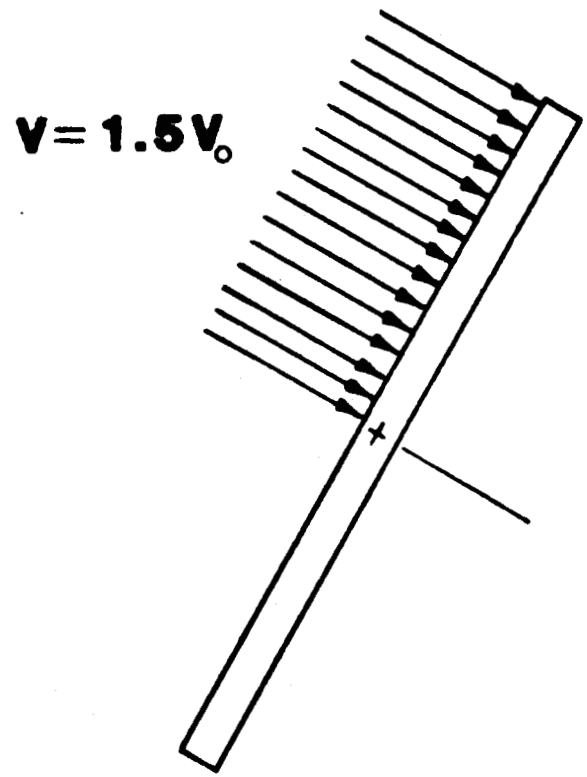

FIG. 2.1 ASSUMED WIND PROFILE FOR SUPPORT DESIGN

After the design phase and prototype fabrication were complete, a brief review of this profile for rear structure design was made. It is our opinion that development of such a profile, although recommended by design literature on similar structures subjected to wind, represents a conservative approach to design. Pressure profile development should be reconsidered in any further optimization work.

2.2 DYNAMIC RESPONSE

The dynamic response of a collector assembly can be divided into three categories: oscillations of the mirror module as a rigid body on flexible supports, vibrations of individual structural members, or deformations of the flexible reflector surface [Ref. 7]. Wind loads have not had significant impacts upon heliostat field performance [Ref. 4, 8], but the stressed membrane mirror module presents a significant departure from past designs in the last category, that of deformations of the flexible reflector surface.

Surface slope error has been divided into two classes based upon the nature of deformation [Ref. 9], and these errors are illustrated in Figure 2.2. Asymmetric error is the result of deformation between supports of the ring; axisymmetric error is the result of membrane sag due to varying pressure loadings. In static response, the axisymmetric error is eliminated by the control system. The dynamic characteristics were investigated primarily for use in determining the required response of that control system.

The spectral distribution selected was proposed by Kaimal for longitudinal variations, and suggested to be more accurate than ANSI developments of fluctuations [Ref. 10]. The longitudinal spectra was applied across the surface of a heliostat as a conservative estimate of gust loadings. Actual developments are discussed in Section 5.0.

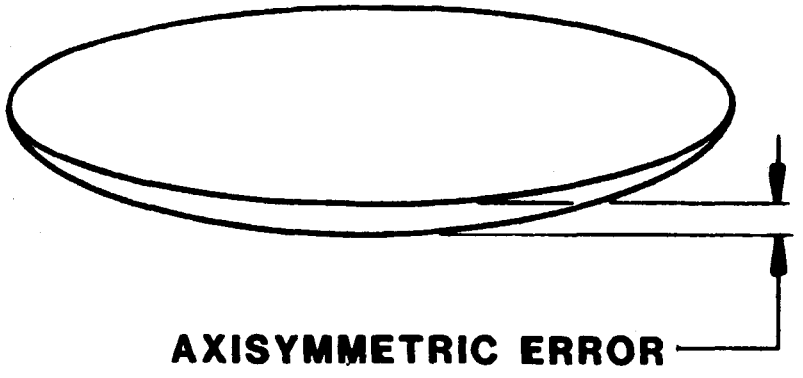

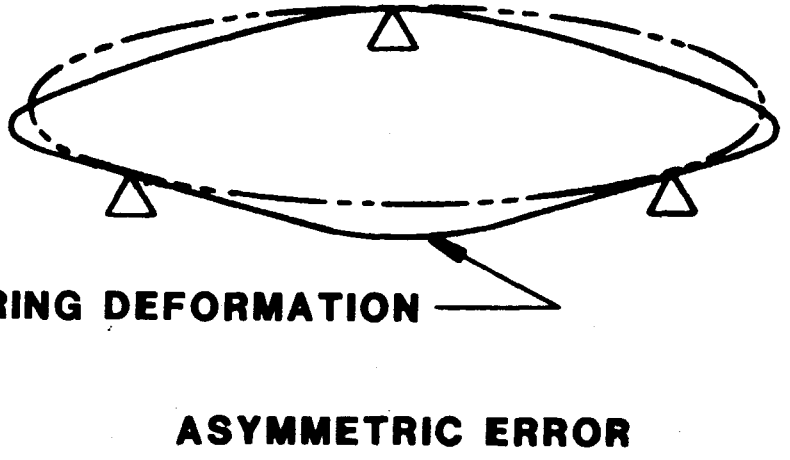

FROM "ANALYTICAL MODELING AND STRUCTURAL RESPONSE OF A STRETCHED MEMBRANE REFLECTIVE MODULE", LM MURPHY, SERI/TR-253-2101

FIG. 2.2 TYPES OF ERROR

SECTION 3.0

MIRROR MODULE

The mirror module is the primary element of the stressed membrane reflector assembly. This monolithic, 150 square meter aperture consists of four major components: the front and rear stressed membrane, the reflector material, the structural ring, and the tension tubes. Figure 3.1 illustrates the relationship of these parts.

In many respects, it is the relationship of the parts that actually provide the unique structural efficiencies of the concept. Consequently, the design development cannot be presented as a series of individual optimizations that are combined to create the final assembly.

To reduce error and increase stability, the membrane is attached to the ring with both a radial and circumferential fix. Aluminum was selected as the material offering the best compromise of cost and corrosion resistance. The 5000 series alloys are readily formable, can be easily welded, resist atmospheric corrosion, and are relatively inexpensive.

The ring was established based on a stress and stability sensitive design. The weight was largely determined by the axial compression load induced by membrane tension. The distribution of the material was dictated by the out of plane stability considerations and error reduction associated with out of plane area moments. The shape selected was a 3 x 12 x 0.090 inch rectangular tube. Membrane preloads were established at sixty pounds per inch to provide protection against stress reversal without substantial increases in the ring weight.

Six supports were used for mirror module optimization work. The weight per unit aperture of the mirror module and the surface normal error decreases with increasing number of supports. Six supports offered the best compromise between lower reflector weight and increased structural weight.

Resistance welding processes were adopted because of their speed, low distortion, and low cost. Vacuum platens were identified as uniquely appropriate material handling devices. This approach allows thin sheet to be continuously supported with a distributed load, maintain flatness, and provide free edges for welding.

The following sub-sections present the development and optimization of the mirror module, an area that received substantial effort in our analysis.

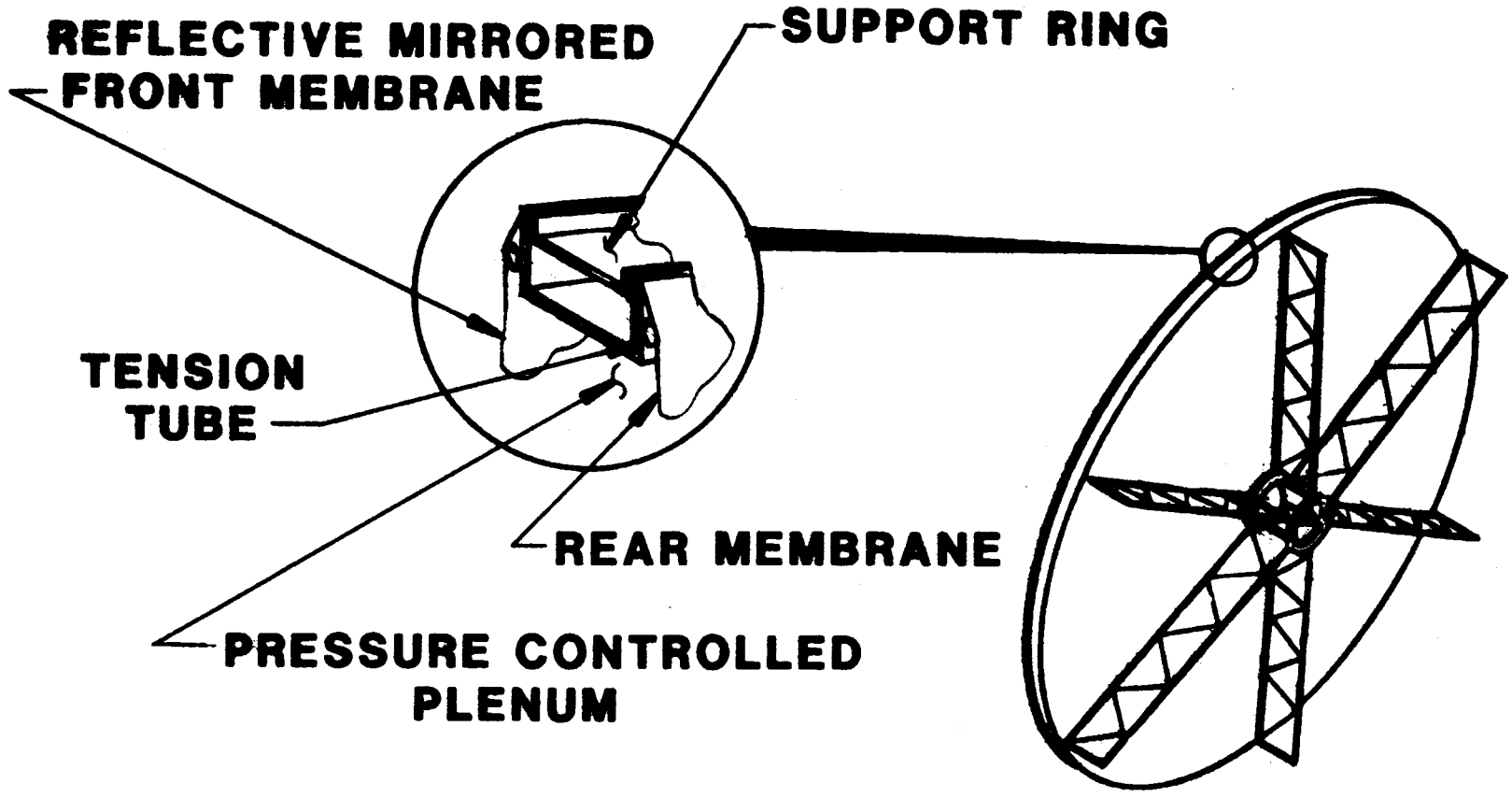

FIG. 3.1 MIRROR MODULE

3.1 ATTACHMENT

The structural response of the ring and membrane are coupled through their attachment. It is largely this coupling that is unique to the approach; our design attempts to make full use of these advantages.

The membrane is considered to be a diaphragm of zero flexural rigidity. Its stiffness is achieved by pre-loading in tension; this tension is translated to the ring as axial compression. Axial compression in the ring requires that design consider stability or buckling, both in and out of plane.

Designs of long slender columns under compressive loads that must resist buckling in more than one direction are not material efficient shapes, though they are unavoidable in some instances. Buckling resistance is provided by flexural rigidity (EI). If material is distributed in such a way as to provide a large area moment in more than one direction, and the section remains compact to avoid local stability problems, the stress state in the column is very small with respect to yield and hence not efficient.

The radial attachment between ring and membrane lends stability to the in-plane response of the ring. If the ring attempts to buckle in the radial direction along one diameter, the length of an opposing diameter must increase. The membrane tension must correspondingly increase. A rigorous development of the bifurcation loads for in-plane response was accomplished by Murphy [Ref. 11]. The structure was modeled as a ring on an elastic foundation; the results suggested that radial buckling occurred at higher modes of deformation and at tension loads two or more orders of magnitude higher than the out of plane bifurcation loads.

Out of plane buckling response is also improved by radial attachment. The response of a ring to deformation is substantially different from a beam; roll and deflection are strongly coupled. For the ring to roll, tension in one membrane must increase while the other decreases. This coupling effect serves to increase the out of plane critical load by a factor of two or more for membrane thicknesses and ring shapes considered in this analysis [Ref. 11].

A circumferential fix does not provide buckling resistance, but does reduce the deflection of the ring between supports. Because both error and stress are proportional to the ring deflection, an error or load critical design is improved by providing a hard fix. Figure 3.2 illustrates the frame deflection versus unit load for the two cases.

Deflection of the ring between supports induces a circumferential strain. If the membrane is fixed in this direction, the membrane

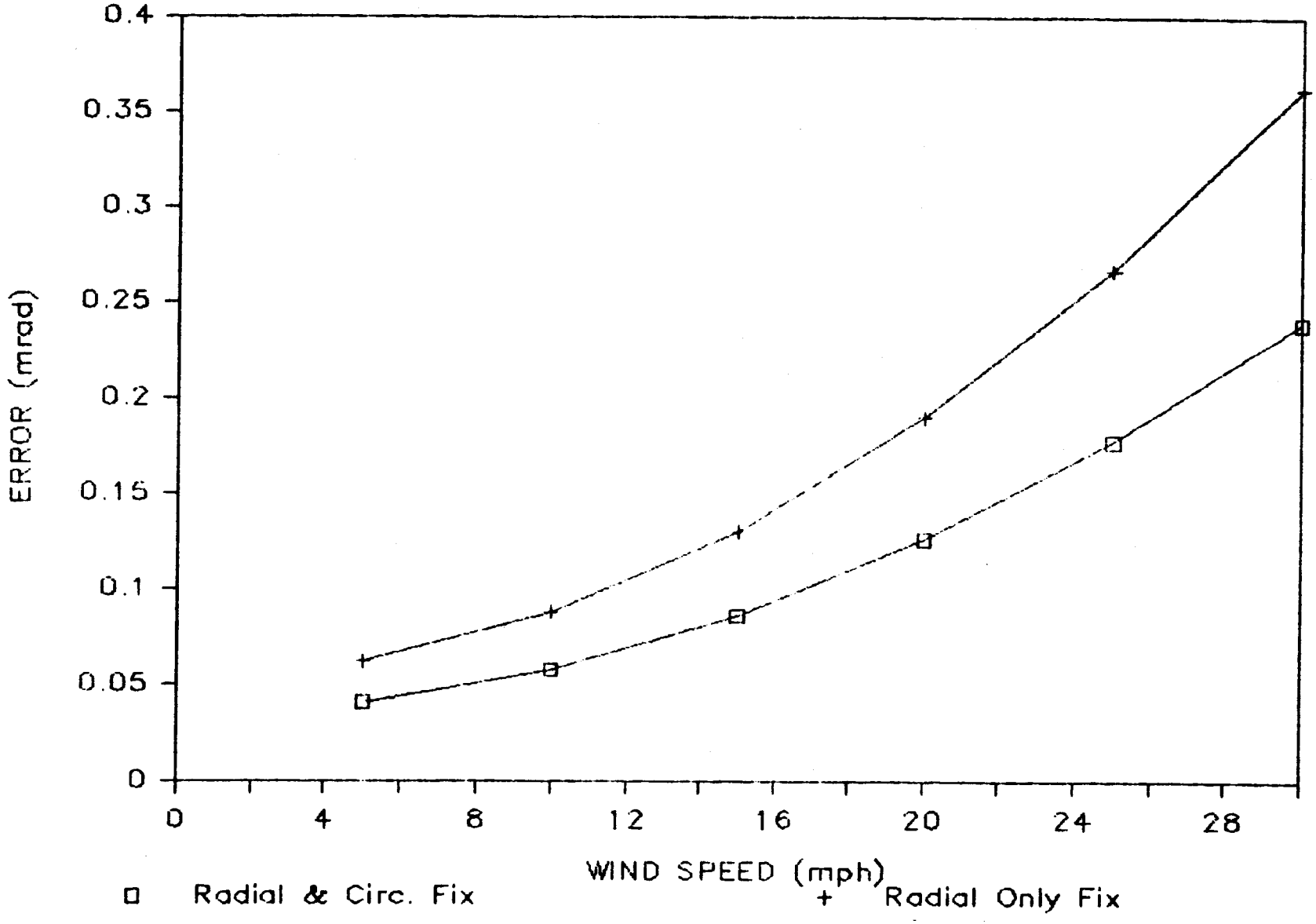

FIG. 3.2 ERROR VS. WIND SPEEDS

is forced to share the circumferential load with the ring. At significant wind speeds (50 mph, worst orientation for stress, 27 mph, worst orientation for error) the circumferential attachment can reduce wind induced error and stress by a substantial margin.

The coupling between membrane and ring have many impacts upon the design of the mirror module. They are essential to the structural efficiency of the concept in that they allow a slender column to be designed upon yield rather than buckling and force all the materials available to resist the load. In the interest of maintaining low weights for inexpensive, high production volume, the design was based on using both radial and circumferential fixes between the membrane and ring.

Two procedures for achieving a fix were identified: adhesive bonding and welding. An immediate problem with adhesive approaches developed. The stress level between the two surfaces was very high and substantial ring depth was required to reduce the shear stress to levels adequate for structural adhesives. The addition of ring material to the in-plane direction would counter the reduction of material offered by a radial fix. Consequently, welding was identified as the preferred method of attachment.

3.2 MATERIALS

The reflective material selected for the stressed membrane was a silvered polymer. It was not the purpose of this design to develop polymer materials and advanced coatings, as these techniques are being investigated by others. Consequently, efforts were limited in the selection of this material.

Cost estimates for silvered polymers in high volume production are not widely available. Under a previous design and development contract, Solar Kinetics worked with a firm involved in metal deposition and polymer production to estimate expense, based upon material costs, of an acrylic and silver reflective material. The results of that work produced estimates of approximately three dollars per square meter. This cost was used for further analysis.

Although direct silvering of the membrane material was not investigated in this effort, it should be noted that the concept is amenable to these approaches. No practical approaches for glass on the membrane were developed.

Stainless steel was rejected on a parametric analysis of costs. The ring cross-section is determined based upon the yield strength of the material. Flexural rigidity has virtually no impact upon the material requirements. Consequently, the ring costs can be determined by looking at the ratio of cost per unit volume to yield stress. In this type of analysis, austenitic stainless showed no promise on a cost basis for ring material.

Ferritic stainless alloys do offer large yield strengths in tempered grades and were parametrically considered. These materials were finally rejected, however, from another structural concern: buckling. In order to take advantage of high yield strengths, the available material must be reduced. Macroscopic ring buckling effects require the material to be distributed to provide both in and out of plane flexural rigidity. When the reduced material is distributed to gain large area moments, wall thickness becomes extremely light and localized buckling failure occurs. Consequently, there is little advantage in moving towards high yield strength materials.

The ferritic stainless alloy group was not considered as a membrane material because it is not a "true" stainless steel. In other words, corrosion would be a serious problem in thin materials. Corrosion protection cost served to eliminate other membrane materials as well. Austenitic alloys would likely be acceptable for membrane fabrication, but as Figure 3.3 illustrates, substantially thinner membranes are required to be competitive in raw material cost. As membrane thickness decreases, handling problems increase.

Finally, the hard attachment discussed in Section 3.1 requires the ring and membrane to have identical thermal expansion properties, galvanic potentials, and be easily welded. Consequently, using an austenitic stainless alloy for the membrane and some different material for the ring was not identified as a desirable approach.

The cost comparison between steel and aluminum for the ring and membrane assembly resulted in a variety of outcomes unique to thin material gages and the stressed membrane concept itself. The cost of thin gage carbon steel is not strictly proportional to material thickness. Discussions with major suppliers of narrow gage material indicated that the expense of bare steel is strongly affected by forming costs below 0.18mm (0.007in).

Corrosion protection of carbon steel is primarily a function of area rather than weight. When coatings were added to bare steel costs, the price per unit area actually began to increase in very light gages due to material handling problems. Narrow gage carbon steel has poor cross-sectional shape control; the sheet is significantly thicker at the center (crown). This creates problems in the coating and coiling process in high speed lines. These companies also indicated that reliable corrosion protection for thirty years could not be guaranteed.

Figures 3.3 and 3.4 illustrate the membrane cost tradeoff for the three materials. The analysis was extended to the ring material to see if differing ring costs would offset the membrane cost. The result of this effort was that aluminum and carbon steel were nearly equal. Typically, steel is the best selection for structural shapes because it offers greater rigidity per unit

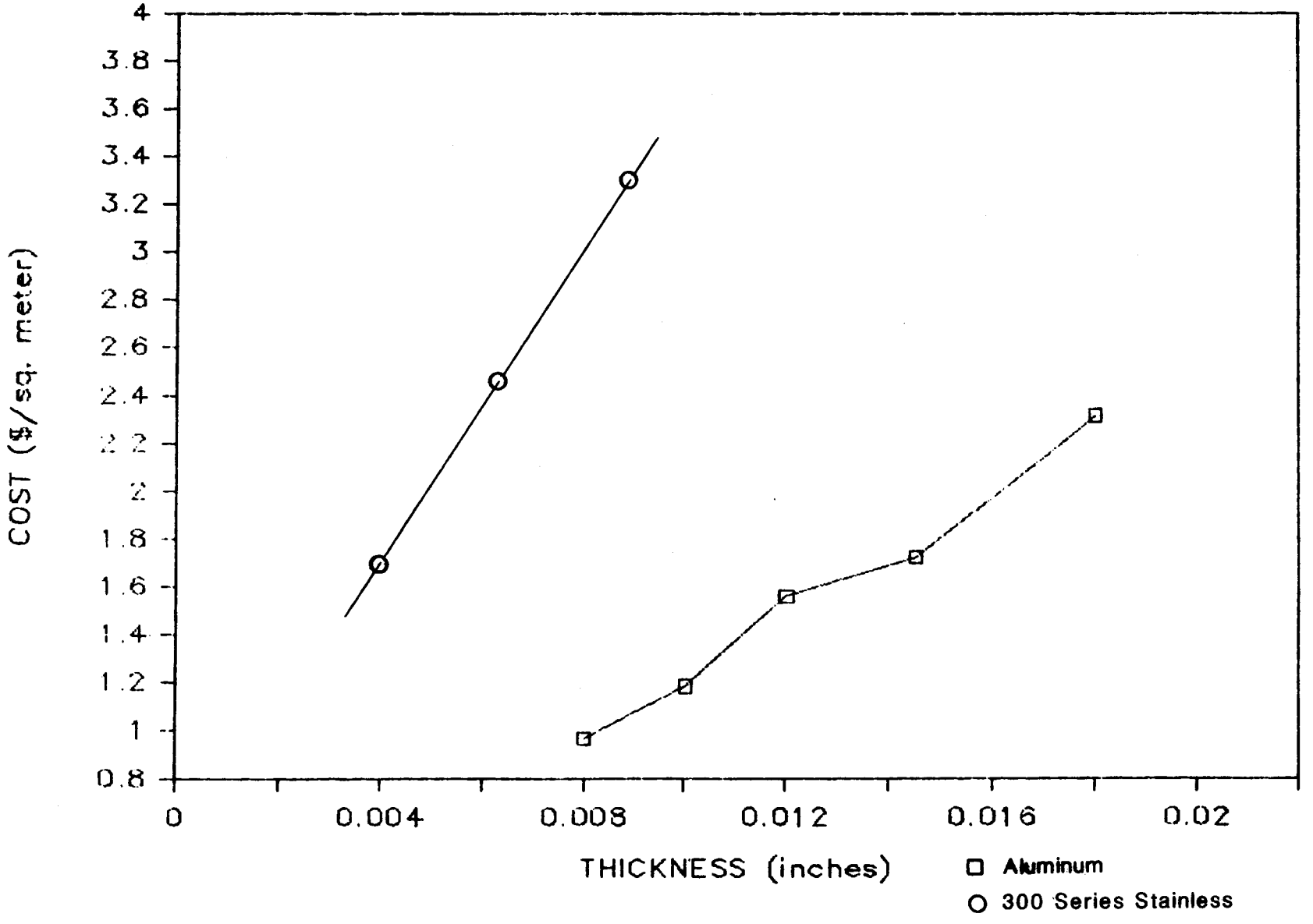

FIG. 3.3 MEMBRANE MATERIAL COSTS

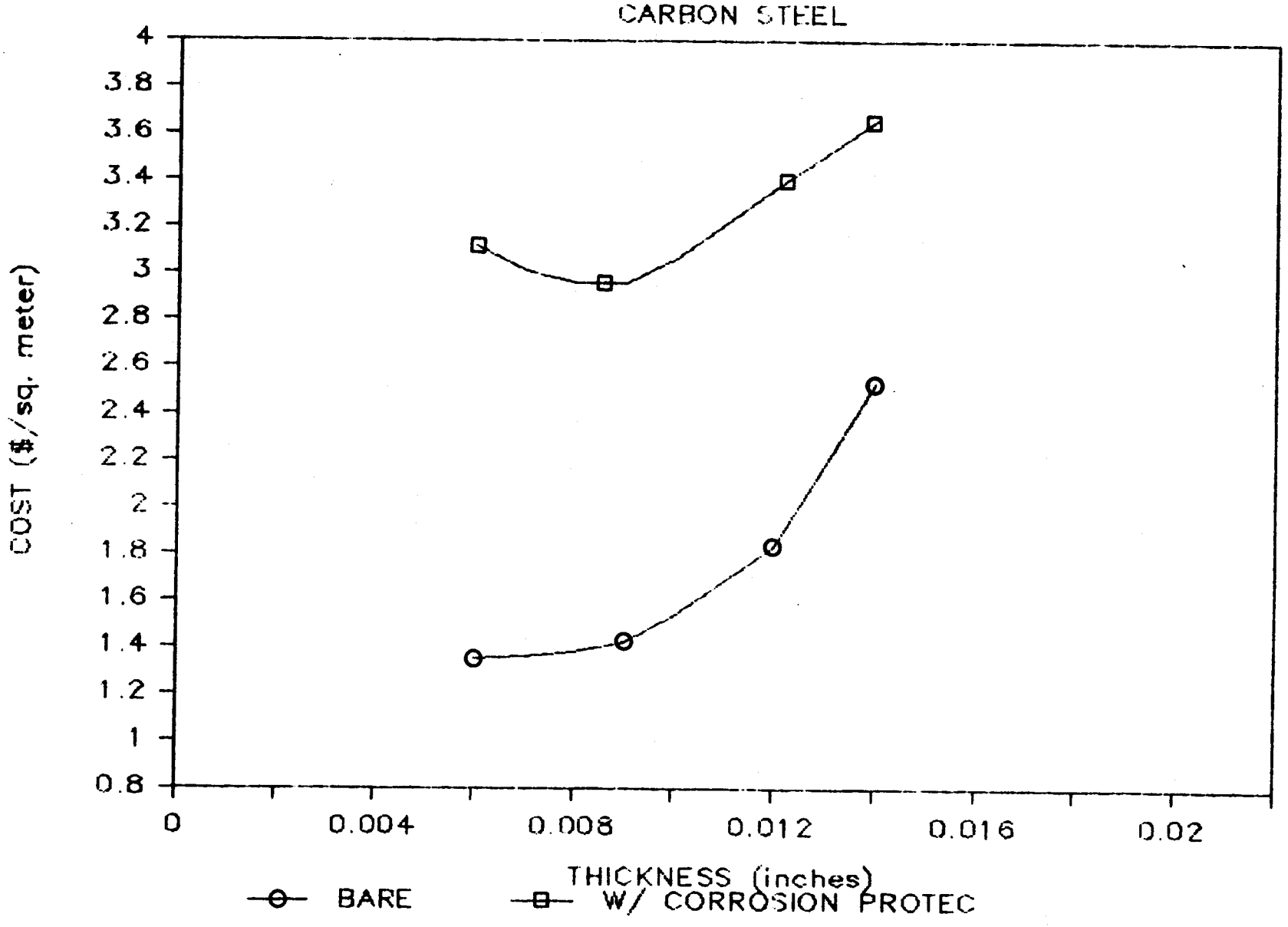

FIG. 3.4 MEMBRANE MATERIAL COSTS

cost. The ring design in the stressed membrane reflector assembly is dominated not by rigidity but by compressive yield. Consequently, the cross-sectional area determines the amount of material required, though there are favorable ways to distribute that mass. The ring cost did not offset membrane cost.

Finally, error in the structure at low wind speeds and at elevations near the zenith was actually worse for carbon steel than aluminum. Although an increase in ring weight is essentially offset by the increase in the stiffness term, the membrane weight is not offset. Aluminum was selected for the design.

3.3 RING

The design of the ring is a crucial development in optimization of the reflector assembly and one of the most complex. The selection of shape, thickness, and tension required a substantial number of tradeoffs; some more easily quantified than others. Because of the large number of variables involved, some reasonable assumptions were made and the sensitivity of these assumptions were tested against the final design.

Initially, the baseline design of a rectangular, hollow tube was adopted. An error budget of 0.6 mrad was allowed for wind and gravity errors at 27 mph in the worst orientation. A stress limit of fifty percent of yield was applied for loads due to 50 mph winds, gravity, and initial tension. The remainder of the stress was allowed for localized loads at the attachment points, and increases in the apparent tension due to diaphragm stretching.

The response to loads was studied in parametric fashion to establish the relative importance of each deformation mode. Stability issues were discussed in the section on attachment. Asymmetric error and wind stress is driven entirely by out of plane response. Stability considerations, wind induced stress, and error suggest that mass can be most efficiently distributed by providing a large moment of inertia in the out of plane direction. The ratio of height to width for the ring was selected to provide an order of magnitude difference in area moments.

A nominal design preload of 50 pounds per inch was selected, and the ring was optimized based upon a two term design approximation established in Ref. 9. The ring thickness was allowed to vary and the sensitivity of weight (and hence cost) per unit aperture was plotted in Figure 3.5.

As ring thickness decreases, the localized loads at the attachment points result in substantial stresses. A portion of the ring was modeled using linear finite element techniques and the stress at the attachment was distributed with doubler plates.

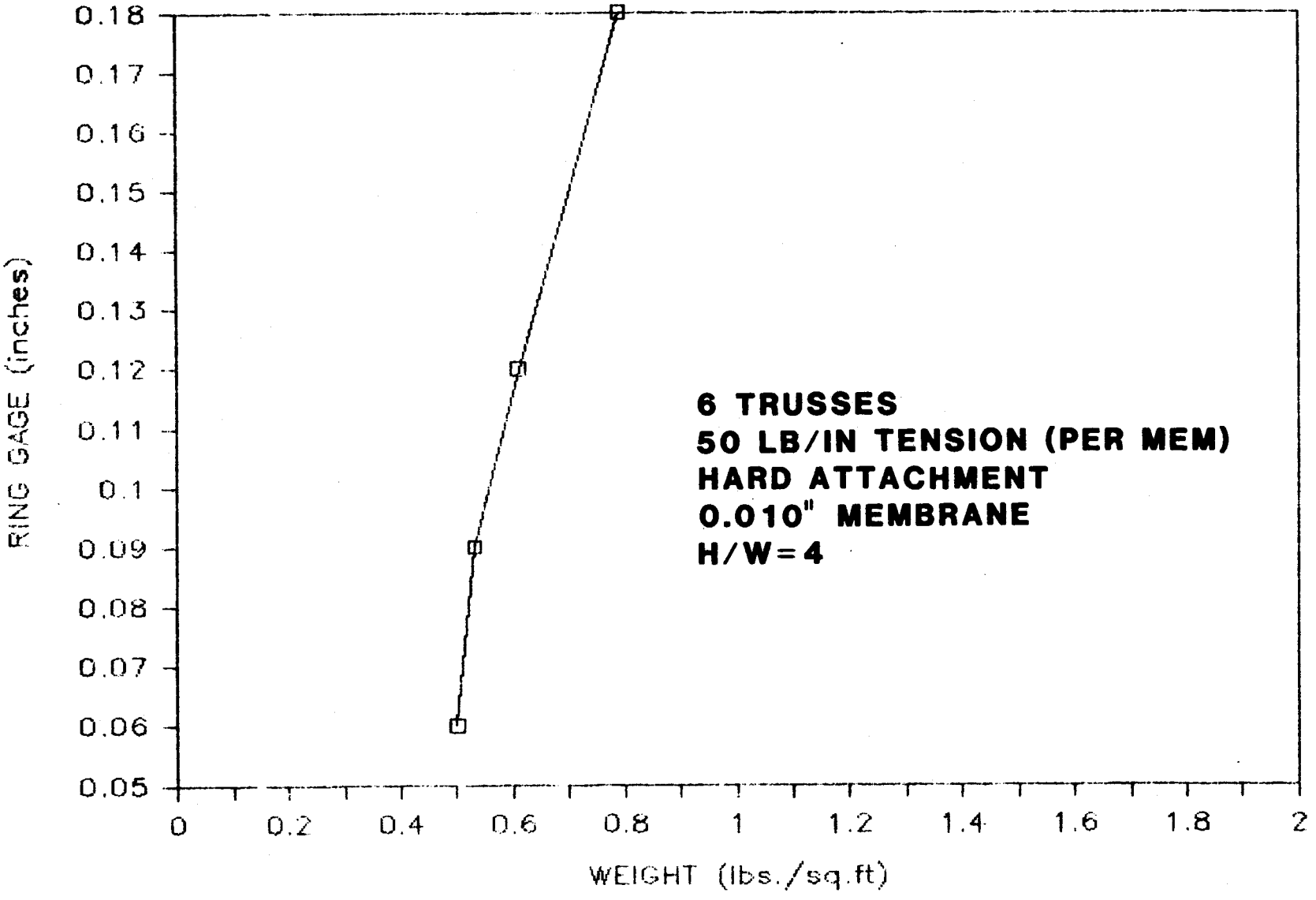

FIG. 3.5 SENSITIVITY OF RING GAGE SELECTION

The weight of doublers for the 0.060 inch wall thickness was more significant than the additional weight associated with 0.090 inch wall.

The initial tension was varied next, and the ring was optimized for each value shown in Figure 3.6. Obviously, the initial tension is a substantial driver in the weight of the mirror module. Some caveats need to be applied to the selection of low tension values, however.

At thirty pounds per inch, the lower limit shown in Figure 3.6, the two term design approximation predicts a stress reversal in the membrane. In other words, the magnitude of the roll in the ring is adequate to unload the membrane along several diametral lines. If the membrane attempts to go into compression it will immediately buckle. It is essential to provide a preload adequate to maintain tension in all loading conditions.

The failure mode associated with buckling is a stability rather than yield phenomenon. As such, it is essential to provide some factor of safety to the critical load deformation. In the absence of substantial data, the application of such a factor does not lend itself to rigorous development. Two major issues were considered in minimum preload development. The first is illustrated in Figure 3.7. An increase in membrane tension has a positive impact upon heliostat performance.

The next consideration required a departure from the linear, two term design approximation used for development. Diaphragm stretching increases the apparent membrane tension. This increase in tension is a result of large deformations with respect to membrane thickness and is independent of the initial preload. In the stow position, with no control, the increase in tension at survival wind conditions was substantial in comparison to the preload. Because this survival load occurs infrequently, the ring stress was allowed to approach eighty-five percent of yield.

In low tension designs, optimized with the first order approximation, the required cross section will actually exceed yield in the survival condition. To return to the eighty-five percent value established above, the cross sectional area must be increased. In other words, the design approximation based on fifty percent of yield under predicts the required mass. When material is added to provide resistance to this non-linear term, the net cost for an increase from thirty to sixty pounds per inch is approximately twenty cents per square meter. Above sixty pounds per inch, the increase shifts to a near linear relationship of thirty cents per square meter for each ten pound per inch increment. Consequently, the preload was established at sixty pounds per inch.

If the ring is adjusted for each value of tension (as presented in Figure 3.6) to maintain the area moment ratio described

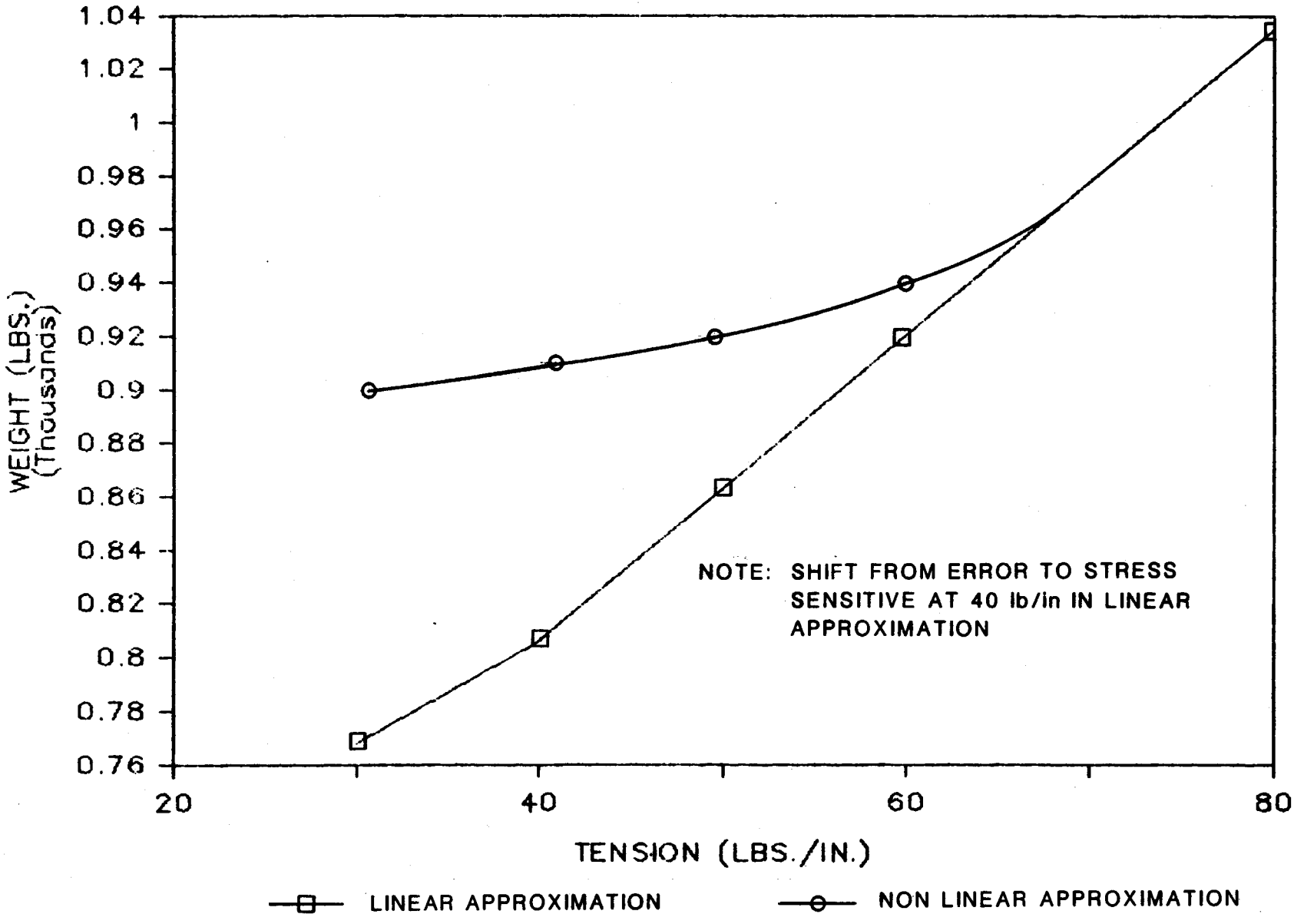

FIG. 3.6 MIRROR MODULE WEIGHT VS. TENSION

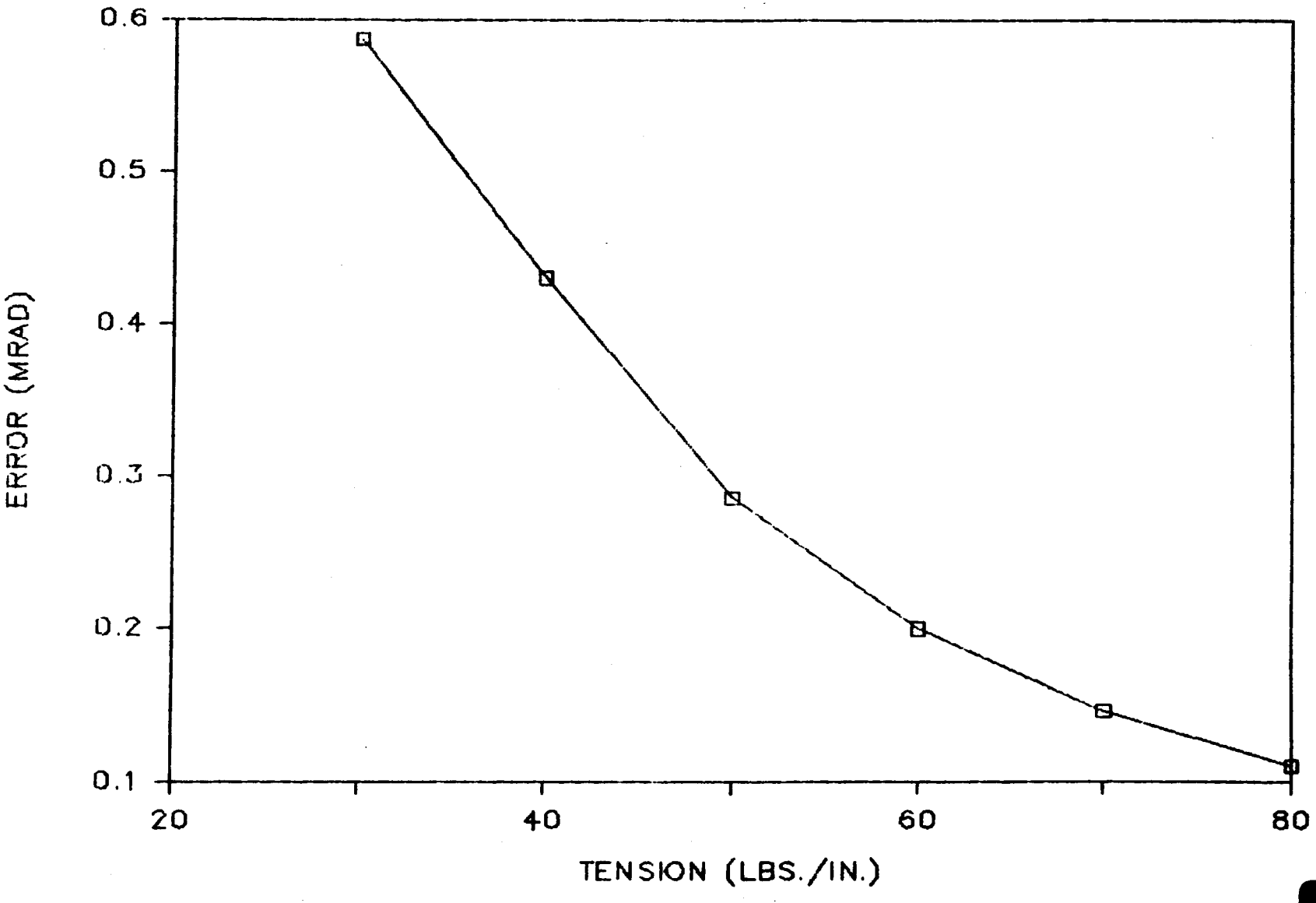

FIG. 3.7 ERROR VS. TENSION

earlier, the safety factor is not linear with preload. As the ring height increases, roll resistance is also improved due to the greater "moment arm" that membrane tension acts through. The safety factor on load reversal is more than two although preload was only doubled.

The result of these assumptions and consequent analysis was:

Height	12 inches
Width	3 inches
Thickness	0.09 inches
Membrane preload	60 pounds per inch

The stress state in the ring is dominated by the membrane preload. Tension in the membrane is transferred to the ring as axial compression. It is the cross sectional area that determines the required weight of the ring. Selection of alternate shapes, area moment ratios, or thickness will not significantly alter the mass. Consequently, the initial assumptions made for the analysis have little impact upon the cost of the reflector assembly.

3.4 MEMBRANE

The selection of the ring, preload tension, and method of attachment for the mirror module are based on factors considered in earlier presentations. The major variable that remained was thickness.

Contact with the aluminum industry indicated that costs do not continue to decrease linearly with weight in thin gages. The change occurred between 0.008 and 0.010 inch thickness. It is at this point that material was classified as foil rather than wrought sheet. Costs purportedly increased because additional processing expense associated with thickness reduction became significant in foil processing.

In addition to a change in the cost to weight ratio for like materials, the availability of tempers and alloys also differed. The 5000 series of aluminum alloys were selected as representing the best combination of weldability, resistance to atmospheric corrosion, and cost. The foil industry offered zero temper and strain hardened only tempers, while wrought suppliers offered strain hardened and stabilized tempers. Zero temper aluminum (dead soft) was considered unacceptable because it is subject to localized yield during handling and is not well suited to resistance welding techniques. Non-stabilized tempers soften at room temperature over time. This softening will reduce the hail resistance of the material. Wrought sheet was selected as the best material for the membrane.

Hail resistance tests on two thicknesses of stressed aluminum were performed by others. Preloaded sheets, 0.005 inches in thickness, failed catastrophically by tearing. Sheets of 0.010 inch material passed the hail test.

Material handling costs are likely to increase exponentially with decreasing thickness. The 0.010 inch tempered aluminum was handled successfully in bench model testing, though these stressed membrane reflector models were two meters in diameter.

Solar Kinetics adopted 0.010 inch material for the design based upon success of the hail test and the availability of stabilized wrought materials. Experience with the fifty square meter prototype assembly alleviated material handling concerns and the final design thickness could decrease by ten or twenty percent.

3.5 TENSION

Consideration was given to applying the membrane loading both before and after mirror module fabrication. Pre-tension suffered some significant problems. If the ring is initially relaxed; in other words, under no axial compression, the membrane tension must be increased to account for ring shrinkage under load. This increase in tension was significant when compared to the final preload and would, in fact, result in planar stress states near membrane yield.

The ring, because of its low moment of inertia in the "in-plane" direction, cannot sustain a compressive load without buckling radially until the membrane tension is coupled. Some consideration was given to shrinking the ring by cooling it, but the approach was abandoned as close temperature control, short assembly times, and substantial thermal mass were significant obstacles.

Post tensioning does not require membrane tensions to overcome ring shrinkage because the deformations occur simultaneously. Two basic methods were considered for post tensioning: mechanical deformation and an inflatable tube. Mechanical deformation induces membrane tension by bending and so tensioning the flange of the ring.

A single stroke tensioning device was considered impractical due to the enormous size, rigidity, and tonnage such a machine would require. Nine of these machines would be required, as they are located in the site manufacturing facility. Efforts turned to the development of a crimping device that would allow progressive deformation on the circumference of the ring.

Mechanical tensioning is extremely sensitive to the position tolerance of the membrane. A second consideration in mechanical post-tensioning involves the rate at which progressive

deformation can proceed. Because the ring has very little buckling resistance before the membrane is coupled, only small deformations can be achieved to remain well away from the critical load.

The addition of an inflatable tube offers a partial solution to both of these problems. Because membrane tension is achieved through force from the tube, and the tube equalizes force because internal pressure is constant, there is a significant reduction in placement sensitivity. Applying pressure to the tube prior to mechanical tensioning effectively couples membrane and ring to avoid radial buckling. Mechanical deformation can then proceed with far fewer passes.

Tensioning the membrane with a tube only was not considered because the inflated tube would load the weld between ring and membrane in peel. This type of loading is unacceptable for resistance welded attachments. If the tube provided all tension, it would also need to be substantially larger in diameter, and consequently, more expensive.

Glass fiber reinforced silicone was selected for the tension tube material to provide for the thirty year life requirement.

Experience gained during the fabrication of a fifty square meter mirror module decreased our concern over uniform tension in the membrane. Some problems in this area were apparent, but these non-uniformities were attributed to a variation in sheet length. The appropriate correction for sheet length variation is to start with a more uniform base material achieved through control of the rolling mill practice and subsequent leveling of the sheet stock in the coil line. Application of tension did not appear to represent significant problems.

In future optimization efforts, we would recommend that the method for applying tension be reviewed. The tube is a relatively expensive component both in capital expense at the central manufacturing facility and in direct material costs. Some concern over the failure of the tube has also been expressed. Although we do not anticipate catastrophic failure of the membrane (the edge crimp provides a residual tension in the event of tube failure), performance would be degraded.

As an alternate approach, a combination of pre and post tension is recommended rather than two methods of post tension. If seventy-five percent of the tension were provided through pre-tension, for example, membrane yield could be avoided. Upon attachment to the ring, the structure would be coupled and a mechanical ring crimp could be implemented without rate sensitive problems. This approach might be implemented through modification of the vacuum platens, for example. If the platen were made from annular rings, each capable of radial expansion, pre-tenison could be provided without encumbering the weld area or requiring enormous and rigid fixturing at the site

manufacturing area. There are other options for applying pre-tension; this approach is offered as an example only. The point is, the stressed membrane mirror module need not rely upon an inflatable tube.

3.6 SUPPORTS

The detailed design of supports is covered in Section 4.0, but some elements are discussed here because of inherent relationships between the mirror module and back structure. The most significant impact is the number of supports available to resist out of plane ring deformations.

The load deformation response of the mirror module has been conceptually described in earlier sections. Although deflection and roll are intimately coupled in any ring, it is useful to simplify response for the purpose of explanation. The vertical deflection of the ring is a function of distance between supports for a given uniform loading condition. As this distance increases, deflection increases. The relationship in non-linear, and is illustrated in Figure 3.8.

The number of struts was varied, and the mirror module design was optimized using the two term design approximation, error budget, and allowable stress developed in an earlier section. The graph illustrates that the reflector changed from an error sensitive to stress sensitive design at four supports (the only error term considered here is asymmetric).

Weight continues to decrease as the number of struts increase because the distance between supports, which roughly corresponds to the unsupported length of a fixed/fixed beam, decreases. The weight of the struts obviously begins to offset mirror module costs at some point. Our analysis indicated that this point occurred at six supports.

The quantity of supports also has an impact upon other sources of error. Three supports define an arbitrary plane; if one support deflects more than another a "tracking" error is induced in the ring. This type of deflection response would occur in reaction to a non-uniform load profile. As the number of supports increase, the magnitude of the "tracking" error decreases but an additional asymmetric error is introduced by the support resistance to deflection. Using the half pressure profile suggested in Section 2.0 as a worst case scenario, the three support approach required an enormous out of plane stiffness to maintain the 1.2 mrad standard deviation term of the mirror normal. The reduction in stiffness requirements as supports increased allowed the total support weight to decrease and, in fact, changed from an error to stress sensitive design. The asymmetric error induced by the support was parametrically determined to be small with respect to the "tracking" term.

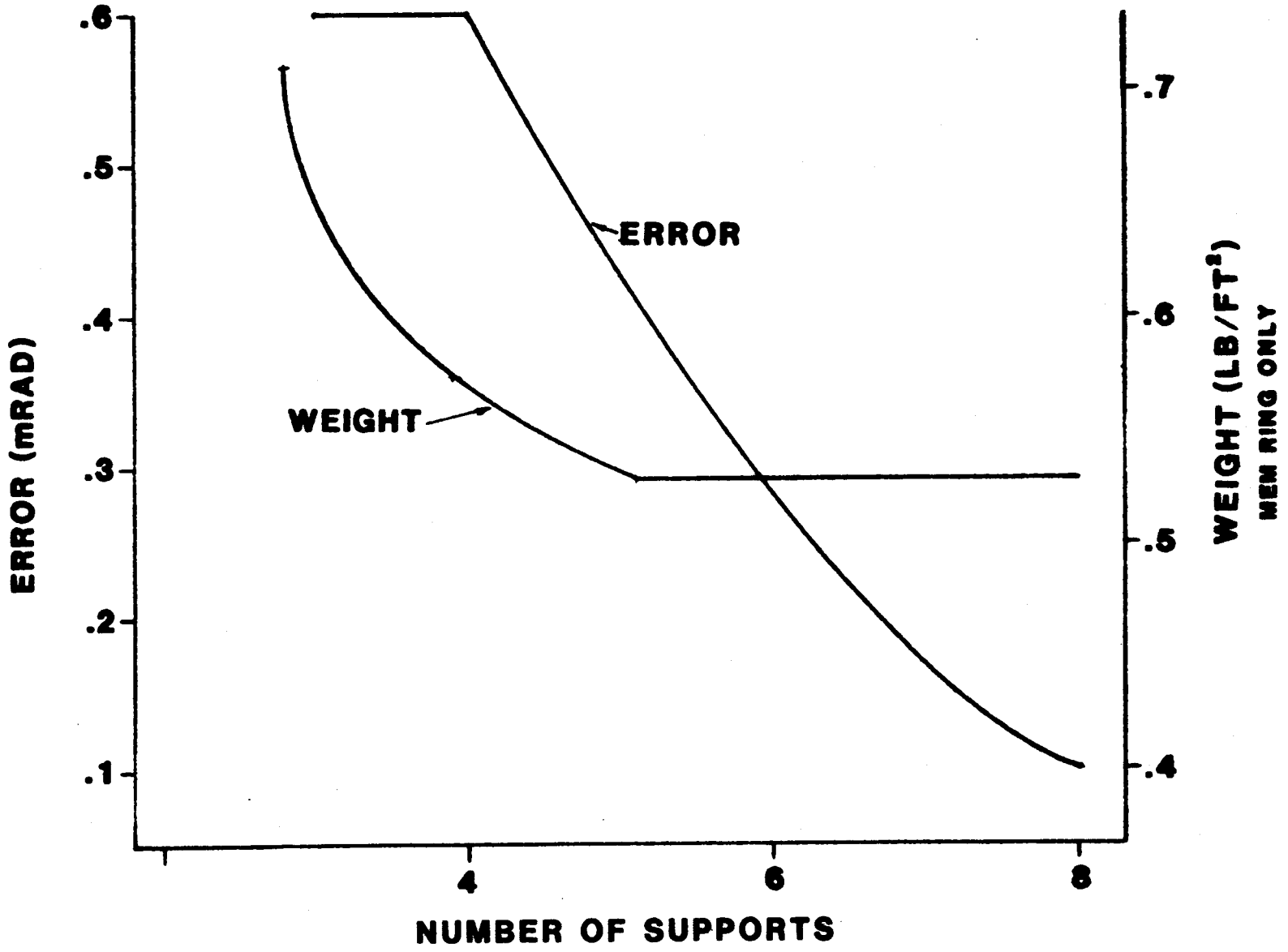

FIG. 3.8 ERROR, WEIGHT VS. NUMBER OF SUPPORTS

Optimization of the quantity of supports was also based upon unfavorable load directions discussed in Sections 2.0 and 4.0. The results of our analysis indicated that six struts were required and all mirror module optimization was based on this quantity.

3.7 MANUFACTURING TECHNIQUES

The manufacturing techniques used for fabrication of the mirror module at both the central and site manufacturing facility are described fully in the manufacturing and cost sections of this report. Two features of our design are discussed briefly here: welding and material handling.

Coiled sheet metal is not truly a uniform thickness, parallel linear edge, constant width, isotropic material. The most significant shape problem of aluminum sheet for welding was camber. Camber is a description of the non-linearity in the center line of a sheet. Although the coil maintains a relatively constant width, the center of the material oscillates about a straight line. When two sheets are butted together, edge to edge, there is no uniform contact. As the gage decreases, camber becomes a more significant problem.

Butt welding processes require close control of the gap between thin sheets; typically a variation of twenty to thirty percent of material thickness is the maximum allowable for successful welds. The camber of a sheet forty feet long exceeds the allowable gap by more than an order of magnitude. The camber problem is eliminated by lapping the sheets.

Fusion and resistance welding processes are suitable for lap welding. Resistance welding was selected over fusion techniques because it is fast, induces less heat into the membrane, and is an industrially proven inexpensive process. Seam welding speeds for 0.010 inch aluminum sheet exceed 180 inches per minute [Ref. 15], an order of magnitude higher than tungsten inert gas approaches. Laser welding is somewhat faster but is not particularly inexpensive.

Heat at the weld zone causes distortion in the membrane material. Resistance welding offers a comparatively low energy input to reduce this distortion.

Resistance welds do not fully penetrate material thickness and are subject to failure by peel. Peel in the membrane to membrane weld is substantially reduced by using two welds at each seam. The weld is then primarily loaded in shear, a stress state that resistance seams are particularly well suited for.

Surface preparation for aluminum resistance welding is dependent upon the alloy and temper. The "half hard" temper 5000 series aluminums selected require that waxes, oil, and dirt must be

removed but do not require etching or mechanical abrasion of weld surfaces. This preparation would also be required for fusion processes and does not represent any additional cost for the technique to be employed.

Resistance welding for ring to membrane attachment was selected for similar reasons. Camber is no longer a problem, but speed and minimal energy input are still required.

As the sheets of aluminum are welded into a membrane, any position or wave distortion is made permanent by the connection. It is essential to hold each sheet flat in order to produce flat membranes. The narrow gage material has virtually no flexural rigidity and will not rest flat under its own weight due to an initially non-uniform stress state.

A vacuum platen is uniquely qualified for this clamping because it holds the sheet with a distributed load. Platen positioning effects the sheet to sheet relationship.

The vacuum platen approach was extended to handle membranes at the site manufacturing facility. The entire membrane must be translated from coil to assembly fixture without applying concentrated loads and maintaining a planar shape. Because the platen is slightly smaller in diameter than the finished membrane, a free edge is provided at the circumference for welding. The membrane need not be released until welding is complete. Therefore, the platen serves as a transfer device and positions the membrane.

Perhaps of greater concern in thin sheet stock is the variation of length across the width of a sheet. This variation has been alluded to in the prototype sections of this document and in earlier sections. The problem did not become apparent until a large radius (i.e. the 8m diameter prototype) mirror module was built. The result of length changes in the base membrane material is a non-uniform tension and waves between the seams. This problem can be addressed through better control of the mill rolling process and leveling in the coil line. Both areas were included in our evaluation of the commercial design. The two meter diameter bench test models did not exhibit the problem, and consequently no effort was made to counter the effect in the prototype assembly. Preliminary analysis of the prototype indicates that the waves are not a serious impediment in the concept. Even when not addressed, we estimate that less than five percent of the optical surface is lost as a result.

SECTION 4.0

SUPPORT STRUCTURE DESIGN

The support structure of the reflective assembly was designed to feed the distributed loads of the mirror module into three connections with the drive unit. The major sources of these loads are wind and gravity.

Since the intent of the stressed membrane heliostat program is to reduce heliostat cost, careful consideration was given to ways in which material costs could be minimized.

4.1 DESIGN CONSIDERATIONS

SAND82-8181, section 2.5.9, "Optimization of the Second Generation Heliostat and Specification", concludes that support structures are more effectively sized on the basis of stress than on slope errors; however, slope error analysis did bias choices in favor of stiff parts where there was no accompanying weight penalty. A structure was designed to be stress critical at 50 mph at any orientation and at 90 mph in stow. Minimal deflection induced slope errors resulted in a 27 mph wind.

4.2 LOADS

Of the two primary sources of loading, wind was the more significant. To develop appropriate design loads, a non-uniform pressure distribution was considered. Placing the mirror module at different angles of attack relative to the wind resulted in loads in, and moments about, the radial, tangential, and azimuth axes of the reflective assembly.

4.3 MATERIAL

Steel was chosen as the support structure material for its relative low cost. Steel also has a high modulus of elasticity, which results in a stiff structure.

4.4 COMPONENTS

The major components of the support structure are as follows:

Trusses

Hub

Hinges

Strapping

The considerations used to design these components are presented in the following paragraphs. The results are also given.

4.4.1 TRUSSES

A heliostat with 150 square meters of reflective surface requires a mirror module of 46 ft. diameter. The truss length is the distance from the hub to the ring diameter. The hub was chosen to be 6 ft. in diameter, so the trusses were 20 ft. in length.

4.4.1.1 TRUSS DEPTH

When the azimuth axis is oriented in any position other than perpendicular to the wind direction, the primary load is parallel to the azimuth axis. Since deflection is inversely proportional to the moment of inertia, and deflections result in slope errors, steps were taken to make the moment of inertia of the trusses as high as possible for a given amount of material. At the same time, the trusses needed to be stress critical at the 50 and 90 mph wind speeds. The primary members were placed in tension or compression by the tip loading.

Since $I = I + Ad^2$, the moment of inertia could be increased by placing the primary members further and further apart without changing the cross-sectional area. Eventually, buckling considerations limit the distance of separation between the primary members. Results of analysis yielded the primary member of Figure 4.1. This member is stress and buckling critical at 50 mph, minimizes structural mass, and results in a very stiff structure.

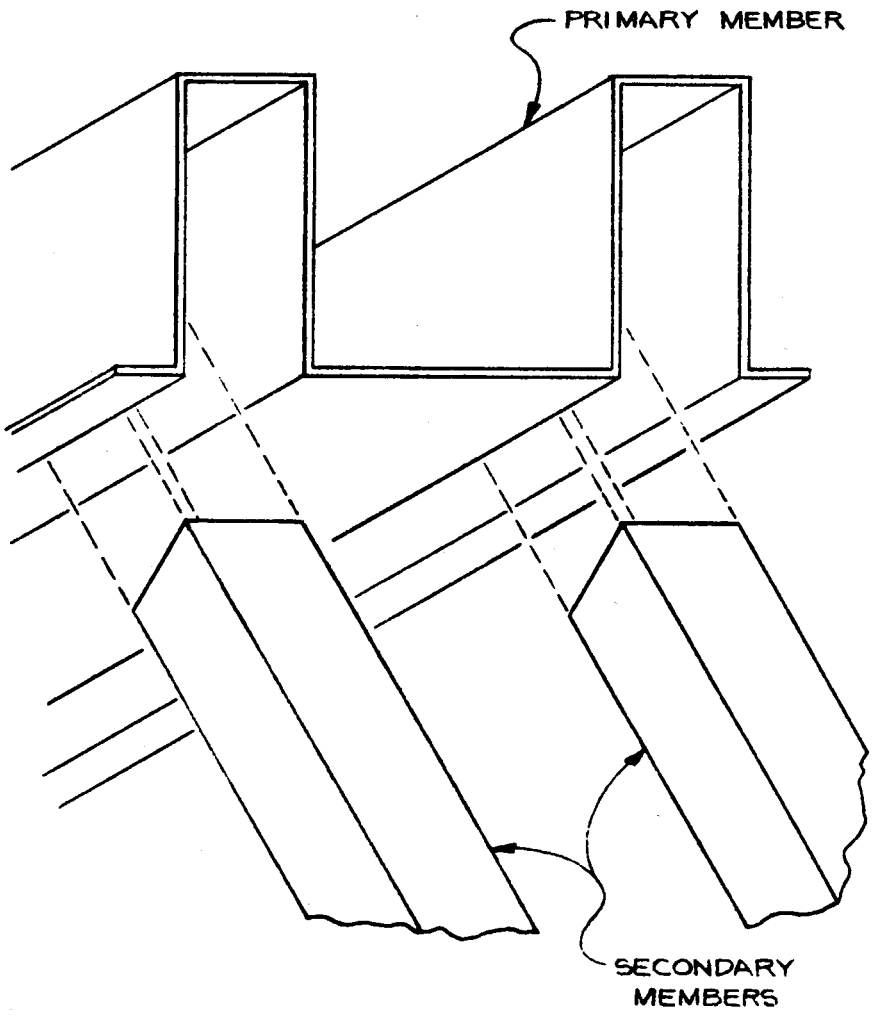

FIG. 4.1 PRIMARY/SECONDARY ATTACHMENT IN TRUSS

4.4.1.2 NUMBER VS. WEIGHT

The minimum number of trusses that could be used to support the mirror module is three. There are a number of reasons to increase the number of trusses. As the number of trusses increase, the tracking error caused by uneven pressure distributions on the mirror module decreases. To effect the same result with fewer trusses would increase the combined truss weight enormously. It should also be recognized that some manufacturing error will always exist in the mirror module. The more places the mirror is held, the more the error can be corrected. With only three trusses, it is not possible to correct for manufacturing error at all.

4.4.1.3 SECONDARY MEMBERS

The secondary members of the truss are designed to resist buckling loads. The secondary member at the tip of the truss is made of thicker gauge. This is to provide an adequate bearing surface for the hinge pin.

The secondary members are twinned 1" x 1/16" tubes. At the truss tip, they are a roll-formed shape to allow the tubes to be connected and cap the end.

4.4.1.4 CONNECTIONS

Primary to secondary member attachments are made with spot welds. Connection to the hub is made with bolts. Fitted inserts (Figure 4.2) insure alignment. The hinge is attached with a bolt with castle-nut through the heavier gauge secondary members at the truss tip (Figure 4.3).

4.4.2 HUB

The hub serves to feed the truss loads into the three drive connection points. Loads at the hub tend to be highly concentrated. Also, small deflections of the hub are greatly magnified at the truss tips. Heavier materials were used for these two reasons.

The hub (Figure 4.4) is built of two hoops of 2" x 6" x 1/4" angle iron held apart by spaced T sections. Six brackets are welded to the underside of the lower hoop.

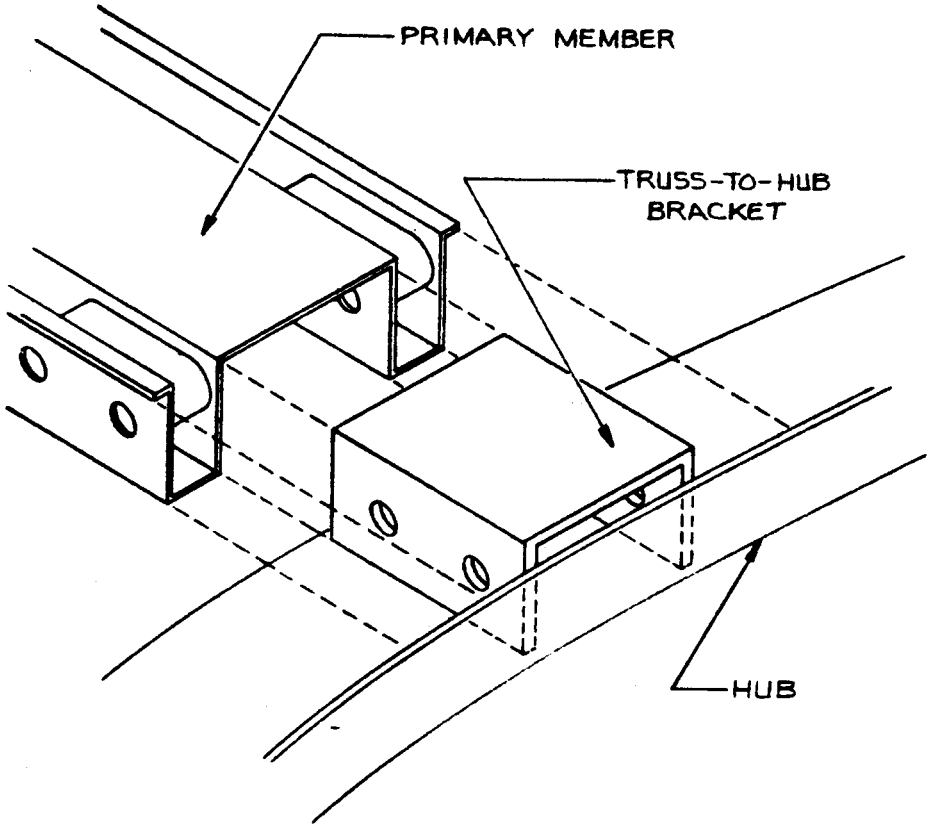

FIG. 4.2 TRUSS/HUB ATTACHMENT

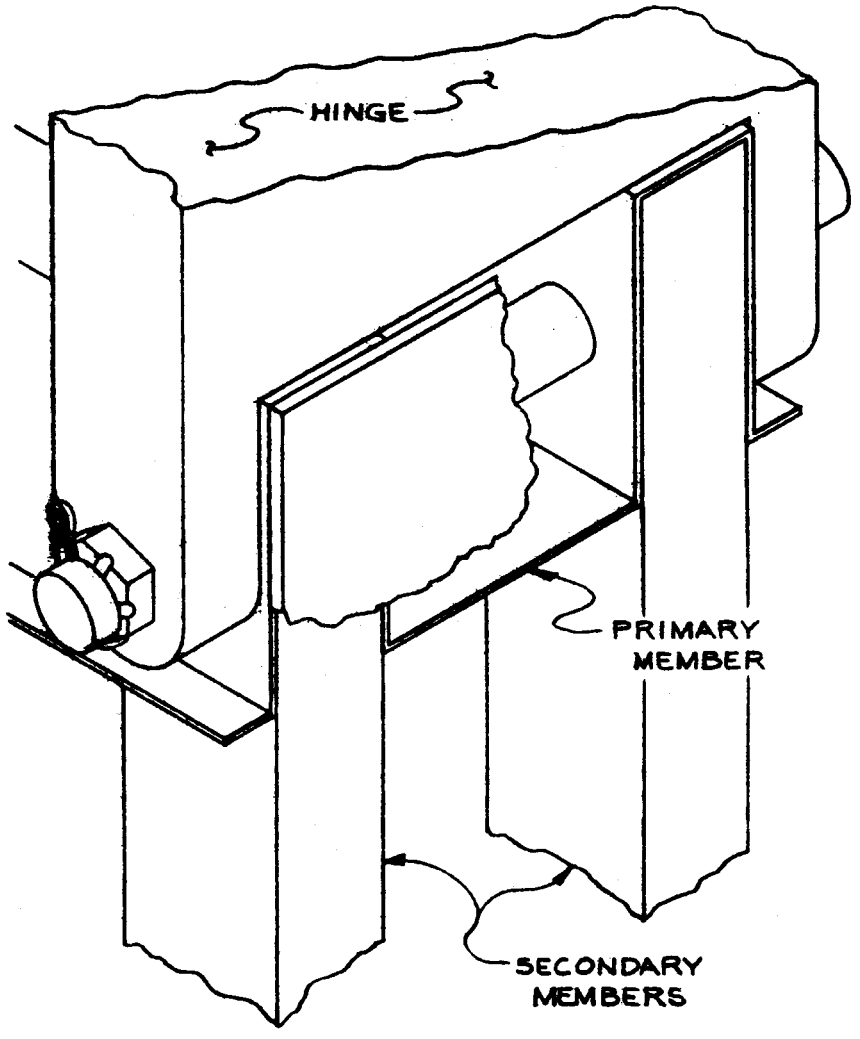

FIG. 4.3 TRUSS/HINGE ATTACHMENT

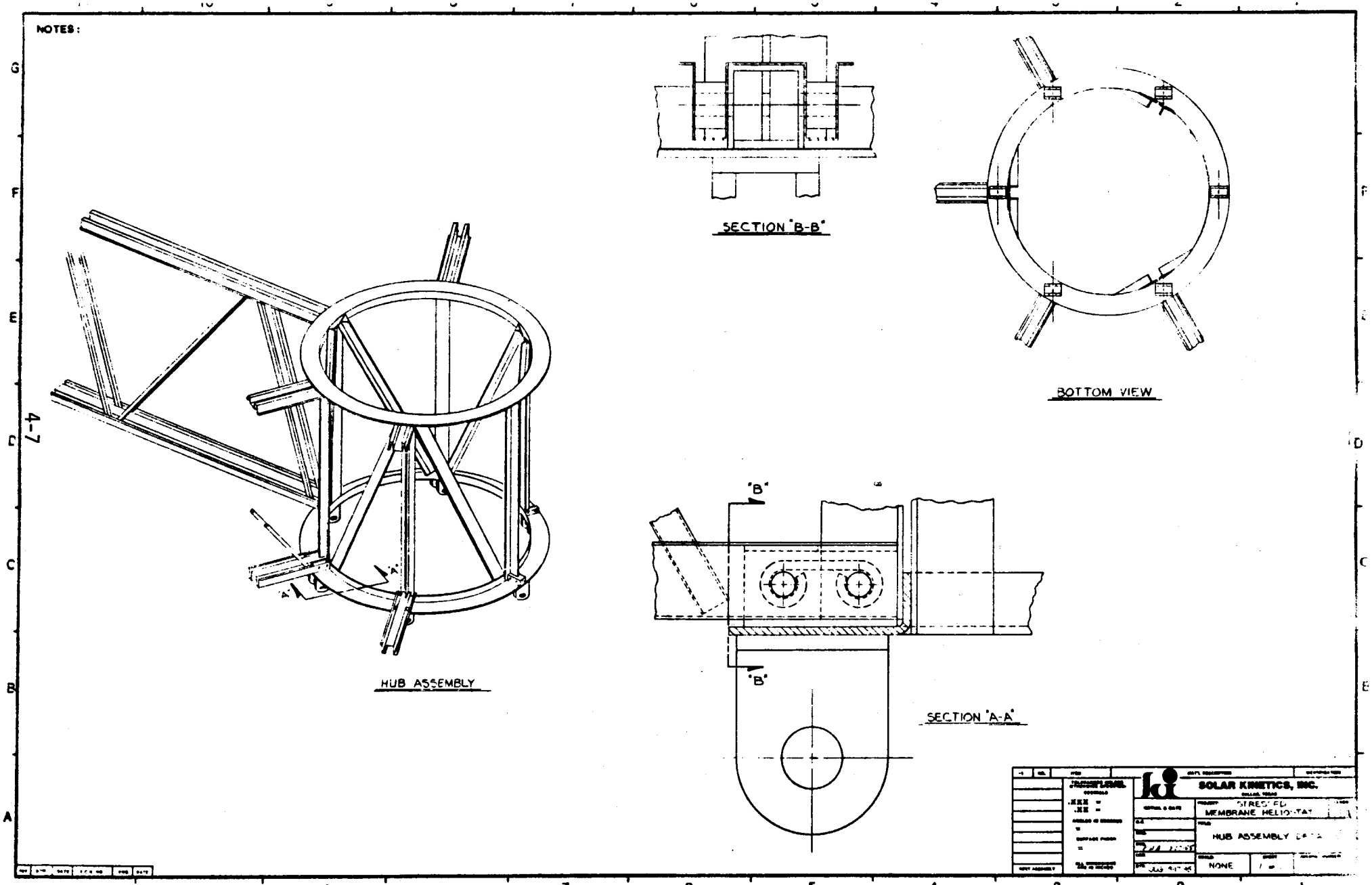

FIG. 4.4 HUB ASSEMBLY

Three of these brackets are used for connecting to the drive. The other three are used by the installation truck to grasp the reflective assembly. Short channel sections are inserted and welded on the inside of the 6" flange of the hoop to offer and attachment point for the trusses.

4.4.3 HINGES

The difference in the thermal expansion coefficients between the mirror module and the support structure requires a hinge that allows radial movement. The hinge is made long enough to hold the mirror module away from the support structure so that the rear membrane cannot be damaged. The hinge is attached to the truss by a bolt that pierces the primary and secondary members at the truss tip (Figure 4.3). The hinge is fastened to the ring with a pin through a welded doubler.

4.4.4 STRAPPING

Side loads on the mirror module result in torsion about the radial axis of the trusses if not prevented through cross-bracing. Such forces arise from pressure gradients along the edge of the mirror module. These gradients can also cause a rotation of the reflective assembly about its optical axis. To prevent such movements, the star strapping pattern of Figure 4.5 is used. The radial pattern permits rotation about the optical axis.

4.5 SUPPORT STRUCTURE WEIGHT

The weights of the components of the support structure are shown in Table 4.1. The total weight of the support structure is 2246 pounds.

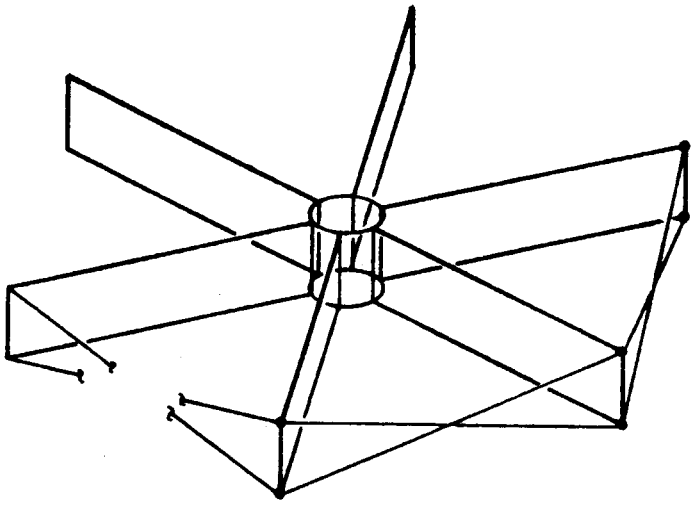

RADIAL PATTERN

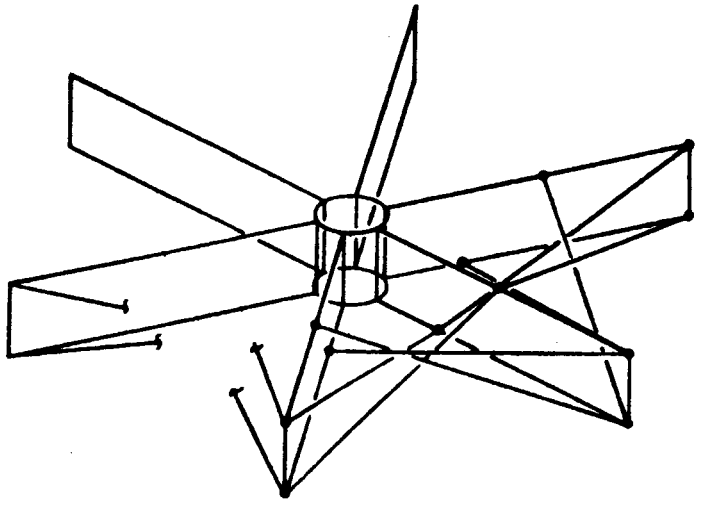

STAR PATTERN

FIG. 4.5 TRUSS STRAPPING

TABLE 4.1

SUPPORT ASSEMBLY WEIGHT

ITEM	WEIGHT(lbs.)	QUANTITY	TOTAL WEIGHT (lbs.)
Truss			
Primary Members	148.60		
Secondary Members*	67.00		
	215.60	6	1293
Hub			
2" x 6" x 1/4" Angle	247.20		
T Bracing	284.00		
	531.20	1	531
Strapping	7.70	24	184
Connectors			
Drive Brackets	15.00	6	105
Truss Brackets	2.25	12	27
Hinges	15.00	6	105
			2246 lbs

* Secondary Members at Truss Tip of Heavier Material

SECTION 5.0

CONTROLS

The stressed membrane reflector assembly requires a pressure system to control the focus of the mirror. Deformation of the front membrane occurs in response to a differential pressure. The pressures required are on the same order of magnitude as the dynamic pressures created by the wind. Consequently, the pressure must be varied actively to maintain focus.

We have elected to use a linear variable displacement transducer (LVDT) mounted firmly to the ring for the commercial design. This transducer was selected because of its infinite mechanical life and high accuracy. Placement of the transducer will be along a quarter line to eliminate problems associated with sag and roll due to front loading conditions.

An axial fan with rotational speed control was selected as a prime mover. This type of actuator provided the best compromise of high volume at low heads, characteristic of the mirror module response.

5.1 RESPONSE

Initial design assumed that the minimum focal length required was 90 meters. As the diameter of the reflector assembly increased, however, the need for short focal lengths was questioned. Large diameter heliostats suffer from off-axis optical errors that are significant in small heliostat arrays. In large arrays, short focal lengths are not required. Receiver aperture is largely determined by the beam spread of distant heliostats and surface error in close heliostats is not as critical because reflected energy is captured anyway.

The stressed membrane reflector assembly suffers some unique disadvantages at short focal lengths. As deflection of a membrane becomes large with respect to its thickness, the apparent tension increases due to diaphragm stretching. The affect of diaphragm tension is quite significant at the short focal lengths.

The two term design approximation used for sizing the ring in Section 3.0 was modified to incorporate diaphragm tension effects. The weight of the ring increases substantially at the short end of the scale (see Figure 5.1). To maintain low cost per unit aperture for large diameter modules, a minimum focal length of 183m (600 feet) was used for design and control response.

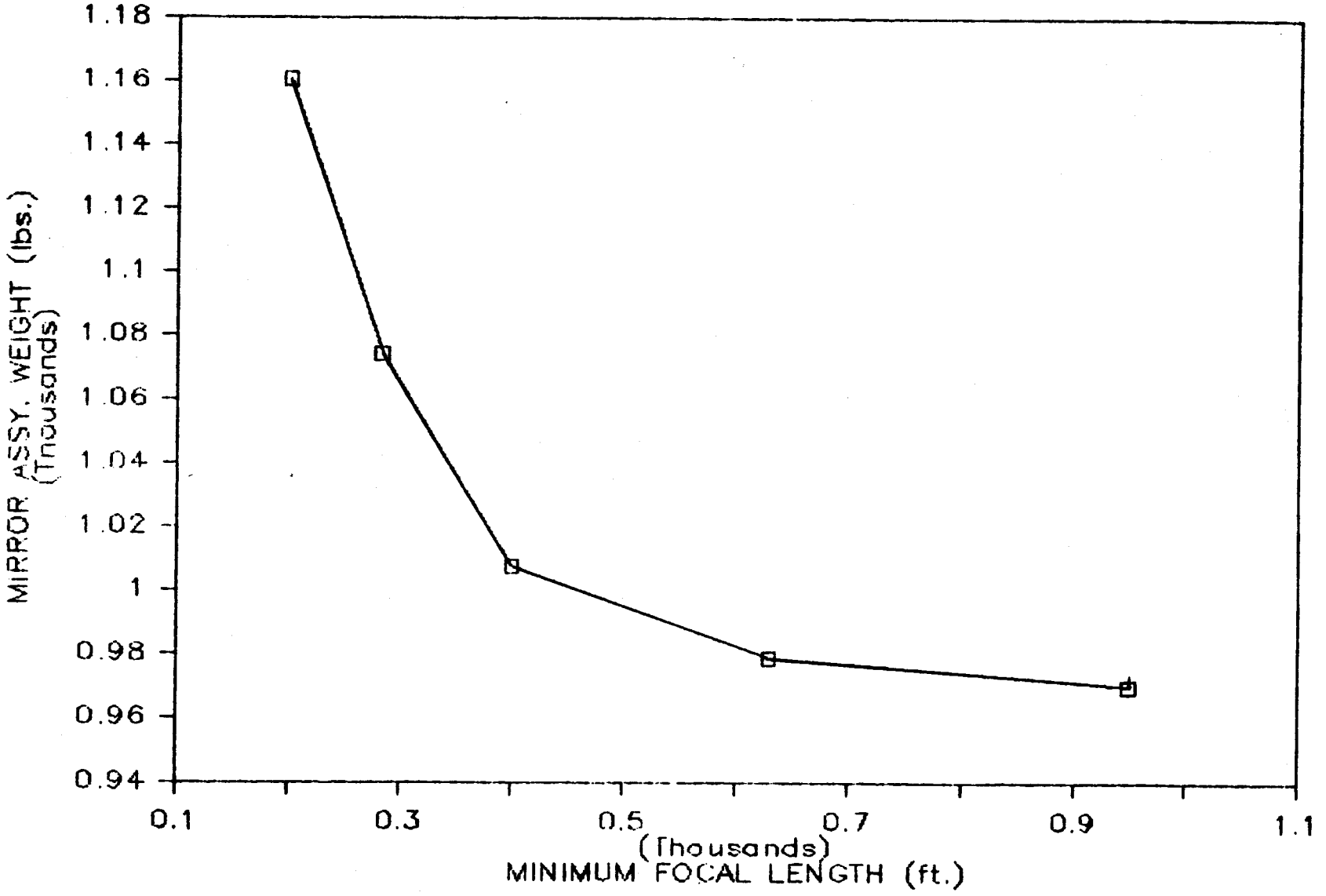

FIG. 5.1 WEIGHT VS. FOCAL LENGTH

SOLAR KINETICS INC.

Because the wind is essentially an oscillating load, the response time was an important consideration in control design. The Kaimal distribution, outlined in Section 2.0, describes the relationship between the variation in dynamic pressure and time. For the operational maximum wind speeds (including gusts), the variation in dynamic pressure was peak near 0.03 Hz though significant energy is available at frequencies higher than this point.

To carefully analyze the response of the heliostat, it is necessary to know the natural frequencies associated with different types of deformation modes. In such a complex structure, it is generally impossible to determine these frequencies and critical dynamic responses by analysis.

During the design phase, several two meter scale models were constructed. One model was taken outside during a very gusty day where the mean wind speed was between 20 and 25 mph. A fan was connected to the unit, and it was focused on a target. The significant variations in the projected image occurred at a frequency of 0.2 to 0.3 Hz.

Dynamic similitude is difficult to establish for scale models; no attempt was made to quantify the results of this test. Some general observations were made, however. First, oscillation frequency of the image is likely to decrease as the diameter of the heliostat increases. The oscillation frequency also appears to be affected by the diameter and length of the flexible control tube attached to the center of the rear membrane.

Based on a peak variation in wind speed occurring at 0.03 Hz for gusts to 27 mph, and an anticipated image oscillation much slower than 0.2 Hz for the large diameter commercial design, the control response time was set to 0.1 Hz. The selection was based upon engineering judgment and limited test results. Further analysis may be necessary based upon experiences gained in prototype testing.

5.2 TRANSDUCER ACCURACY

Three methods of measurement were investigated on a parametric basis: differential pressure, slope, and displacement. Pressures measurement would control focal length by looking at the differential between internal and external pressure. This approach was not investigated in depth due to problems in measuring dynamic pressure. If a single sensor is used, it is subject to micro-effects in wind velocity variations that the membrane does not respond to. Several sensors would be required over the surface of the membrane and this requirement was deemed impossible to implement at low cost. Slope and displacement transducers allow direct measurement of the variables being controlled. They also make use of an averaging effect induced by the large unsupported length of the membrane itself.

Slope measurement devices investigated were primarily limited to inclinometers placed on the front membrane itself. An advantage of this approach was that by carefully selecting the position of the transducers, three inclinometers could provide a good indication of average focal length and provide an absolute position reference for tracking. The required accuracy of such a device is substantial because it must look at very small slopes due to focus imposed upon large changes in slope due to heliostat position. The cost of such transducers was prohibitive.

Displacement and slope measuring transducers not referenced to gravity have to be referenced to some structure of the reflector assembly. The support structure was ruled out due to the large relative motion between the support arms and mirror module. The rear membrane is also not a reference position because in winds the pressure differential across rear and front are not identical or constant. By default, the ring is the only remaining structure.

An investigation into the deformation characteristics of the ring and membrane was performed to identify the best position for attachment. Under a uniform load, ring deformation is maximum halfway between supports and minimum at the supports. The quarter point is the best estimate of membrane position for various ring deflections. Roll is maximum at a support and halfway between supports, though in opposite directions; the roll at the quarter point (15 degrees from a strut placed on 60 degree intervals) is zero. The best estimate of membrane position is obtained along the quarter point.

Our analysis allowed one milliradian of axisymmetric error in the membrane position. Using the analysis developed in [Ref. 9], this error budget translates to approximately 4.8mm (0.19in) of deflection at the center. The resolution of the displacement transducer should be substantially better than the required accuracy of the membrane. For a reasonable and stable control system, we estimated an accuracy of plus or minus 0.5 to 1.0 mm (0.02 to 0.04 in) measured at the center of the reflector assembly would be adequate.

The design requirements also included the ability to be able to achieve any focal length between flat and fully concave. Originally, full concavity was defined as 90m focal length though this requirement was amended to 182m by Solar Kinetics (see 5.1). A focal length of 182m results in a center deflection of 67mm (2.64 in). Therefore, the requirement to measure within 0.5 to 1.0 mm is imposed upon the total measurement range. Accuracy, expressed as a percentage of range, should exceed 0.7 to 1.5 percent.

The response of the control system was defined at 0.1 Hz in an earlier section. Because membrane deflection will vary in response to wind oscillations, and the control system should

respond to the mean of these oscillations, we estimated that measurements should be taken on one second intervals as a minimum. Sensor response should therefore be much faster than one second to provide stable readings.

As membrane deflection was greatest at the center, our initial efforts were devoted to placing a sensor at that point. Bench testing, with a small sensor strung between high tension cables and located at the center, indicated that the oscillations of the sensor were an order of magnitude or more greater than the required measurement accuracy and occurred at frequencies of less than ten Hertz. Efforts at damping the motion, much like a bow string is damped, were unsuccessful.

The membrane deflection is greatest at the center, but not insignificant relatively close to the ring. The relationship for uniform loading is:

$$w(r) = w(o)\ (1-(r/a)^2)$$

where $w(r)$ = deflection of membrane at r
$w(o)$ = deflection of membrane in center
r = radial coordinate measured from center of membrane
a = membrane radius.

Moving the transducer closer to the ring to eliminate sensor hum in suspension systems was considered. If the sensor is placed within one meter of the ring on the seven meter radius design proposed here, the deflection of the membrane to maintain accuracy is reduced by one fourth. In other words, the absolute accuracy required is 0.13 to 0.25 mm (0.005 to 0.010 in). Accuracy expressed as a percent of range does not change because the total measurement length decreases by the same ratio.

There are some additional caveats that should be considered in the selection of transducer position. The load deformation response suggests that there is no measurement error associated with ring roll or sag at the quarter point based upon equal membrane tension, zero manufacturing error, and uniform pressure profiles. Equal membrane tensions are achieved because the tension tube tends to transfer load from one side to another. Manufacturing error is not zero, but can be nullified by calibration after the mirror module is attached to the trusses.

Non-uniform pressure profiles are more difficult to quantify. The non-uniformity is likely to cause additional deflection and roll in the ring. If the sensor is fixed to the ring, the measurement error due to roll increases in direct proportion to the distance from ring to sensor. The measurement error associated with deflection is minimized at the center, though the magnitude of the error diminishes rapidly. For example, if the non-uniform ring deflection at the quarter point is one-half of

the maximum uniform deflection, the measurement error is less than the required sensor accuracy at one meter from the ring. Consequently, for the commercial design, we intend to place a sensor at the quarter point approximately one meter from the ring.

An LVDT was selected for displacement measurement because it provided a significant number of important features. First, the accuracy of the instrument is adequate on both an absolute and percent of range basis. Null repeatability is also excellent in an LVDT. Long life and reliability are provided because there is no mechanical contact between core and coil,. The input and output signals of the transformer are inherently isolated from each other making the sensor an effective analog computing element without the need for buffer amplifiers. Cost for the transducer element, in large quantitities, was minimal.

5.3 PRIME MOVER

The load deformation response of the reflector assembly is characterized based upon the pressure differentials across the membranes. These pressure differentials distend the membrane, and significantly alter the volume of the plenum. In some respects, the focal control system can be more easily explained in terms of volume rather than pressure characteristics.

The response time of the mirror module was defined earlier as 0.1 Hertz, and the Kaimal distribution was used to describe the potential dynamic pressure changes. The leeward side of the heliostat is exposed to a suction. The magnitude of this negative pressure was assumed at sixty percent of the windward dynamic pressure [Ref. 16]. Because the period of wind oscillation that can be addressed is relatively long, the pressure profile from velocity variations was assumed to be fully developed across the surface. The pressure changes required at a mean wind speed of just over 22 mph with gusts to 27 mph varied according to azimuth angle and the direction of the wind. A worst case analysis was performed assuming that the angle was 90°, and calculations for a forward and rearward wind were made. The actual pressure change from mean was relatively small, on the order of 0.003 psi. The volume increase due to rear membrane position change varied according to the initial focal length. The range was relatively small; the volume change was between 65 and 85 cubic feet. If the full ten seconds is allowed for making the adjustment, the control system need provide a pressure change of only 0.003 psi, but the associated volumetric flow rate is 400 to 500 cubic feet per minute (CFM).

The two meter module placed in a 20 mph mean wind described in Section 5.1 did in fact show significant variation in the image size on a periodic basis. We feel that it is necessary to respond to dynamic variations in wind pressure to control surface

error in the reflector assembly. The high volume, low pressure characteristics required for this type of response led us to investigate axial flow fans as the control actuator.

An axial fan delivers flow in direct proportion of its rotational speed. Static pressure increases with the square of revolutions per minute (rpm) and horsepower increases with the cube. Adjustment of the motor rpm in an axial fan system therefore offers flow and static pressure control. Motor speed control is relatively easy and inexpensive to implement.

Fan selection was based upon achieving adequate flow rates and heads for dynamic response and low power requirements to maintain focus against static wind and gravity forces. An eighteen inch diameter propeller fan was finally selected on this basis. A sixteen inch axial fan was very nearly identical in air delivery and power requirements, though operating speeds were higher. If the final fan selection changes from eighteen to sixteen inches, there is little change in power or cost estimates.

The eighteen inch fan response is illustrated in Figures 5.2, 5.3, and 5.4. The 1200 foot focal length and thirty degree azimuth angle were selected to represent a typical rather than worst design case. Maximum dynamic power requirements to achieve the flow rates identified earlier at heads that correspond to maintaining focus in operational wind speeds were virtually the same as for static requirements. The maximum power requirement for the worst combination of orientation and wind was approximately 180W (0.25 horsepower).

5.4 CONVEXITY

A relatively powerful fan was required to maintain focus in severe wind speeds and dynamic oscillations of pressure in the worst orientations. An investigation of the abilities of using the existing pressure control to achieve defocus was accomplished. Several factors were incorporated into our analysis including adjusting flow rate based upon static pressure differentials, in rush through the fan opening due to the delta in internal and rear pressures, time to accelerate the fan in the proper direction, and the limits of deflection imposed by an increase in apparent tension due to diaphragm stretching.

The results are shown in Figures 5.3 and 5.4. The pressure control system optimized for control purposes could not achieve a convex radius of 1200 ft. in five seconds irrespective of wind conditions. It should be noted that substantial convexity can be achieved in short time periods, however. In five seconds, no wind, the heliostat has achieved a convex radius of less than 1700 feet. A 1200 foot convex radius is not reached for six seconds. Under the most severe wind conditions, the heliostat reaches a convex radius of 1700 feet in approximately ten seconds. The 1200 ft. radius is not reached for fourteen seconds.

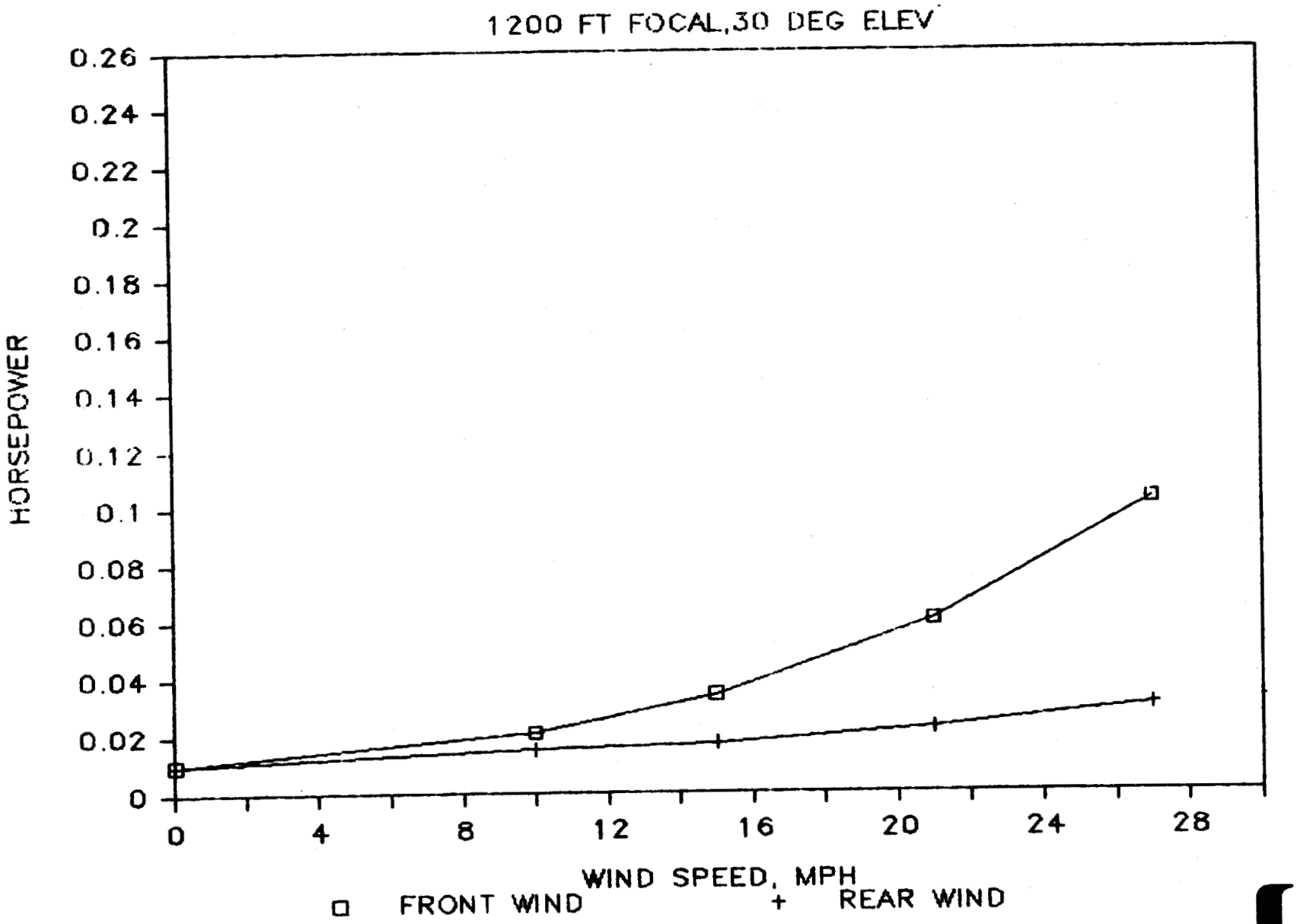

FIG. 5.2 POWER VS. WIND SPEED

SOLAR KINETICS INC.

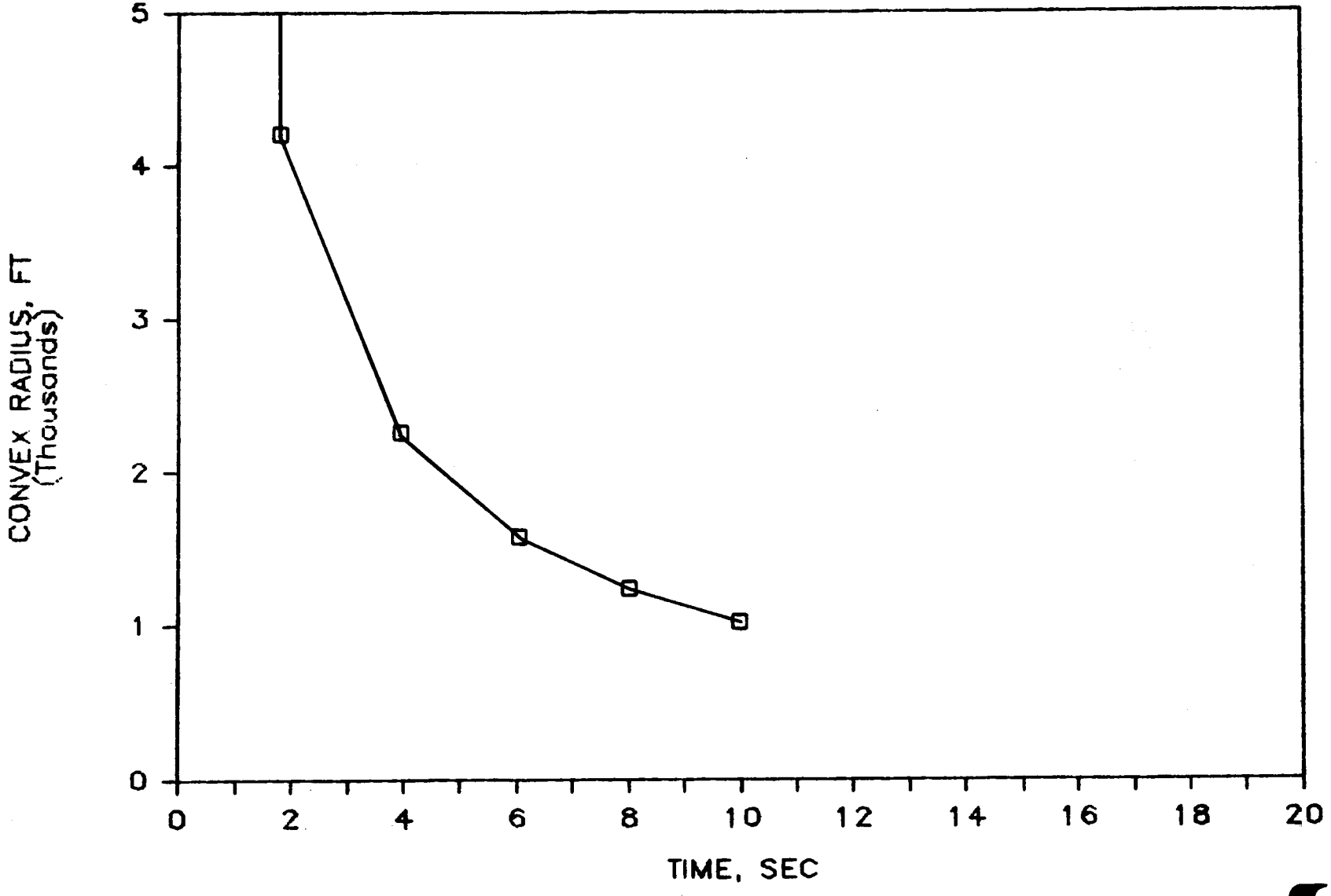

FIG. 5.3 CONVEX RADIUS VS. TIME, NO WIND

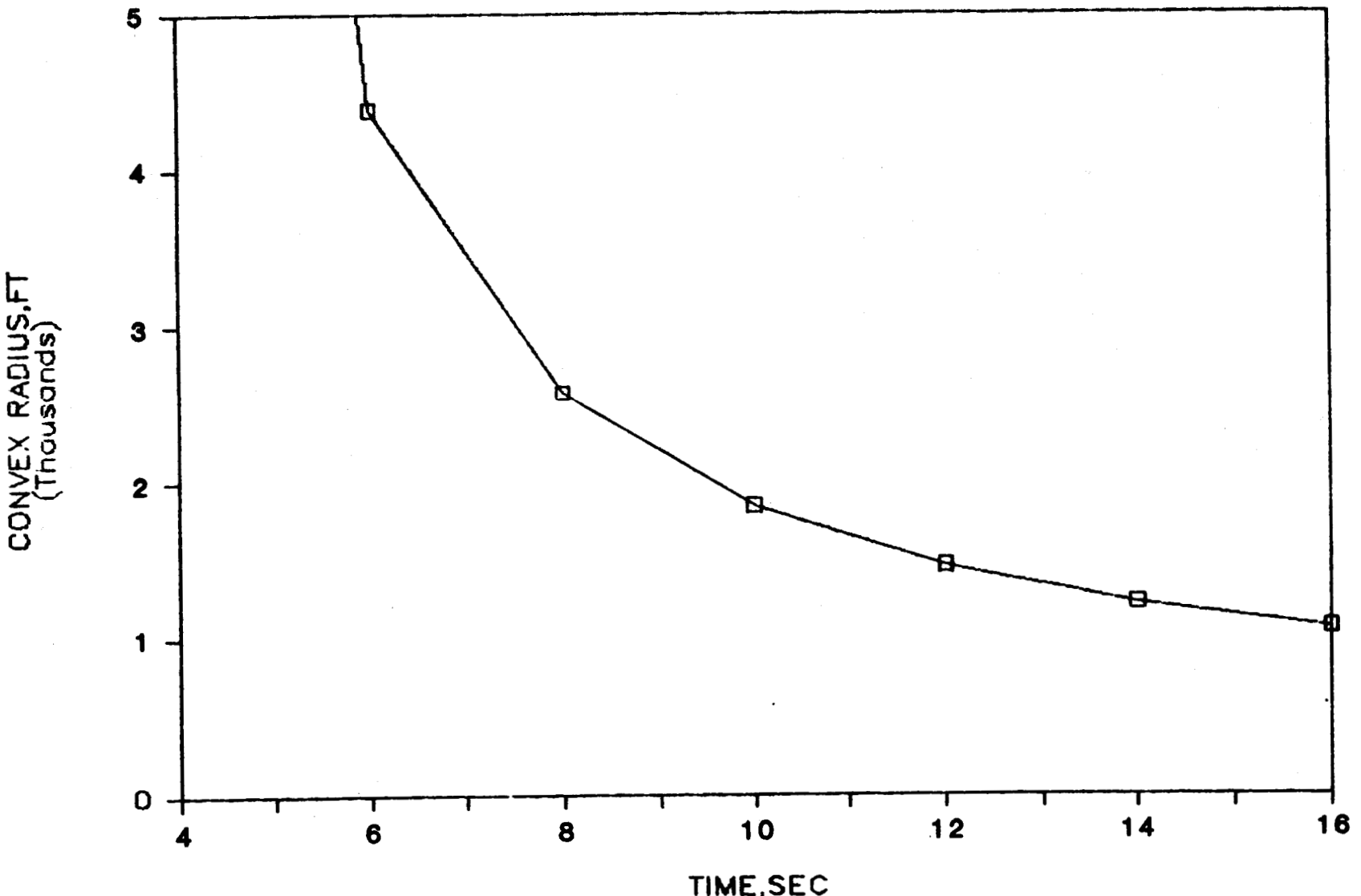

FIG. 5.4 CONVEX RADIUS VS. TIME, 27 MPH WIND

SOLAR KINETICS INC.

Additions to the control system to provide faster convexity were briefly investigated. Increasing the available power was considered. By replacing the quarter horsepower fan with a half horsepower unit, the 1200 foot requirement can be achieved in less then five seconds. The expense of increasing motor size is not limited to the additional motor horsepower but also requires additional field wiring expenses, larger auxiliary power units, and additional parasitic demands due to oversized efficiency problems.

It is not clear that in large fields, a 1700 foot convex radius is inadequate due to the larger slant ranges associated with large heliostat aperture. There is a cubic relationship between diameter and volume, while the aperture increases only with the square. Consequently, the smaller diameter heliostats have no problem with defocus requirements of 1200 ft. radius in five seconds.

Methods for maintaining or instigating convexity on power failure were not thoroughly investigated. The fan is capable, however, of maintaining convexity in a 50 mph wind with power.

5.5 MOUNTING

The optimum point to add and withdraw air from the heliostat was the center of the rear membrane. The drive hub provided a convenient mounting point for the assembly. A flexible tube connects the fan tube with the rear membrane and a diffuser is provided at the end of that tube to avoid direct impingement of the air stream on the membrane. Vanes are provided on each side of the fan tube to straighten flow and therefore reduce fan inefficiencies associated with turbulent and circular flow patterns.

A filter element is provided at the rear of the fan assembly to prevent the introduction of dust and miscellaneous foreign matter to the mirror module. This element has substantial surface area in comparison to fan diameter. Pressure drop is not expected to be a substantial problem due to the large area ratio and extremely high porosity. The element is inherently self-cleaning because the fan is often exhausting air from the mirror module. Filter change intervals should be long, and the element can be removed and replaced very quickly. Figure 5.5 shows the assembly.

5.6 MISCELLANEOUS CONTROL ELEMENTS

Solar Kinetics selected a pulse width modulated (PWM) DC motor to regulate fan speed. This type of system provides electronic commutation to eliminate brushes. Rotational speed feedback can be provided along with communication and speed control in a motor

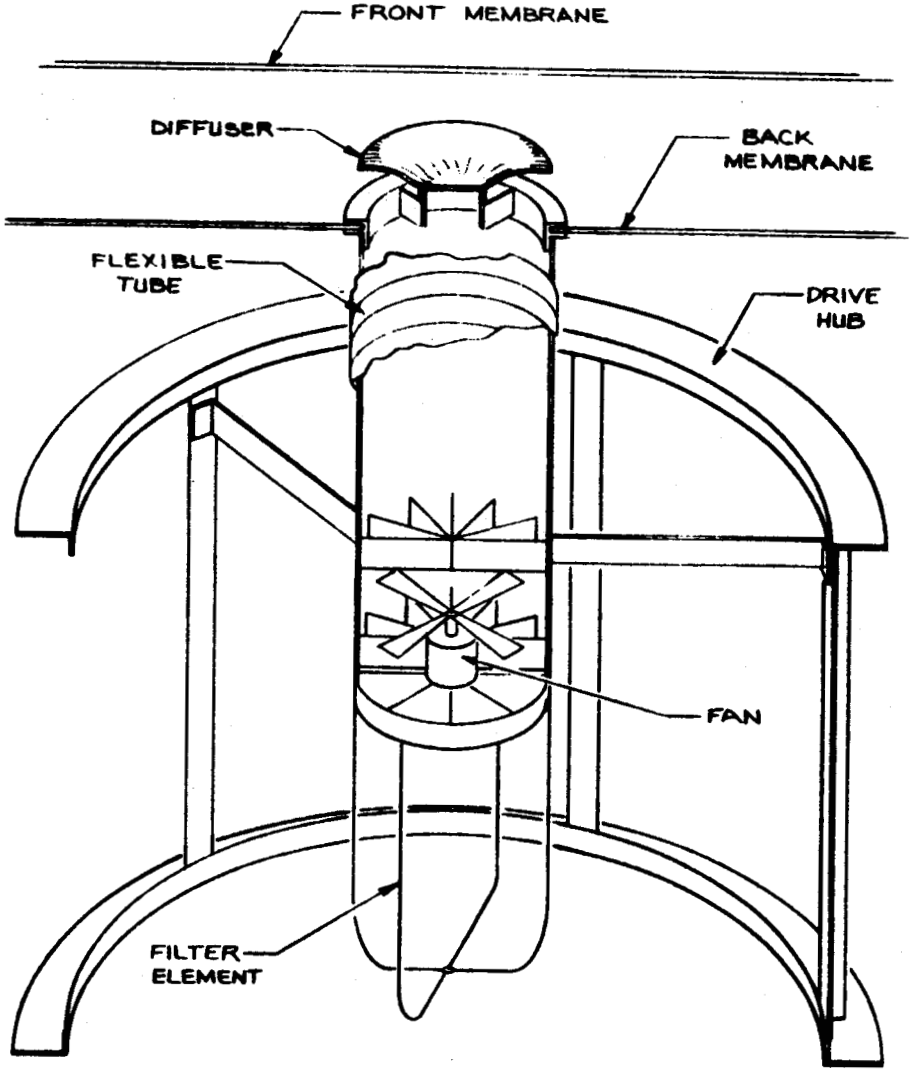

FIG. 5.5 ACTUATOR ASSEMBLY

mounted electronic package that costs less than one hundred dollars (including motor) in large volume. The packaged unit provides speed control based upon analog or digital input; discrete controls for dynamic braking and direction are also provided.

LVDT response must be translated for the microprocessor to read position. Costs for these translator circuits were estimated at fifty dollars for large volume. Some refinement in cost may be possible in this area. The additional processing required for membrane position to speed can likely be handled by the existing microprocessor associated with tracking controls. No additional cost was added for processing capabilities.

The load and consequently deflection of the mirror module is oscillatory. Response to control system changes involves a significant time lag. This situation is classically controlled by proportional/integral logic.

SECTION 6.0

INTRODUCTION

TO MANUFACTURING AND COST

The following sections present the manufacturing process and cost for producing 150m^2 stressed membrane heliostats at a rate of 50,000 per year. This task was completed by Solar Kinetics, Inc. under Phase I of Sandia Laboratories Contract No. 91-8808A. The objective of the contract was the development of the reflector assembly and support structure, and did not include the balance of heliostat (pedestal, drive, heliostat controls, etc.). For this reason, the design and production technique for the BOH is not addressed. Costs for the BOH, however, have been estimated in order to give a complete heliostat cost.

As detailed in this report, the manufacturing of most of the components is done at a central plant. Because of the heliostat size, production of the 46 ft. diameter ring and final assembly of the reflector is done at the site of each heliostat field. Nine simultaneous site operations are used to match the production ability of the central plant.

Reflector assembly and support structure installed costs represent 51% of the complete heliostat cost, or $28.30 per m^2. The heliostat installed cost, including the BOH, is estimated to be $55.26 per m^2. Based upon the same inflation figures quoted throughout this text, we estimated the total cost of a glass to metal heliostat of identical aperture to be $71.19 per square meter of aperture.

SECTION 7.0

CENTRAL MANUFACTURING FACILITY

7.1 INTRODUCTION

A method for manufacturing 50,000 stressed membrane reflector assemblies has been developed and is described in the following sections. This manufacturing scenario includes details of all significant or unique operations at the central manufacturing facility (CMF) along with labor, equipment and floor space requirements. The development was performed in order to identify special tooling and equipment requirements and to provide a means by which a credible estimate of capital and life cycle cost could be made.

7.2 PRODUCTION RATES

The annual production volume, as established by the contract, is 50,000 reflector assemblies. To assess the rate requirements of the CMF, a plant efficiency factor of 85% was chosen. This factor is applied to the ideal production capacity to account for down time, labor inefficiencies, re-work and scrap. As an example, if a process was to produce 50,000 parts per year, it must have the capacity to produce parts at a rate of 58,824 (50,000/.85) per year. This factor is based on SKI's experience and is a reasonable value in industry. At this production volume and efficiency, the CMF must have the capability of producing components for 14.7 reflectors an hour. This translates to 29.4 membranes and 88.2 struts per hour. Production rates are broken down further in Table 7.1. Major items that are not listed in this table are purchased. These include the hinges, some doublers and miscellaneous hardware. Such parts are not cost effective to produce in these volumes.

7.3 DEGREE OF AUTOMATION

In determining the degree of automation of each manufacturing process, it was first assumed that each process would be fully automated. The advantages and disadvantages of using manual labor at each step instead of automated equipment was then considered. Where manual labor proved cost effective, it was incorporated into the process and the automated system was removed. In some cases, semi-automatic processes are employed. Laborers proved most beneficial for tasks that are not repetitious, for complex actions, or as operators of semi-automatic equipment.

TABLE 7.1

PRODUCTION RATES
Based on 50,000 Reflector Assemblies Per Year

COMPONENT	QUANTITY		PRODUCTION RATE		MINUTES PER UNIT PRODUCED**
	Per Mirror Module	Per Year	Per Day*	Per Hour**	
Membrane	2	100,000	400	29	2.0
Truss	6	300,000	1200	88	0.7
Hub	1	50,000	200	15	4.1
Tensioning Tube	2	100,000	400	29	2.0
Hinge	6	300,000	1200	88	0.7
Control Assy.	1	50,000	200	15	4.1
Strut Straps	24	1,200,000	4800	353	0.2

* Based on 250 Days Per Year

** Based on 250 Days Per Year
16 Hours Per Day and
85% Plant Efficiency

7.4 PRODUCTION DESCRIPTION

The CMF production process for each of the major components is described in the following text. A summary of all processes is presented in Figure 7.1.

7.4.1 MEMBRANE PRODUCTION

The membranes are made from ten (10) .010" thick aluminum sheets joined by resistance seam welded lap joints. The sheets are constructed in a continuous, linear coil line as shown in Figure 7.2. Four coil lines run in parallel; two producing laminated front membranes and two producing unlaminated rear membranes.

The first two processes in the coil line are leveling and cleaning. The cleaning removes dirt, oil and oxide to provide a good surface for reflector adhesion and welding.

The next process is lamination of the reflective film on the aluminum sheets. This process is complicated by the fact that a resistance weld cannot be made through reflective film. By using reflective film that is slightly narrower than the aluminum sheets, the edges of the aluminum are left bare for welding. The ends of each sheet must also be left bare for welding to the ring. This is done by first laying a none adhesive disposable template on the sheet where no film is desired. The film is then applied to the sheet and template. Numerically controlled knives then shear the film along the edge of the template, and the template, with the unwanted film, is removed.

The edges of the film are sealed against corrosion by a coat of acrylic. Two of the acrylic spray heads are stationary and one is numerically controlled to follow the curved edge of the film.

Laser shears cut the sheets with a seven meter radius to final shape. Drop (aluminum waste) is limited to approximately 4% by this process. Coil speed for each line averages 47 feet per minute (fpm).

The sheets from this process are transferred to one of two electric resistance seam welders (see Figure 7.3). Each welder has six rolling electrodes on a translating bridge. The welding current is passed from the rolling electrodes through the aluminum sheets into a flat copper bar which is actively cooled. When fouled, the upper electrodes are replaced with dressed electrodes. When the copper bar is fouled, it is indexed laterally to provide a clean surface along the line of the weld.

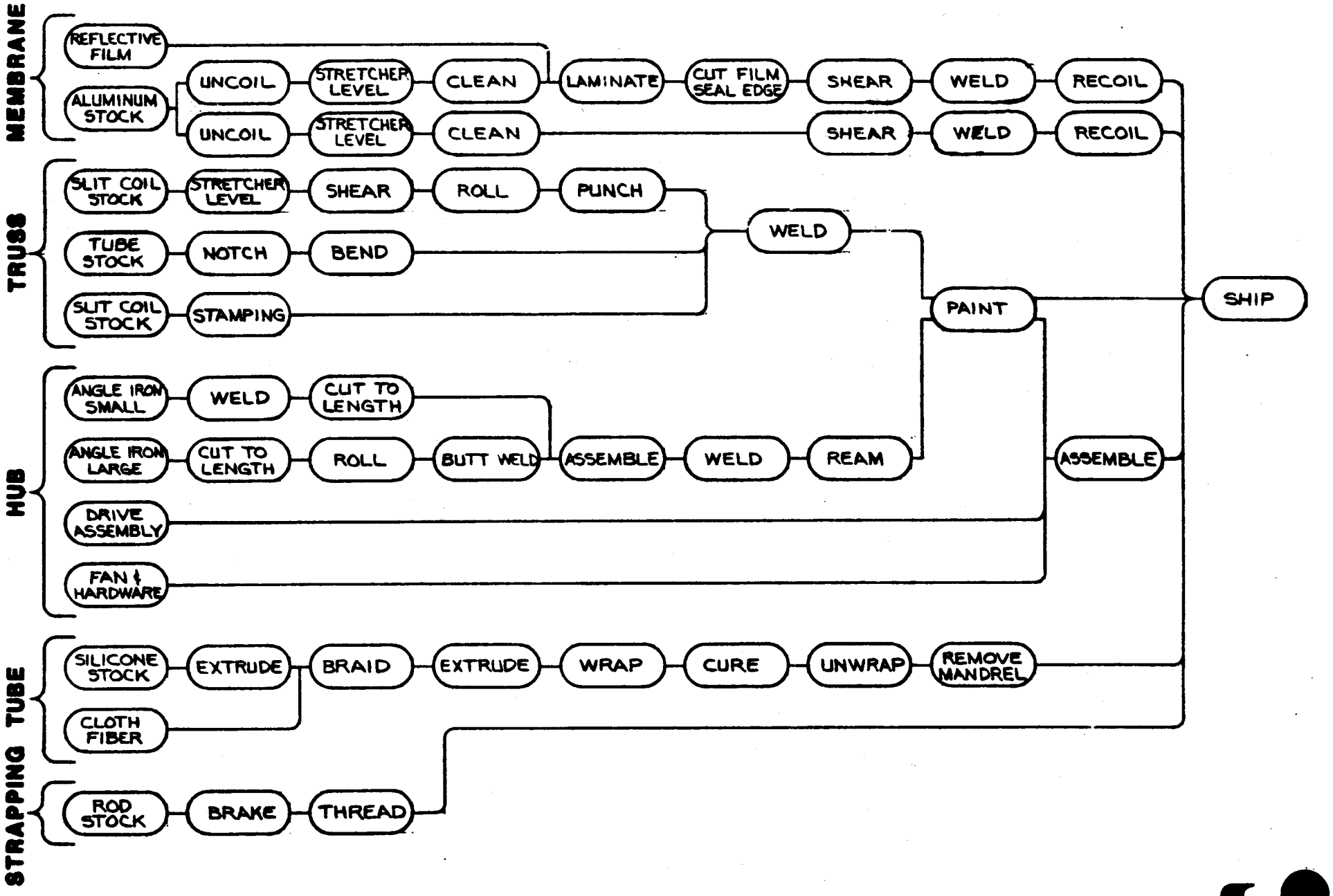

FIG. 7.1 CMF PRODUCTION FLOW

SOLAR KINETICS INC.

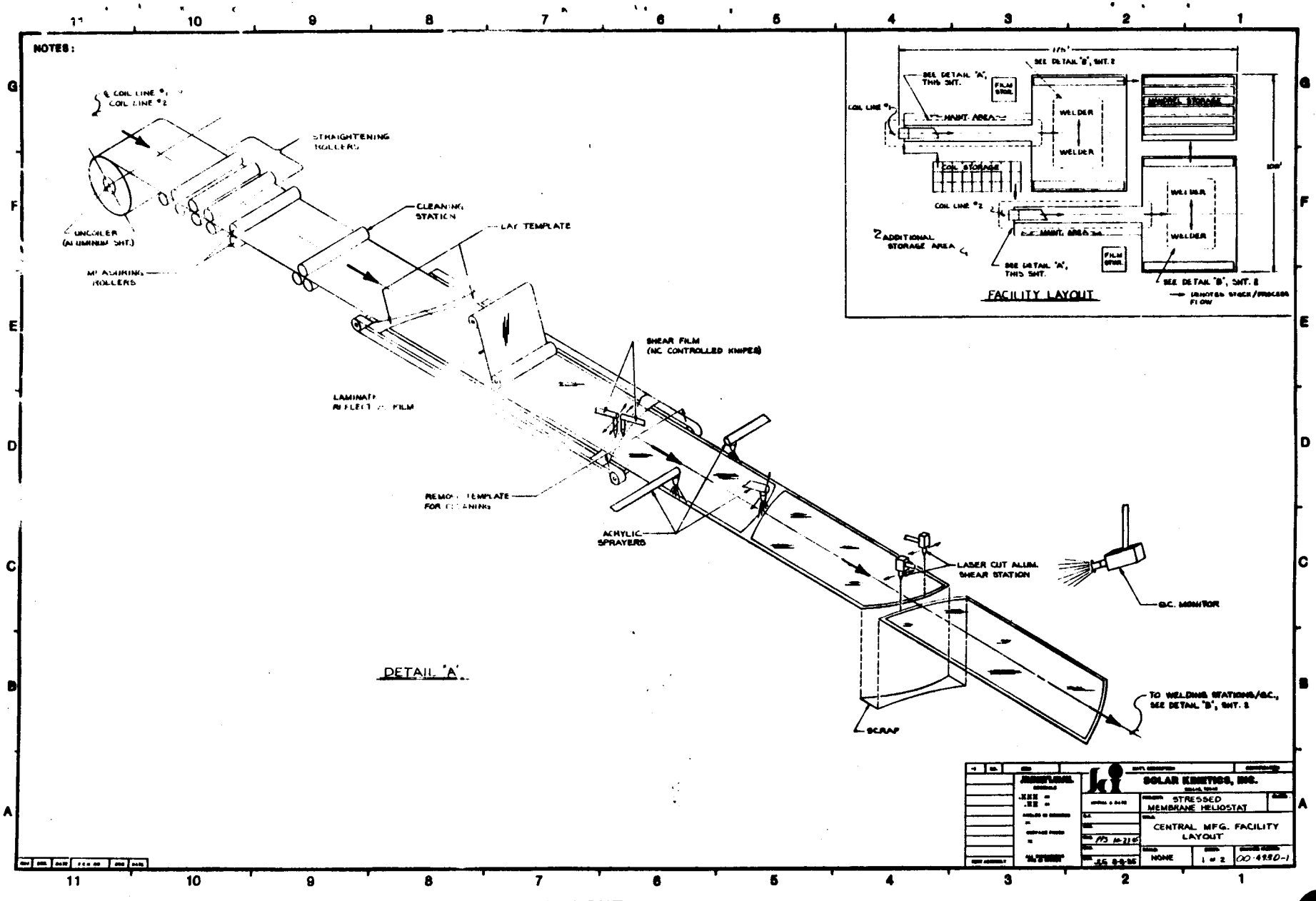

FIG. 7.2 MEMBRANE FABRICATION - COIL LINE

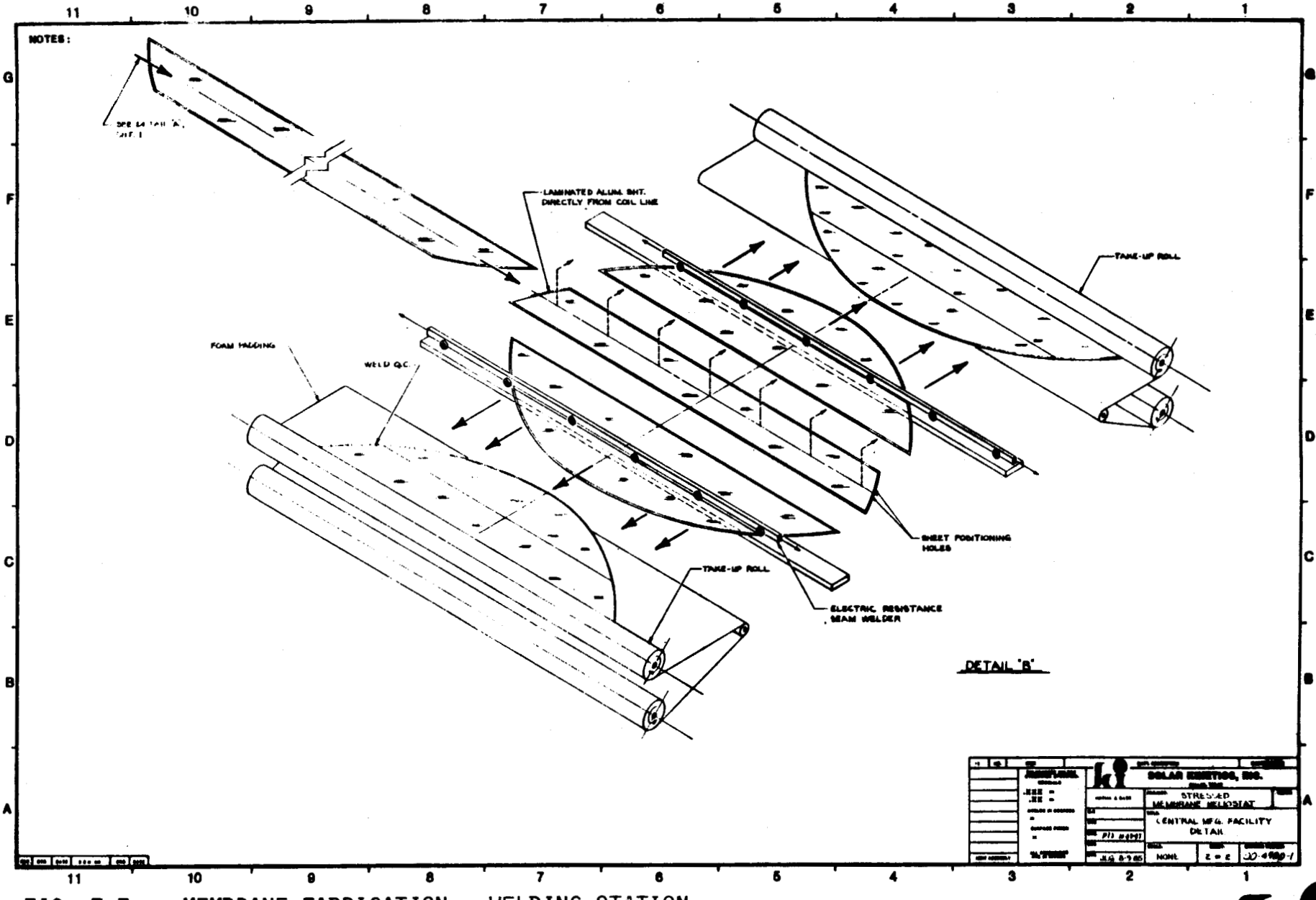

FIG. 7.3 MEMBRANE FABRICATION - WELDING STATION

SOLAR KINETICS INC.

When the bar becomes completely fouled (at the end of the day), it is removed and milled clean by the maintenance crew. In this way, tip dressing has little impact on production. Welding speed per machine is 32 seconds per seam. This allows 30 seconds for transfer and 58 seconds for accurate positioning of each sheet.

The assembled membranes are rolled onto a mandrel for transportation to the site. Based on trucking weight limits, 145 rear membranes are carried per roll, and 120 front membranes are carried per roll. Because the seams of the membrane are lapped, they are twice as thick as the rest of the membrane. When the membranes are rolled over each other on the mandrel, this extra height would damage the membrane directly above and below it if no precaution was taken. A layer of foam is rolled between each membrane layer to prevent this "print through" effect.

The mandrel used to feed the foam is also used as the membrane take-up roll after it has been emptied. The same mandrels that are used to ship the membranes to the sites are also used to return the foam to the CMF.

The membrane rolls are filled once every 40 manufacturing hours at each welding station. When full, they are transferred to an adjacent storage area by an overhead crane to await shipping.

7.4.2 TRUSS PRODUCTION

The trusses are made from roll-formed primary members separated by bent square tube secondary members. Two identical and parallel process lines are used for truss manufacture.

The truss flanges are produced from slit (in-house slitting), pre-coated, carbon steel stock (see Figure 7.4). The coiled stock is leveled, cleaned and sheared to length. Each piece of stock is rolled into a double hat section and transferred to a punching station where all mounting holes and miscellaneous notches are accurately punched. The coil speed for this process is 41 fpm.

The webbing is made from purchased, galvanized square tubing. The zig-zag pattern of the webbing is made by bending the tube at several points. The tubing is notched through three walls at the point of the bend. In this way, only one wall of the tube is

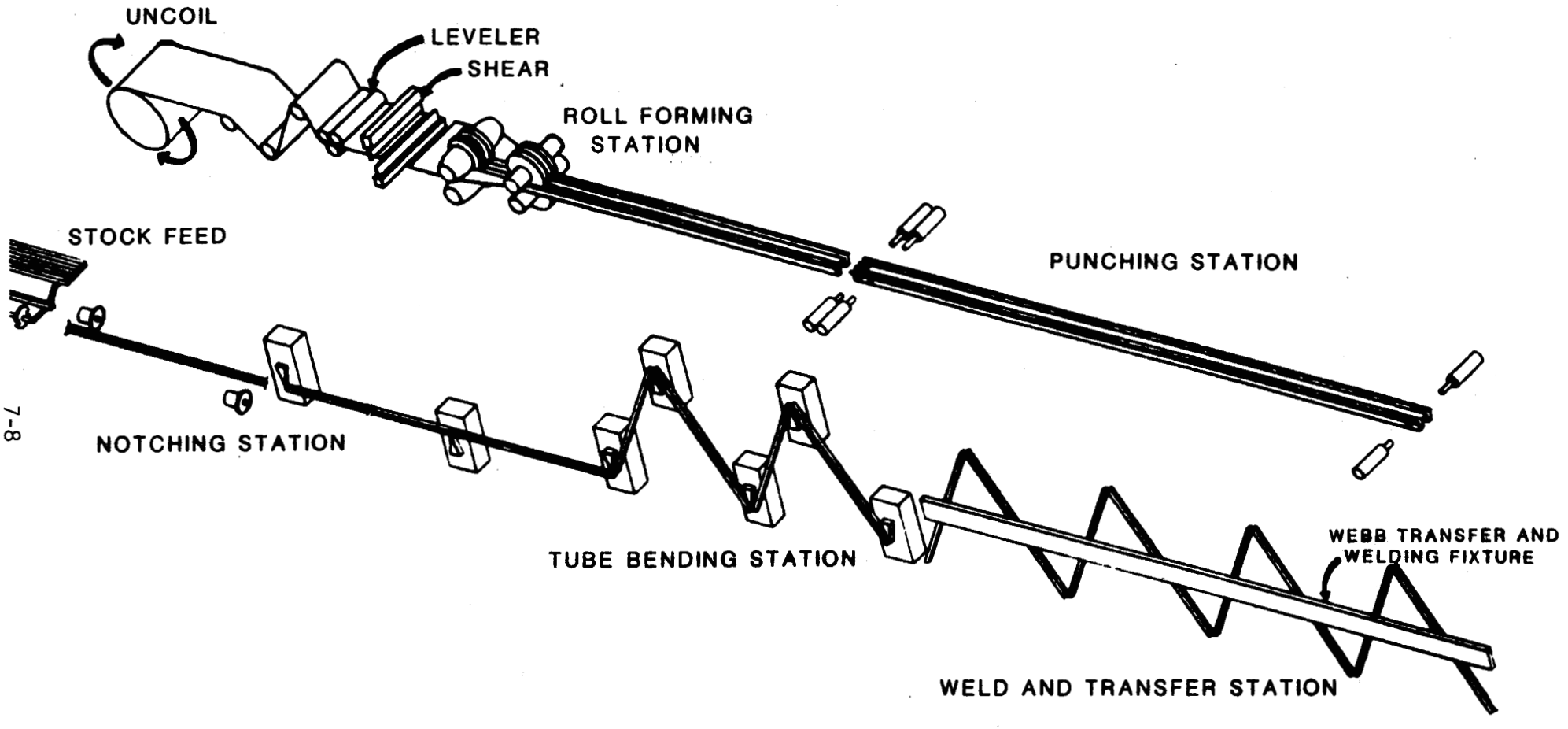

FIG. 7.4 TRUSS FABRICATION - COIL LINE

bent and the cross section remains undistorted. Figure 7.4 shows that the notching is done with an indexing band saw and the tubing is bent with a set of moving fulcrums. Because of the notches, the bending force required is very low and the fulcrums serve primarily as guides for the process.

The tube has little rigidity of its own and is supported by a fixture that attaches to the midpoint of each section. This fixture allows transfer of the part to the assembly area, positions, and holds the part during assembly.

Critical positioning of the strut is provided by the punched holes in the flanges. After positioning, a gang spot welder joins all the parts. Doublers are then positioned and welded by another gang welder (Figure 7.5).

Positioning and welding of each assembly is completed in 84 seconds and the part is transferred to the paint line.

7.4.3. HUB PRODUCTION

There are four types of parts that comprise the hub: the rings (two each), the bracing (12 each), the drive and assembly brackets (six each), and the truss brackets (12 each). These four parts are manufactured separately and assembled in an automated welding process.

The rings are made from hot rolled structural steel angle. The angle is purchased in straight lengths, and is cut to the required length in large quantities by an auto-indexing band saw. Each piece is then fed through an angle roll to produce the circular shape. Butt welding of the joint is performed manually with a mig welder.

The bracing is constructed from two structural steel angles welded back-to-back to form a tee cross section. The angle is purchased in standard 40 foot lengths and welded into a tee shape with an automatically controlled mig head. These tee sections are cut to size in bulk by the same auto-indexing band saw used for the rings. The bracing is then transferred to the hub assembly area.

The drive and assembly brackets are best made as stampings. The size of the stampings, however, requires a large tonnage press and it is not cost effective to have in-plant equipment for these production volumes. Consequently, these stampings will be purchased.

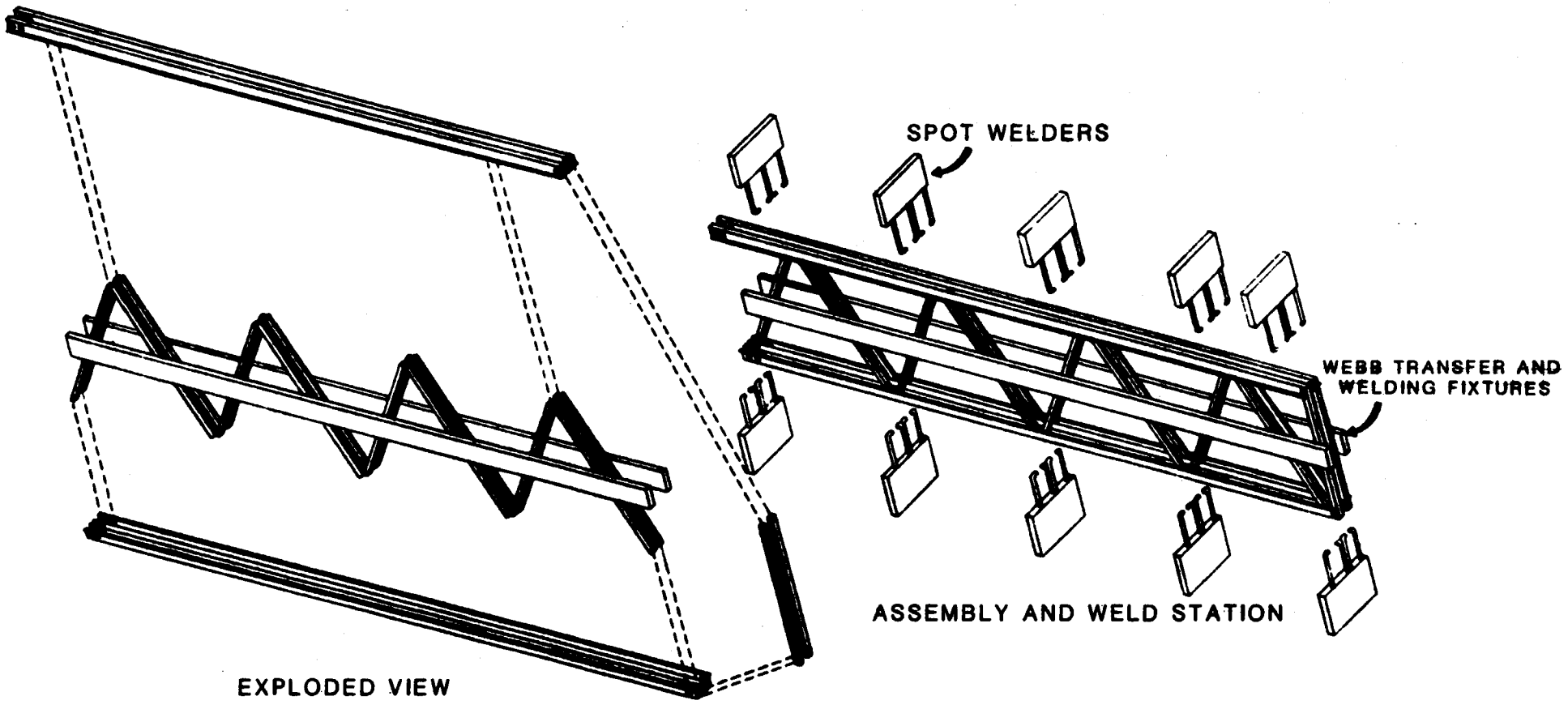

FIG. 7.5 TRUSS FABRICATION - WELD STATION

The truss attachment brackets are considerably thinner than the drive brackets and are needed in twice the quantity. Equipment for stamping these parts is cost effective. The brackets are made from slit (in-house slitting) carbon steel coil stock. The coiled stock is fed into a two stage auto-indexing press. The first stage punches holes and cuts the perimeter, the second stage brakes the edges. The stamping speed is 16 seconds per part.

Assembly of the components of the hub is divided into four stations. At the first station, one laborer mounts the two rings, the strut brackets and the six vertical braces in an assembly fixture. Locating is accomplished by fixing the strut brackets through mounting holes. In this way, the strut mounting holes are accurately positioned in relation to each other. Misalignment due to weld shrinkage is nullified by reaming these holes after final welding.

This fixture is transferred to the second station where two robot welders weld the unit together.

The weldment and fixture is conveyed to the third station and the diagonal braces, drive, and mounting brackets are manually positioned for welding.

Welding is done by a single robot welder at the fourth station.

The fifth station drills holes in the uprights and accurately reams all remaining holes.

The hub is transferred to the paint line and the fixture is returned to station one. Each station completes its operation in 4.1 minutes.

The floor space layout of the hub production area is shown in Figure 7.6. The total area required is 6,600 square feet.

7.4.4 TUBING

The tension tube is cost effective to produce captively because of the high volume required (1.4 million feet per year). A layer of the rubber material is extruded onto a 140 foot flexible mandrel. Four carrier braiders then simultaneously lay the reinforcing material on the tube followed by another layer of rubber. The tube is compressed with a temporary layer of cloth and is fed through an autoclave for cure. After cure, the temporary cloth and mandrel are removed. Two identical lines are employed to meet the production requirements.

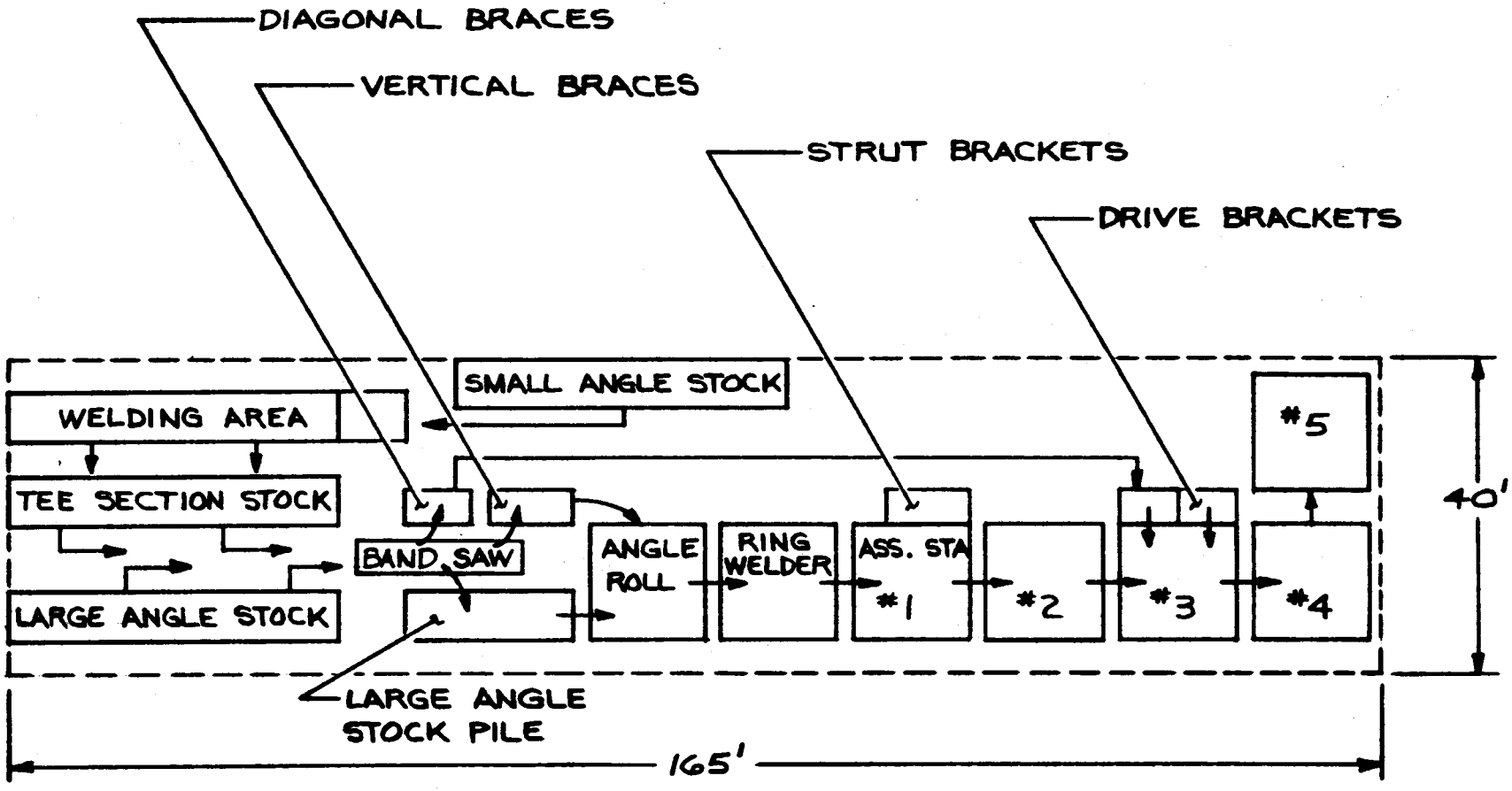

FIG. 7.6 HUB PRODUCTION

7.4.5 STRAPPING

Strapping is made from galvanized, carbon steel rod that is purchased in the desired length. CMF processing is restricted to threading and braking. The strapping is crated for shipping.

7.4.6 CONTROLS

Manufacturing work at the CMF on the focus controls is limited to stamping the assorted metal components and mounting the fan assembly.

The stamped parts include the LVDT mounting bracket, the access hole collar, and plug. These parts are made from aluminum coil stock and are shipped unassembled.

The fan assembly (purchased with fan, housing, and filter) is mounted after the hub exits the paint line. This unit is also fitted with the tracking drive assembly for shipping.

7.4.7 SLITTING

Coil stock for the strut flanges and the strut-to-hub brackets and spacers are slit in-house. This process slits the original stock into the desired width and recoils for use in the strut, controls, and hub production areas. Slitting speed is 80 feet per minute.

7.5 PLANT DESCRIPTION

The CMF is a high bay sheet metal building with an adjacent single story office facility. The high bay area (Figure 7.7) is 325 by 375 feet. The floor space requirements are broken down in Table 7.2. Total manufacturing floor space is 74,900 square feet, and total enclosed floor space is 142,000 square feet.

7.6 LABOR

Production at the CMF will proceed through two eight hour shifts. Two shifts are used to reduce the equipment and floor space required thereby reducing capital costs. The disadvantage of paying second shift premiums are negligible by comparison. Production does not occur during the third shift so that the equipment can be serviced.

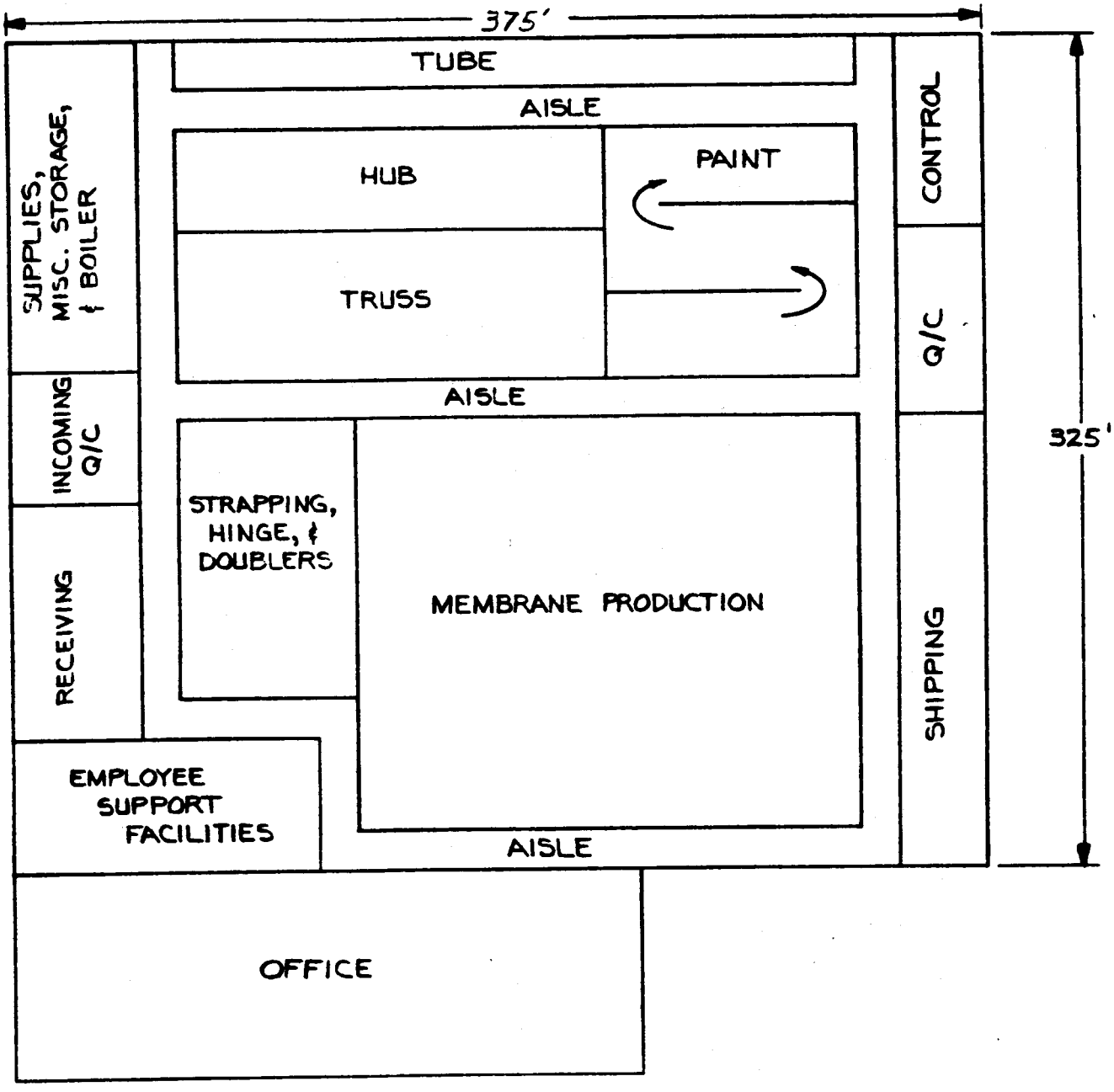

FIG. 7.7 CMF LAYOUT

TABLE 7.2

CMF SPACE ALLOCATIONS

COMPONENTS	FLOOR SPACE (ft^2)
Reflective Assembly	
Membrane	34,000
Inflatable Tube	5,400
Focus Controls	2,500
Support Structure	
Truss	9,000
Hub	6,600
Paint	10,000
Misc. Hardware	7,500
* Mfg Floor Space	75,000
Total Enclosed Floor Space	142,000

* Aisle Space Excluded

The total number of employees required at the CMF is 204 (see Table 7.3). There are 114 direct laborers required and 118 indirect laborers. Indirect laborers include janitors, supervisors, clerical workers and all other employees who do not directly participate in hardware production. The indirect labor is based on an estimate of 35 workers required for shipping, receiving, maintenance, and quality control, plus 75% of the direct labor for other tasks.

7.7 EQUIPMENT REQUIREMENTS

The necessary CMF production equipment is itemized in Table 7.4. Equipment cost is detailed in the cost section of this report.

TABLE 7.3

CMF LABOR REQUIREMENTS

	Number of Employees
Reflector Assembly	
Membrane	12
Tube	2
Controls	8
Support Structure	
Truss	9
Hub	11
Straps	1
Paint	10
Slitting	2
Stampings	2
Direct Laborers per Shift	57
Total Direct Laborers	114
Total Indirect Laborers	90
Total Number of Employees	204

TABLE 7.4

CMF EQUIPMENT LIST

DESCRIPTION	QUANTITY REQ'D.
Membrane Production Equipment	
Upender	4
Uncoiler	4
Levelers	4
Cleaners	4
Template System	2
Laminators	2
Film Shears	2
Laser Shears	4
Acrylic Sealers	2
Feed Systems	4
Positioners	4
Vacuum Chucks	4
Film Q.C.	2
Welder	4
Positioners	4
Q.C. Weld	40
Recoiler	8
Mandrel	68
Miscellaneous	Lot
Truss Equipment	
Web Feed System	2
Web Notcher	2
Web Bender	2
Web Transfer Fixture	8
Flange Uncoiler	2
Flange Leveler	2
Flange Roll Former	2
Flange Punch	2
Assembly Fixture	2
Gang Welder	2
Transfer Equipment	Lot

TABLE 7.4 (Con't.)

DESCRIPTION	QUANTITY REQ'D.
Hub Equipment	
Tee Section Welder	1
Band Saw	1
Roll Former	1
Mig Welder	1
Assembly Fixture	8
Robot Mig Welder	3
Multi-Head Reamer	1
Transfer Equipment	Lot
Tube Equipment	
Extruder	2
Braiders	8
Wrapper	2
Autoclave	1
Transfer Equipment	Lot
Recoilers	2
Boiler	1
General Plant Equipment	
Paint Line	Lot
Fork Lifts	8
Compressors	4
O.H. Crane	1
Leasehold Imp	Lot
Stamping Ram & Dies	2

SECTION 8.0

TRANSPORTATION

Materials are shipped from the CMF to the site on standard open flat bed trailers. Average trip distance, and the assumptions concerning the transportation equipment, are taken from Reference 19. These assumptions are summarized below for the readers' convenience:

- Average Round Trip Distance of 533 Miles
- Standard Open Flat Bed Trailers
- Maximum Load of 45,000 Pounds
- Volume of 96" Wide by 108" High and 600" Long
- Tractor Life of 600,000 Miles

Transportation has been considered for only the reflective assembly. The balance of heliostat (such as pedestals) has not been addressed. Transportation costs are included in the cost presentations for BOH components.

8.1 TRAILER LOADING

The major components to be transported are as follows:

Ring Coil Stock

Membranes

Hub/Drive Assembly

Trusses

Truss Strapping

The major components will be sent on trailers dedicated to and appropriately fitted for a particular component.

The ring coil stock will be sent on pallets from the coil stock supplier. The trailer would be weight limited.

Membranes are sent to the site on large trailer mounted mandrels. Foam lining is rolled with the membranes to prevent damage in shipping. One hundred forty five rear membranes or 120 front membranes can be rolled on a single mandrel.

The hub, drive and fan are assembled at the CMF. Special racks will allow sixteen of these assemblies to be placed on each trailer. Elevation tubes are shipped on the same trailer, but are not connected until after the reflective assembly is on the pedestal.

Trusses are shipped in a stacking position of sixteen abreast by two long by two high. This permits sixty-four trusses to be shipped in each load.

Truss strapping is bundled before shipping. Loads will be weight limited.

A summary of the shipping requirements is listed in Table 8.1. The analysis shows that 0.1854 truckloads are required per reflective assembly.

At a production level of 50,000 units/year, the CMF would dispatch 37 trucks per day to the installation sites. The average round trip per driver would be 2 days; a fleet of 74 tractors would be required. The number of trailers required is as follows:

Available for loading and storing finished goods at the factory:	74
Enroute:	74
Unloading and buffer stock at the site:	109
Total trailers required:	257

Customized racks and tie-downs would be fitted on the trailers to reduce the need for crating.

TABLE 8.1

TRANSPORTATION (MAJOR COMPONENTS)

COMPONENT	QUANTITY PER TRUCK	WEIGHT PER UNIT (lbs.)	WEIGHT PER TRUCKLOAD	TRUCKLOADS PER HELIOSTAT	TRUCKLOADS PER DAY (200 HELIOSTATS)
Coil Stock	-	-	45,000	.0100	2.000
Membranes					
Rear	145	240	45,000	.0069	1.379
Front	120	300	45,000	.0083	1.667
Hub/Drive Assembly	16	2700	43,200	.0625	12.500
Trusses	64	214	13,696	.0940	18.750
Strapping	6429	7	45,000	.0037	.747
				.1854	37.043

SECTION 9.0

SITE MANUFACTURING FACILITY

The site manufacturing facility (SMF) provides for fabrication and final assembly. Site assembly is required because of the size of the mirror module (46 ft in diameter). Generally, items that can be made at the CMF are shipped in because of higher CMF efficiencies and the low quantity produced (3000 heliostats) per site. Site tasks are limited and procedures kept simple so that local labor can be used. Machinery is built simply and ruggedly to allow quick setup and tear down.

9.1 SITE SCHEDULES

Three thousand heliostats are required at each site for a 50 MWe field. With a single shift work crew and a production line capability of 27 heliostats per day, nine sites must be operated concurrently to achieve a 50,000 heliostat per year production rate. Each of these facilities will be at a location for approximately 26 weeks. Three weeks of this time will be spent dismantling, moving, and setting up the SMF.

The assembly line is based on a 14 minute work cycle at each station and a 0.79 productivity factor; therefore, work advances to the next station on approximately 18 minute intervals.

Pedestal placement and field wiring will be performed by a separate crew prior to the reflector assembley installation. No inside storage will be provided, as the pedestals need no protection, and the wiring components can be stored inside their shipping trailers.

Construction trades and assembly labor will be obtained locally for each site. A permanent crew will be dedicated to the setup, dismantling, and supervision of all nine site facilities.

9.2 PRODUCTION AREAS AND PLANT LAYOUT

The combined floor space necessary to construct the reflective assemblies is 20,200 sq. ft. The SMF building consists of a metal structure on a concrete slab foundation. Equipment used to move reflective assembly components are floor-mounted. All work on the reflective assembly is done in the horizontal plane, so that the building requires no special bracing or more than

eighteen feet of clearance. The building is designed for rapid dismantling and reuse at subsequent sites. To increase durability, the metal siding is of heavier gauge than conventional construction. The site office is housed in a portable building.

Components of the reflective assemblies are unloaded directly from trucks to their respective work stations. Warehouse space is not required. After the contents of a trailer have been exhausted, the empty trailer is returned to the CMF.

The SMF work in constructing the reflective assembly is divided into four areas. This facility, in Figure 9.1, provides areas for ring fabrication, membrane attachment, hub preparation, and final assembly. The tasks accomplished at each station are shown in Table 9.1.

The first work station manufactures the ring of the mirror module. At the second station, the membranes are attached to the ring and tensioned. The hub/drive assembly is unloaded and placed in a fixtured cart at the third work station. At the fourth work station, the support structure is built, and the mirror module is connected to the trusses.

Figure 9.2 and 9.3 depict the assembly line flow. The processes at each work station are described in the following paragraphs.

9.3 SITE PRODUCTION DESCRIPTION

9.3.1 WORK STATION #1 - RING FABRICATION

The ring is manufactured at the site from coil stock. The necessary equipment (uncoilers, levelers, roll formers, pyramid rollers, welders, tube reelers and cut-off saw) is skid mounted (Figure 9.3). An operator controls the manufacturing sequence of the line.

Two parallel coils of aluminum are uncoiled and leveled. The stock is run through roll formers to shape two channels of appropriate dimensions. A set of parallel pyramid rollers bend the channels to a radius of 7 meters. The pyramid rollers are controlled to eliminate twisting of the channels. A welding unit joins the edges of the two channels to form a closed cross section. The aluminum is captured by the first of a series of guide rollers. These guide rollers are spaced around the circumference of the circle to insure circular trueness and accurate placement of the doublers. At the end of the first revolution, the aluminum is severed by a skid-mounted cut-off saw.

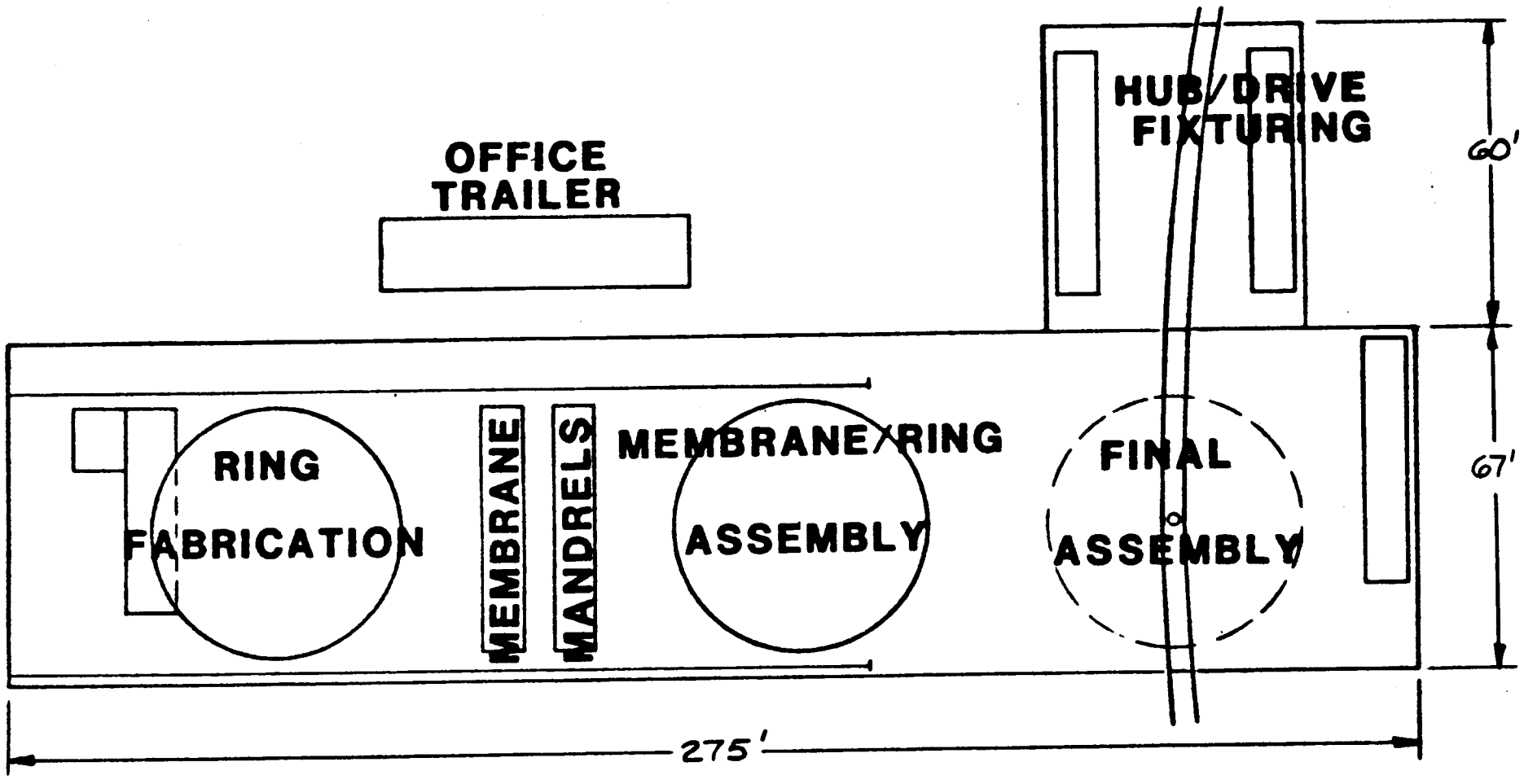

FIG. 9.1 SMF LAYOUT

SOLAR KINETICS INC.

TABLE 9.1

WORK STATION	TASKS PERFORMED	COMPONENTS USED
#1, Ring Assembly	Ring Rolled Strut Doubler Attached LVDT Installed Tube Placed	Coil Stock Doublers LVDT Assembly Tube
#2, Membrane/Ring Assembly	Rear Membrane Hole Reinforced Membranes Attached Tubes Inflated & Membranes Crimped	Reinforcing Flanges Membranes
#3, Hub/Drive Fixturing	Drive Hub Placed in Fixtured Cart	Drive Hub Fan & Fan Controls
#4, Final Assembly	Support Struts Attached to Hub Strapping Connected Mirror Module Attached Fan Shroud Attached Controls Connected	Struts Strapping

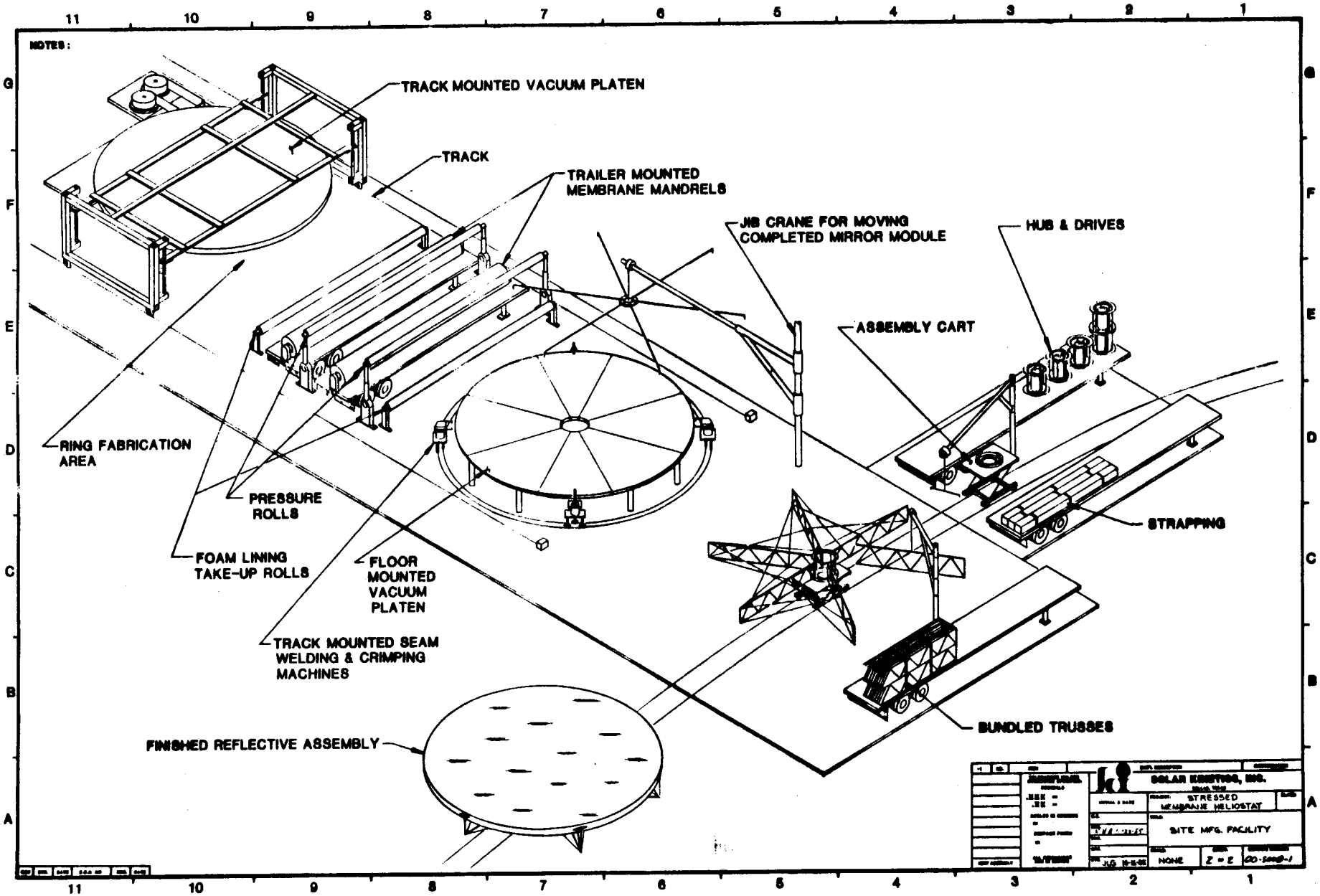

FIG. 9.2 SITE MANUFACTURING FACILITY

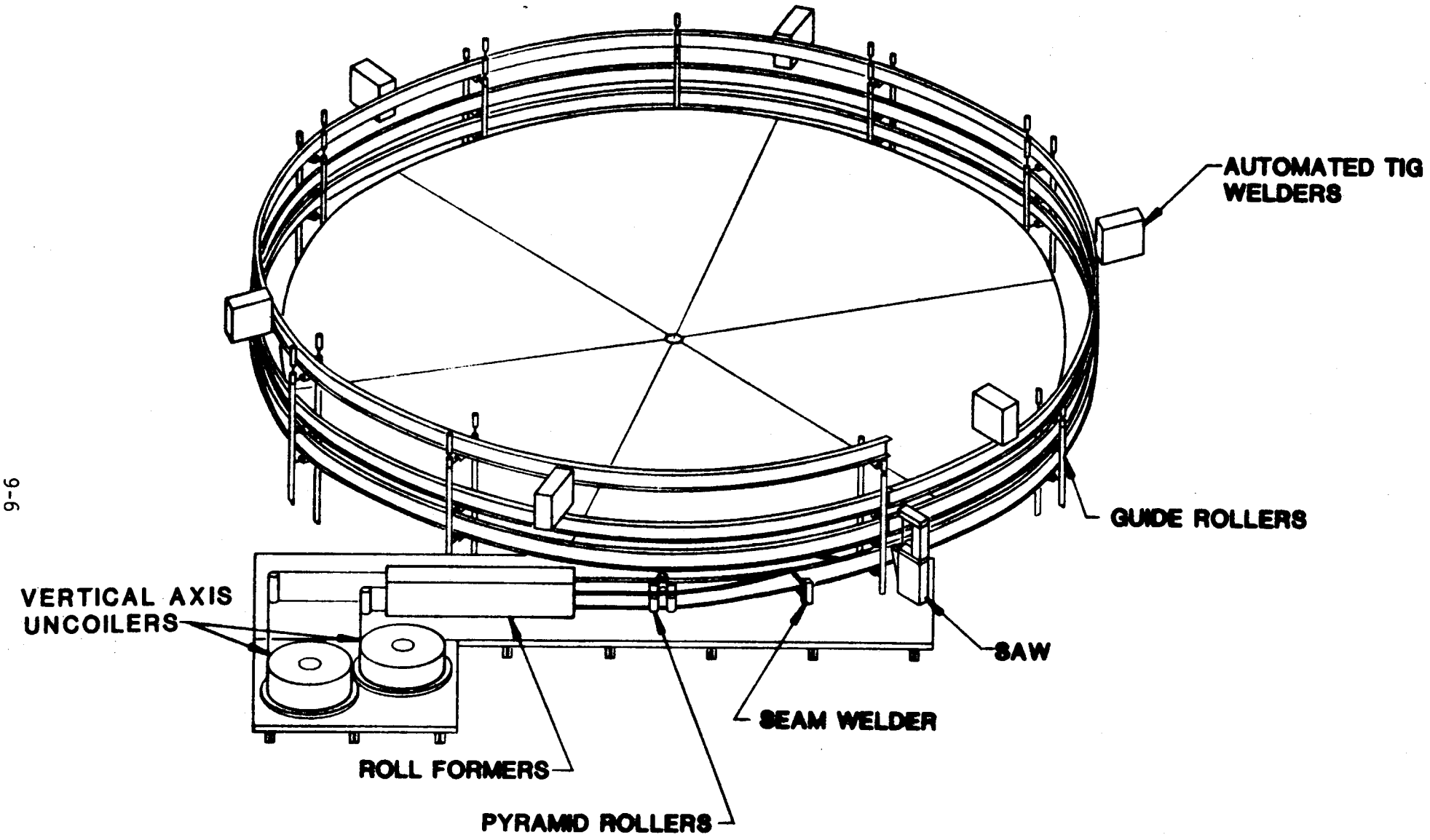

FIG. 9.3 RING PRODUCTION

The second spiral acts as a capacitor, freeing the subsequent operations from the rolling of the ring.

The guide rollers of the third spiral move in the vertical axis. This allows the aluminum spiral to be brought into a defined plane before the ends are butt welded to form a closed ring. The ring is then revolved as precut lengths of silicone tubing are pressed into the channel in the upper and lower surface of the aluminum ring. This tubing will be inflated later to partially tension the membrane. After the tubing has been placed, the four ends are passed through drilled holes in the ring and connected to barbed fittings. Doublers for the trusses are positioned and attached to the outside wall of the ring by six automated TIG seam welders. The LVDT support arm is also positioned at this station.

The track mounted vacuum platen grabs the finished ring with air clamps and moves it to the second work station. Doublers are loaded into the TIG welders by the work crew to complete the work cycle.

9.3.2 WORK STATION #2 - MEMBRANE TO RING ATTACHMENT

The membranes are shipped to the SMF on trailer mounted mandrels. A foam lining is wound with the membranes to prevent damage. Two membrane mandrel trailers sit side by side at the SMF; one with reflective membranes for the front of the mirror module, the other unsurfaced for the rear. The foam lining is taken up by adjacent rolls as the membranes are used.

The vacuum platens used in the membrane handling are 46 feet in diameter. They are constructed of 18" aluminum honey-comb and aluminum sheathing. Vacuum ports on the active surface are connected by a capillary network. Underneath, hoses connect the ports to a vacuum pump. The activation of ports is sequenced to increase membrane flatness. Wrinkles in the membrane can be swept out by a controlled cycle of the vacuum ports. Two vacuum platens are used at the SMF. One of these is floor mounted and is used much like an assembly table. The other vacuum platen is suspended from a track-mounted framework. It is used to move, position, and clamp the membranes and ring.

There are two holes in the floor mounted vacuum platen. The larger of the holes is located at the center. Machinery beneath the platen cuts the rear membrane for the fan duct and fastens the hole reinforcement. The smaller hole is located 3 feet in from the edge of the vacuum platen. It contains machinery cutting a six inch access hole, attaching the reinforcement, and provides for pressing the core of the LVDT against the front membrane while the adhesive sets.

A track circles the floor mounted vacuum platen. Four machines rest on this track. The machines have two functions; first, to seam weld the membranes to the ring, and second, to crimp the finished edge to increase membrane tension.

To begin the assembly, the upper vacuum platen drives forward over the rear membrane mandrel. A roll insures contact between the membrane and vacuum platen (Figure 9.5). Vacuum ports are opened sequentially as the platen continues to drive forward. The upper platen transfers the rear membrane to the lower platen. As the upper platen raises and returns to pick up the ring, holes are radiused in the back membrane and the flanges for the fan and access holes are attached with adhesives. The upper platen returns, places the ring, and then travels back to pick up the front membrane. Assembly workers thread the leads of the LVDT through a grommeted hole in the access flange and apply an adhesive to the top of the pad on the LVDT core (Figure 9.4). Finally, the upper platen lowers the front membrane on top of the ring. During welding, the platens sandwich the ring and membranes and act as the assembly fixture.

The four seam welding machines circle the platens, joining the two membranes to the ring. The upper platen, no longer needed, returns to the initial position. The pressure tube is partially inflated, and then the machines index back to their starting position while crimping the edge of the channel. The tube is fully inflated. The leads on the LVDT are briefly connected to a calibration device that displays the necessary offset to correct for assembly errors; the figure is recorded by one of the workers on the side of the ring. A jib crane lifts the completed mirror module and moves it to the final assembly area.

9.3.3 WORK STATION #3 - HUB FIXTURING

The hubs are shipped to the SMF attached to the drive unit. The control fan and shroud are also installed inside the hub. An operator uses a jib crane to place these assemblies on fixtured carts. The fixtured carts are able to lower the drive into a floor recess to bring the hub lower to the ground at the next station. They also index the hub so that the support structure can be built more rapidly off of the hub. The carts roll along a track. This permits several finished reflective assemblies to be stored outside on a circular track and partially frees SMF operations from installation.

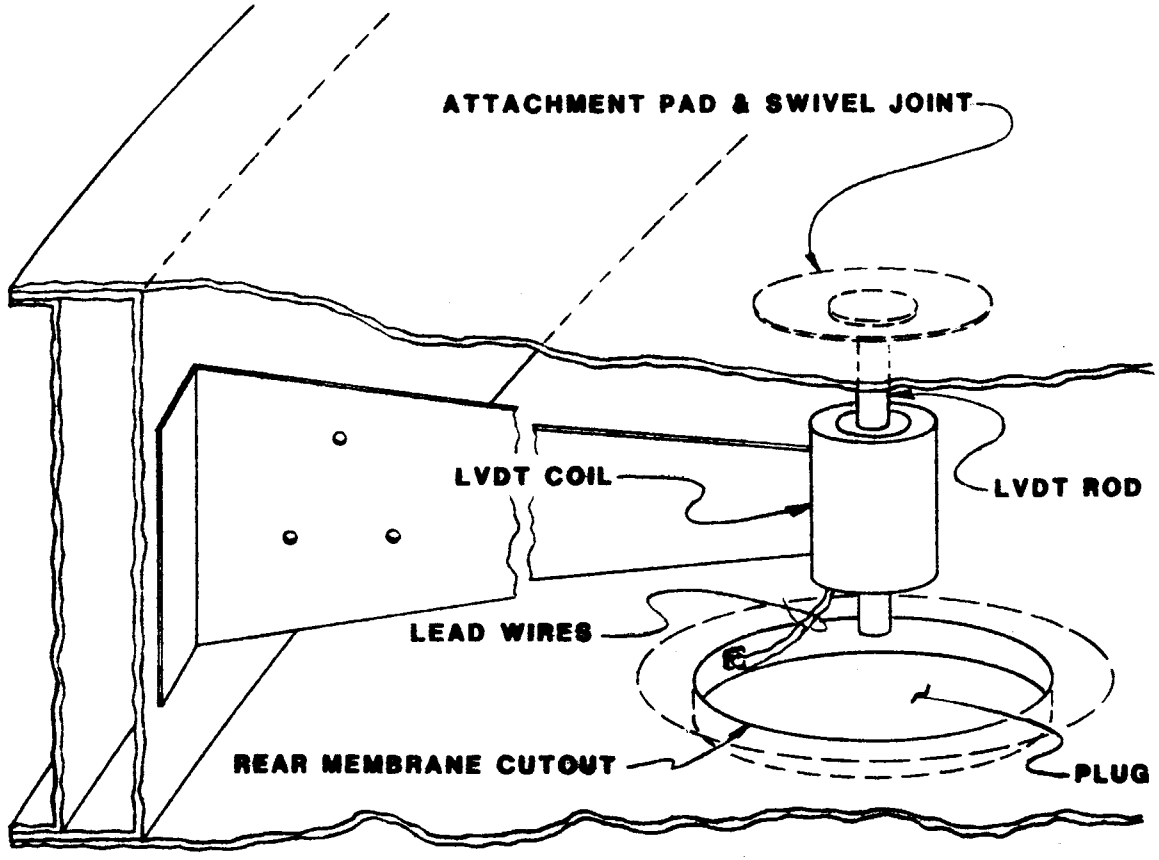

FIG. 9.4 LVDT MOUNT

STRESSED MEMBRANE

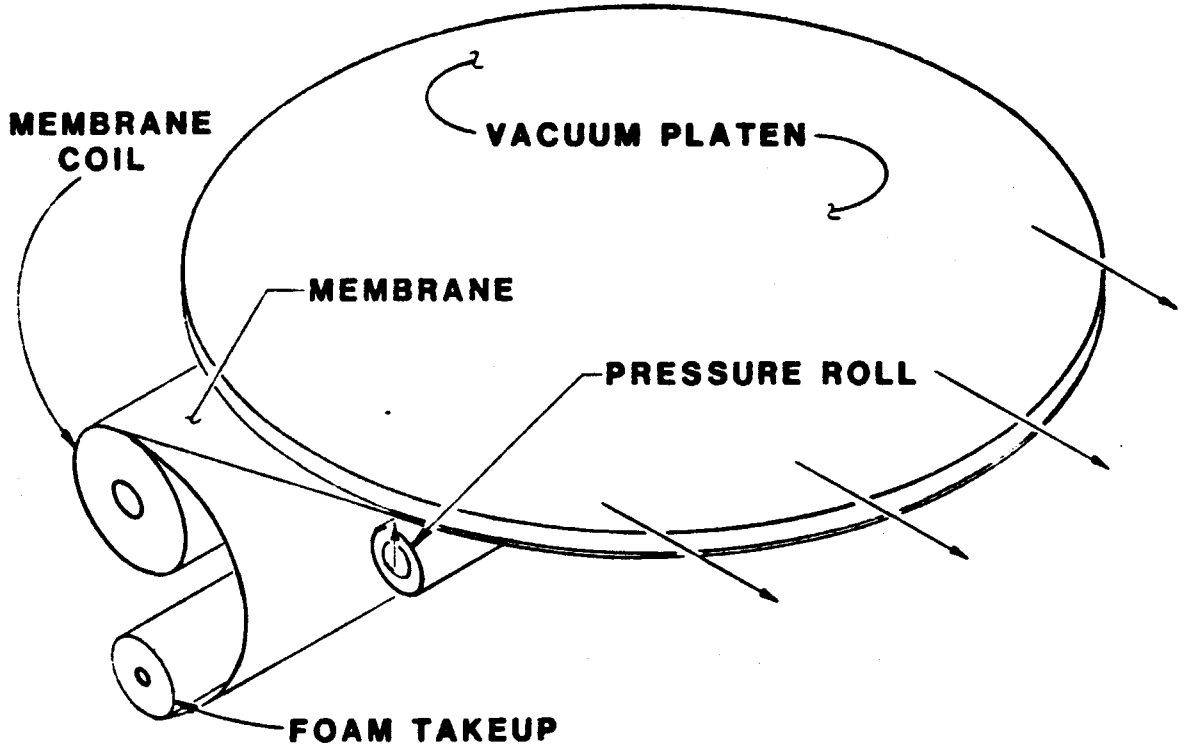

FIG. 9.5 MEMBRANE TRANSFER

9.3.4 WORK STATION #4 - FINAL ASSEMBLY

The completed drive and hub are wheeled into the final assembly area. The cart lowers the drive unit into a floor recess to place the hub a more convenient work height. Trusses are individually removed from a trailer and placed with the aid of a jib crane. The cart indexes the hub to aid in the assembly. A two man crew fasten the trusses to the hub with bolts. Strapping rods are installed by the other two members of the crew. The threaded bent ends of the strapping rods are pushed through pre-punched holes on the trusses, and fastened with nuts (Figure 9.6). Air or electric nut drivers are used to speed the operation. The final set of strapping is pulled into place with the aid of a small rachet winch to insure a taut fit.

After the assembly of the support structure is completed, the mirror module is positioned overhead with a jib crane. The connecting hinges are fastened to the truss tips and mirror modules with pins.

The LVDT leads are connected to a wiring harness on the hub, and the fan shroud is connected to the rear membrane. The finished reflective assembly is pushed out the door to await the installation truck.

9.4 INSTALLATION

Trucks of special construction will be used to install the reflective assemblies in the field. Hydraulic arms with base, elbow, and wrist action make it possible for the trucks to grasp the reflective assembly out of the carts, move them to the field, and position them on the pedestals (Figure 9.7). An articulated gripping device aligns with connections on the base of the hub for speedy pickup and release.

A secondary suspension system under the boom isolates the motions of the truck from the reflective assembly. Weights on the truck bed provide stability against overturning moments.

An installation crew of two men meets the transport truck at the pedestal. A lift truck raises the men level with the top of the pedestal. The reflective assembly is lowered until the drive mates its flange atop the pedestal. The installation crew fasten the drive in place with nuts using air tools. The transport truck releases the reflective assembly and returns to the SMF.

The installation team finish tightening the nuts and make the control and power supply hookups. They then move to the next pedestal to meet the returning transport truck.

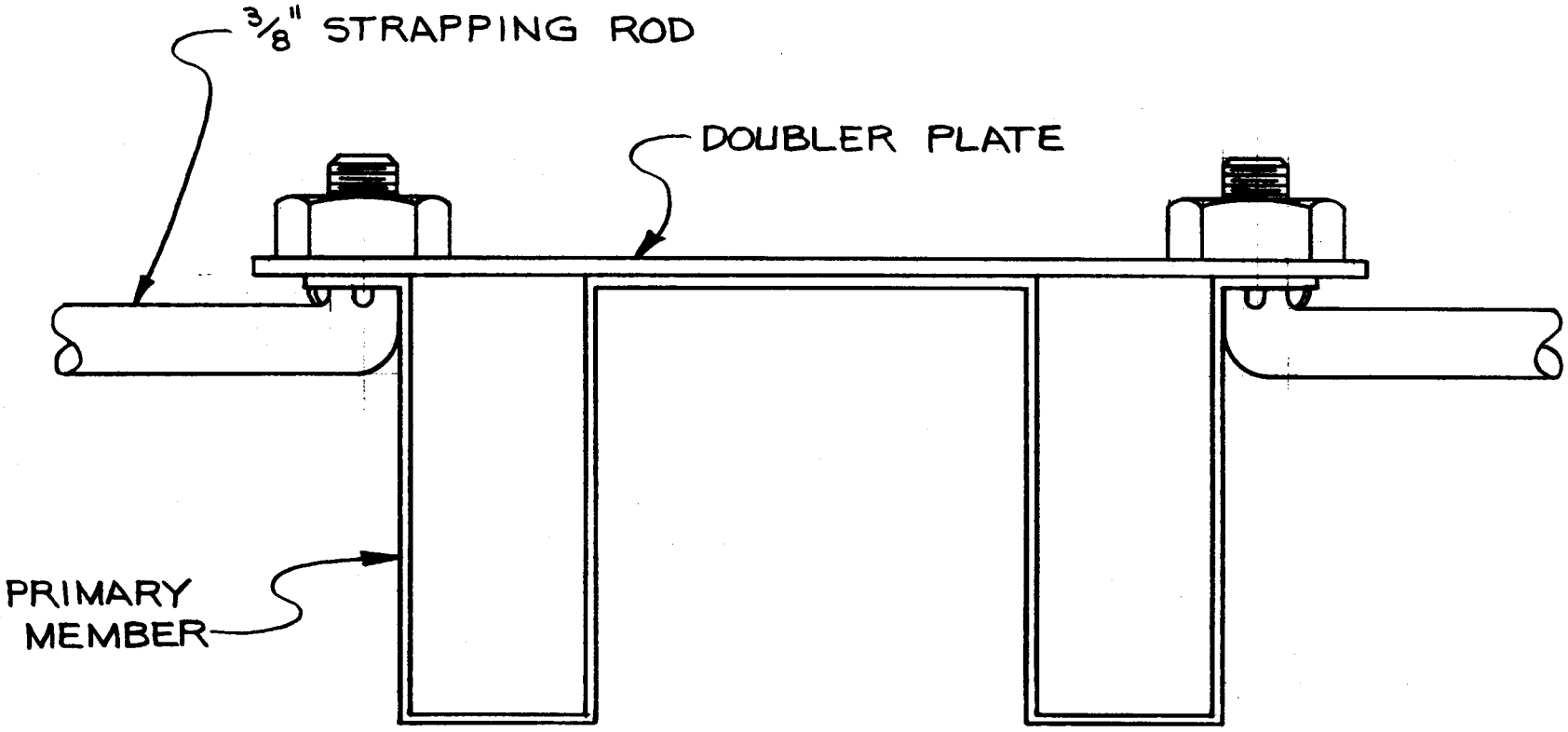

FIG. 9.6 TRUSS STRAPPING ATTACHMENT

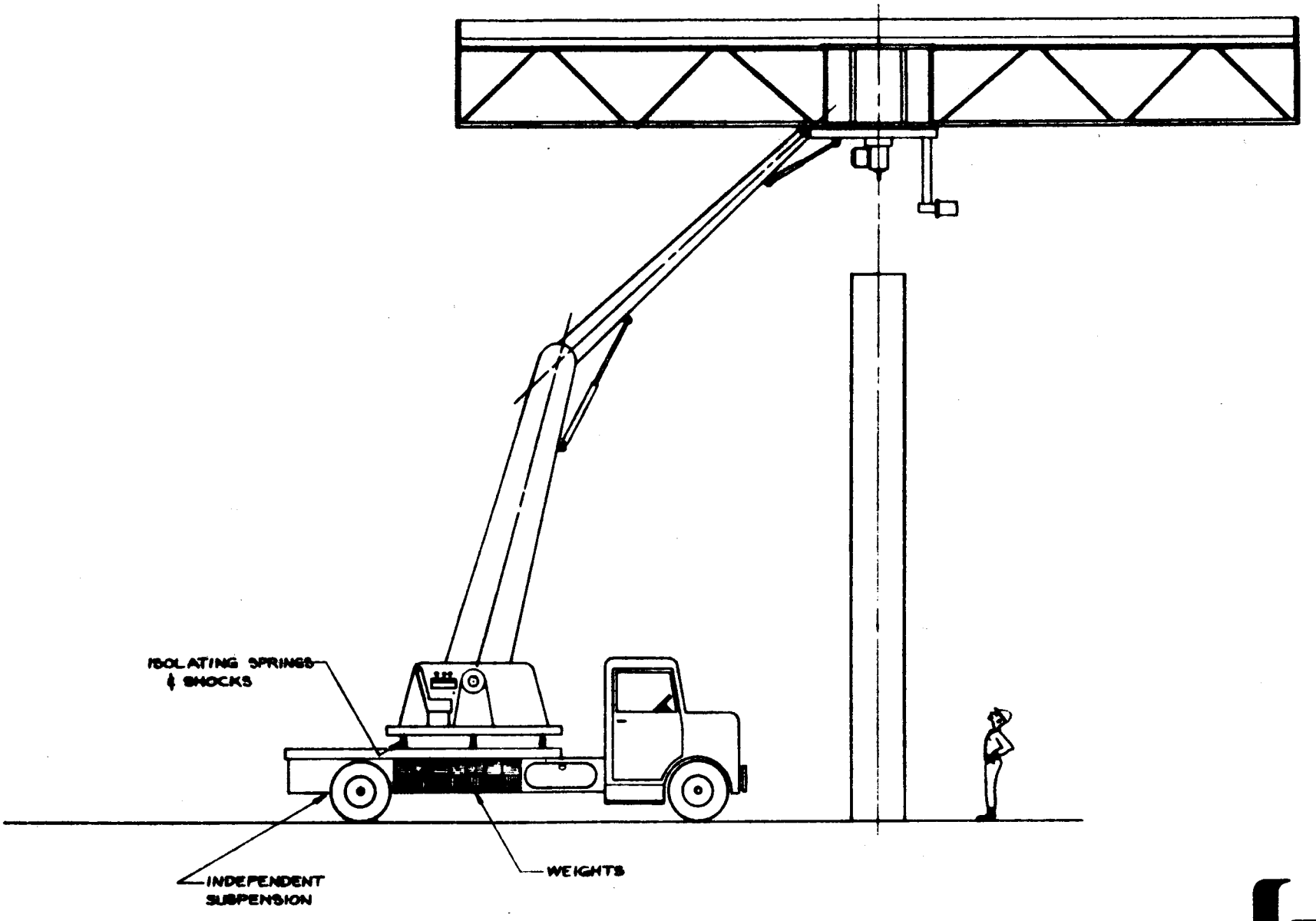

FIG. 9.7 INSTALLATION

9.5 PRODUCTION TIME TABLE

Work Station No. 1	Time/Minutes
Ring Forming Crew - 2 Workers Required	
Roll ring from coil stock @ 25/min	0*
Cut spiral & level	0*
Close ring & weld doublers	8
Attach LVDT support arms & install end fittings on tubing	10
	18

Work Station No. 2	Time/Minutes
Membrane to Ring Attachment - 4 Workers Required	
Place rear membrane	1.5
Cut hole & insert doubler	2.0
Place ring	2.0
Place top membrane	2.0
Seam weld	4.0
Partially inflate tube	.5
Crimp	4.0
Fully inflate tube	1.0
Remove vacuum chuck & attach hooks	1.0
	18.0

* Process simultaneous with subsequent operations.

Work Station No. 3	
Hub/Drive Crew - 1 Worker Required	
Place drive on Cart	18
	18

Work Station No. 4	
Final Assembly Crew - 4 Workers Required	
Connect struts to hub with bolts	4
Install Strapping	8
Position mirror module and connect with pins	4
Connect LVDT leads and fan shroud	2
	18

Installation

Transport Truck - 2 Crews of 2	
Pick up reflective assembly	2
Move to pedestal	10
Position reflective assembly	8
Hold in place	10
Return to SMF	6
	36

Installation Crew - 2 Crews of 2	
Position reflective assembly	8
Bolt down	16
Connect wiring	2
Move to next pedestal	10
	36

9.6 LABOR REQUIREMENTS

The following support personnel are required to maintain the SMF operations:

1 Foreman

1 Inspector

1 Fill-in Worker

1 Support Worker

1 Maintenance Worker

The foreman directs the entire operation. The inspector signs for all deliveries, and with the help of the support worker, inspects shipped parts for damage. The fill-in worker assists as required to keep progress at the work stations synchronized. The support worker assists the inspector and delivers bulk materials to the various work stations. The combined labor requirements

to operate a SMF and install the reflective assemblies are:

Assembly	Workers
Work Station No. 1	2
Work Station No. 2	4
Work Station No. 3	1
Work Station No. 4	4
Support Personnel	5
	16

Installation	
Transport	4
Installation	4
	8

24 Workers Per Site

SECTION 10.0

HELIOSTAT MAINTENANCE

Maintenance requirements for a field of heliostats includes both scheduled and unscheduled maintenance. Scheduled maintenance includes mirror washing and inspection. Unscheduled maintenance involves component failures.

The emphasis of this contract is on the reflector assembly and optimization or redesign of the balance of heliostat (BOH) was not included. Since most of the maintenance for a field of heliostats is directly related to the BOH, the maintenance requirements are based on second generation studies and adjusted for differences in reflector assembly design. Martin Marietta Corporation's (MMC) maintenance plan is used as a base line Ref. 17].

10.1 SCHEDULED MAINTENANCE

Mirror washing procedures, equipment, and labor for the SMH would not change significantly over that used by MMC. They estimated an average of 12 washes per year were required. Each wash for a field of 3,000 heliostats required a two-man crew 80 hours to complete.

Inspection includes an annual visual inspection for oil leaks, corrosion, vegetation growth, and reflector damage.

Microprocessor maintenance is subcontracted to a computer manufacturer as recommended by MMC.

The focus control system air filter will require periodic replacement. This task is unique to the SMH but could easily be performed during the annual inspection.

10.2 UNSCHEDULED MAINTENANCE

Failure rates for the heliostat components are defined in Table 10.1. It is noteworthy that although there are more components to fail on a SMH than on a second generation heliostat, the per unit aperture failure rate is lower because of the increased size of each heliostat.

TABLE 10.1

RELIABILITY OF FIELD REPLACEABLE COMPONENTS

COMPONENT	FAILURE 10^6 HOURS	NO. OF UNITS PER SITE	3,000 UNIT FIELD LIFETIME FAILURES*
Heliostat Controller Including Power Supply	16.09	3,000	4,827
Heliostat Field Controller	4.08	192	78
Encoder	1.20	6,000	720
Drive Motor	4.60	6,000	2,760
Cables	.61	3,000	183
Drive Mechanism	.30	3,000	90
Fan Motor	5.80	3,000	1,740
Fan Motor Control	4.08	3,000	1,224
LVDT Read Circuit	1.40	3,000	420
LVDT	.80	3,000	240
Structure	0	3,000	-
			12,282

Mean Time Between Failures (MTBF) = 8.14 Hrs. of Operation.

*Assumes 100,000 Hours Operating Time.

Based on MMC's second generation data [Ref 17] and estimates for components unique to the SMH.

Unscheduled maintenance procedures for the BOH components (drive, heliostat control, structure) are clearly defined in the second generation documentation, and the reader is referred to Reference 17 for details.

Components in the SMH that will require service but are not covered in the second generation design are the fan motor, the fan motor control circuit, the LVDT, and the LVDT read circuit.

The fan motor control circuit and the LVDT read circuit are both located at the level of the drive. Access to these circuits will require the same operator-controlled mobile work platform used to service the drive controls. These two circuits will be removable so that field service will be limited to problem isolation and unit replacement.

The fan motor will be accessed in a similar fashion and field service is also limited to problem isolation and replacement.

LVDT access is through the removable hand hole cap on the rear membrane. The LVDT core can be unscrewed from the front membrane, and the coil is unfastened with a set screw. Field service of the LVDT is also limited to problem isolation and replacement.

SECTION 11.0

COSTS

11.1 INTRODUCTION

Based on the SMH design and production procedure developed by SKI, a cost for the heliostats was generated. This cost is presented as a function of annual production rate and cumulative total number of heliostats produced.

The following assumptions apply to this cost analysis:

- Costs are reported in August 1985 dollars.
- Base line production rate of 50,000 heliostats per year; 150m^2 aperture area per heliostat.
- A relatively stable product design throughout its life cycle.
- Minimal marketing expense required to obtain and maintain a stable sales volume.
- Base line costs are based on the 50,000th unit produced.

11.2 CAPITAL COSTS

Capital costs are divided into equipment costs, building costs, and land and development costs for both the CMF and the SMF.

11.2.1 CMF EQUIPMENT

The CMF equipment required to produce 50,000 mirror modules per year is based on the following:

	Equipment Cost
Membrane	$ 6,786,000
Truss	2,020,000
Hub	1,031,000
Tube	1,994,000
General	7,660,000
	$19,491,000

These costs are based on equipment cost estimates presented in Table 11.1. A description of these machines is presented in the CMF description section of this report.

TABLE 11.1

CMF EQUIPMENT COSTS

DESCRIPTION	COST ($1,000)	QTY.REQ'D.	EXT. ($1,000)
Membrane Production Equipment			
Upender	21	4	84
Uncoiler	23	4	92
Levelers	33	4	132
Cleaners	22	4	88
Template System	25	2	50
Laminators	32	2	64
Film Shears	50	2	100
Laser Shears	84	4	336
Acrylic Sealers	40	2	80
Feed Systems	100	4	400
Positioners	100	4	400
Vacuum Chucks	50	4	200
Film Q.C.	60	2	120
Welder	800	4	3200
Positioners	80	4	320
Q.C. Weld	40	8	320
Recoiler	45	8	360
Mandrel	5	68	340
Miscellaneous		Lot	100
			6786
Truss Equipment			
Web Feed System	16	2	32
Web Notcher	20	2	40
Web Bender	80	2	160
Web Transfer Fixture	4	8	32
Flange Uncoiler	15	2	30
Flange Leveler	33	2	66
Flange Roll Former	50	2	100
Flange Punch	110	2	220
Assembly Fixture	20	2	40
Gang Welder	400	2	800
Transfer Equipment		Lot	500
			2020

CMF EQUIPMENT COSTS (Con't.)

DESCRIPTION	COST ($1,000)	QTY.REQ'D.	EXT. ($1,000)
Hub Equipment			
Tee Section Welder	24	1	24
Band Saw	13	1	13
Roll Former	45	1	45
Mig Welder	12	1	12
Assembly Fixture	4	8	32
Robot Mig Welder	175	3	525
Multi-Head Reamer	80	1	80
Transfer Equipment		Lot	300
			1031
Tube Equipment			
Extruder	68	2	136
Braiders	150	8	1200
Wrapper	55	2	110
Autoclave	100	1	100
Transfer Equipment		Lot	100
Recoilers	14	2	28
Boiler	320	1	320
			1994
General Plant Equipment			
Paint Line		Lot	3400
Fork Lifts	26	8	208
Compressors	14	4	56
O.H. Crane	660	1	660
Leasehold Imp		Lot	1500
Stamping Ram & Dies	84	4	336
Maintenance Equipment		Lot	500
Miscellaneous		Lot	1000
			7660

Cost Based on August 1985 Dollars Total: $19,491,000

11.2.2 CMF BUILDING

The building required for the CMF has 121,000 ft^2 high bay area with 20,000 ft^2 of offices and miscellaneous facilities. Cost of office and facilities space was estimated to be \$57/ft^2, and cost of the manufacturing area was estimated at \$43/ft^2. On this basis, the CMF building cost is \$6,340,000.

11.2.3 CMF LAND AND IMPROVEMENTS

Land requirement for the CMF is 17 acres with an estimated improved cost of \$20,000 per acre. On this basis, the CMF land cost is \$340,000.

11.2.4 SMF EQUIPMENT

The required equipment cost for each SMF is broken down as follows:

	Equipment Costs
Ring Fabrication	\$ 646,000
Ring to Membrane Attachment	435,000
Hub Placement	75,000
Final Assembly	40,000
General	75,000
Installation	300,000
	\$1,571,000 per site

This cost is based on the cost of each piece of equipment as presented in Table 11.2. With site operations at nine independent locations, the total SMF equipment cost is \$14,139,000.

11.2.5 SMF BUILDING

Each SMF consisted of a 20,200 ft^2 sheet metal building with a reinforced concrete foundation. The building is made from durable, heavy gage metal and is transferred from site to site for its expected life of five years. The slab, however, is not portable and represents a site-retained capital expense.

The cost for the moveable building was estimated to be \$40 per ft^2 (\$808,000 per site) which is \$7,272,000 for all the sites. The site-specific building costs are estimated to be \$10 per ft^2 or \$202,000 per site.

TABLE 11.2

SMF EQUIPMENT COSTS

DESCRIPTION	COST ($1,000)	QTY.REQ'D.	EXT. ($1,000)
Ring Fabrication			
10' x 12' Skid	3	1	3
10' x 40' Skid	5	1	5
Vertical Axis Uncoilers	15	2	30
Roll Former	35	2	70
Pyramid Rollers	50	2	100
Dual Seam Welder	30	1	30
Guide Roller Fixtures	3	12	36
Cut-off Saw	15	1	15
Manual TIG Welder	7	1	7
Automated TIG Welder	45	6	270
Tube Laying Machine	80	1	80
			646
Ring to Membrane Attachment			
Pressure Rolls	5	2	10
Mandrel Uncoilers	2	2	4
Overhead Vacuum Chuck	100	1	100
Floor Mounted Vacuum Chuck	70	1	70
Membrane Hole Cutter	10	1	10
Seam Welder	20	4	80
Crimper	30	4	120
Translater	10	4	40
Tub Inflater	1	1	1
			435
Hub Placement			
Jib Crane	15	1	15
Fixtured Carts	10	6	60
			75
Final Assembly			
Jib Crane	20	2	40
			40

SMF EQUIPMENT COSTS (Con't.)

Description	COST ($1,000)	QTY.REQ'D.	EXT. ($1,000)
General			
Forklift	25	1	25
Generator	5	1	5
Office Trailer	25	1	25
Misc. Hand Tools		Lot	20
			75
Installation			
10 Ton Truck, Modified Suspension & Hydraulic Arm	120	2	240
Cherry Picker	30	2	60
			300
			$ 1,571,000 per site
		Total (9x) =	$14,139,000

Cost Based on August 1985 Dollars.

11.2.6 SITE-RETAINED CAPITAL

Initial spares, special tools, and mirror washing equipment are left at each site for operation and maintenance. A significant part of this cost is the mirror washing equipment which, based on Martin Marietta Corporation's estimate [Ref 17], are $97,500 per truck with one truck per site. Spares and tools are expected to cost $58.10 per heliostat. These prices have been adjusted for inflation.

11.2.7 CAPITAL COST SUMMARY

The initial capital investment is summarized below:

	Cost
CMF Equipment	$19,491,000
CMF Building	6,340,000
CMF Land & Improvements	340,000
SMF Equipment	14,139,000
SMF Building	7,272,000
Site-Specific Capital	4,660,000
	$52,242,000

11.3 MANUFACTURING COST

The manufacturing costs have been broken down into costs for direct materials, direct labor, indirect labor, depreciation and property taxes with insurance. These costs include those incurred at the CMF as well as those incurred at each site.

11.3.1 DIRECT MATERIALS

The direct material costs are given in Table 11.3. Costs for raw material are based on vendor estimates at a volume equivalent to 50,000 heliostats per year. These costs are $.83 per lbs. of .010" aluminum membrane material, $.90 per lbs. of aluminum ring material, and $.25 per lbs. for hot rolled structural steel, and $2.09 per lbs. for raw silicone. Prices for purchased parts are based on estimates and vendor quotes. The cost of the film was chosen to be $.30 per ft^2.

11.3.2 DIRECT LABOR

Direct labor is defined as the labor that directly participates in the manufacture, installation or checkout of the heliostat or its parts. This includes most workers at both the site and the CMF.

TABLE 11.3

DIRECT MATERIAL COSTS

	QTY. PER HELIOSTAT	COST ($/HELIOSTAT)*
Membrane	2	$ 380.14
Film		475.31
Ring	1	403.20
Ring Doubler	6	54.00
Truss Primary	6	297.00
Truss Secondary	6	128.70
Tip Doubler	6	27.72
Strapping	24	59.40
Hub Rings	2	91.50
Hub Bracing	1	68.25
Drive Brackets	6	26.25
Hub-to-Truss Brackets	12	18.00
Hinge	6	47.00
Hinge Pins	12	4.80
Tensioning Tube	2	73.60
Controls		250.00
Paint		9.00
Misc. Hardware & Doublers		30.00
	92	$2,443.87

Total = $16.29/m^2

*Based on August 1985 Dollars.

The number of direct laborers at the CMF working on the reflective assembly is 44 and on the support structure is 70. Direct labor at each site requires 24 employees.

The cost of this labor accounts for the base wage, Social Security payments, unemployment insurance, Workmen's Compensation, company contributions to insurance policies and pension funds, vacations, holidays, premiums and other fringes. The cost is also based on the actual number of hours spent on a task. In this way, inefficiencies are included in the labor figure.

Wages at the CMF are based on SKI's experience of the wages required to obtain and keep qualified laborers. The base wage is $8.45 per hour with $3.80 in fringes.

Labor at the sites is primarily local people who will not travel from site-to-site. In this way, no large additional expense is incurred with having employees working out of town. The wages were, therefore, set the same as at the CMF.

Based on this, the cost of membrane production at the CMF is $.14 per m^2. This low labor cost is due to the highly automated membrane production line. The support structure direct labor cost is $.23 per m^2 at the CMF. All direct labor at the sites will be $.91 per m^2. The total direct labor cost is, therefore, $1.28 per m^2.

11.3.3 CONSUMABLES

Consumables are all material and supplies that are necessary during production but do not appear in the final product. Consumables include all material waste, operating and processing supplies, non-durable tooling and equipment, and utilities.

Material drop is based on estimates of the expected drop per component and is approximately 2% of the direct material. Supplies, non-durable tooling, and utilities are also strongly tied to the production rate and are estimated to represent 5% of the direct material cost. On this basis, the consumables cost $1.12 per m^2.

11.3.4 INDIRECT

Indirect costs include all costs (labor and supplies) incurred by plant maintenance, engineering, receiving, shipping, clerical, drafting, purchasing, inspecting, first line supervisor, and other employees not covered under G&A or direct labor.

Part of the indirect cost is tied directly to the production rate, such as first line supervision, receiving and inspection. This part of indirect cost has been estimated to be 35% of the direct labor rate, or $.45 per m^2.

Engineering, clerical and drafting remain fairly constant regardless of production rate. This cost is estimated to be 50% of the direct labor at the planned production rate, or $.64 per m^2.

11.3.5 DEPRECIATION

Depreciation is based on the capital cost of $52,242,000. Based on a straight line depreciation, this cost is $2.22 per m^2 (see Table 11.4). With a variable production rate, the depreciation per m^2 varies as shown:

% of Planned Capacity	Depreciation Cost ($/m2)
50	4.22
100	2.11
135	1.56

11.3.6 PROPERTY TAXES AND INSURANCE

Property taxes and insurance were estimated as a percentage of the average asset value over a ten year period. A rate of .025 was chosen as follows:

Asset	First Year	Tenth Year
CMF Building	$ 6,340,000	$3,170,000
CMF Land	340,000	340,000
All Other	45,562,000	-0-
	$52,242,000	$3,510,000

Avg = 27,876,000
Rate = 2.5%
Total = 696,900

This corresponds to the following rate per m^2:

% of Planned Production	Taxes and Insurances ($/m2)
50	.18
100	.09
135	.07

TABLE 11.4

DEPRECIATION

	INITIAL COST	LIFE (YEARS)	DEPRECIATION COST ($/m2)
CMF Building	$ 6,340,000	20	.04
CMF Land	340,000	00	-
CMF Equipment	19,491,000	10	.26
SMF Building	7,272,000	5	.19
SMF Equipment	14,139,000	5	.38
Site Specific Capital	4,660,000	.5	1.24
			$2.11/m^2

Based On: 50,000 Units Per Year.
No Salvage Value.
Straight Line Depreciation.
August 1985 Dollars.

11.4 TRANSPORTATION COST

Transportation costs are based on 74 tractors and 257 trailers. Depreciation, driver wages and taxes associated with transportation are recorded as transportation costs since they are so strongly tied to miles traveled.

11.4.1 EQUIPMENT

Equipment costs were computed as follows:

74 tractors @ $77,000 =	$5,698,000
257 trailers @ $14,000 =	3,598,000
	$9,296,000

Trailer costs include associated racks, tarps and tie-downs.

Expected tractor life is 600,000 miles for a total fleet mileage of 44,400,000 miles; therefore, transportation capital cost is $.21 per mile.

11.4.2 COST PER MILE

Other transportation costs are based on those reported in Reference 19 and adjusted for inflation based on the Consumer Price Index. The cost per mile is then:

	Cost Per Mile
Depreciation	$ .21
Fuel	.26
Tires	.13
Maintenance	.21
Insurance, Taxes, etc.	.25
Driver	.47
	$1.53

11.4.3 COST PER SQUARE METER

The cost per square meter of reflective aperture is based on an average round trip distance of 533 miles and a packing factor of .185 loads per heliostat, and the above mentioned cost per mile. This results in a cost of $1.00 per m^2.

11.5 OTHER BUSINESS COSTS

A business will incur other expenses that have not yet been discussed. These include research and development, general and administration, taxes and profit.

11.5.1 RESEARCH AND DEVELOPMENT

In order to keep the product competitive in the market, research and development must be a continual effort. The R&D cost was estimated at \$.27 per m^2.

11.5.2 GENERAL AND ADMINISTRATION

This cost includes marketing and administrative costs. Included in this is the General Manager and his staff, the Marketing Department, and the Accounting and Finance Department. Based on the number of personnel required to perform these tasks, a cost of \$2.37 per m^2 was assigned to G&A.

11.5.3 TAXES

State and federal income taxes are estimated to be \$1.05 per m^2.

11.5.4 PROFIT

The required after-taxes profit is defined as an internal rate of return of 15% with a 10 year life. Including all capital costs (transportation capital also), this value is \$1.63 per m^2.

11.6 BALANCE OF HELIOSTAT COSTS

The design of the balance of heliostat (BOH) was not considered in this contract; rather, a BOH cost was estimated from second generation heliostat work and is used to give an estimate of the expected overall SMH cost.

The cost of the BOH is broken down into seven categories: drive, pedestal, drive electrical, controls, field wiring, foundation, and field assembly and check-out.

11.6.1 DRIVE

Based on Sandia estimates of drive costs for $150m^2$ heliostats, the drive cost is set at \$11.00 per m^2.

11.6.2 PEDESTAL

Pedestal cost, as the remainder of the BOH costs, is based on McDonnell Douglas results of optimization of the second generation heliostat [Ref 4]. MDAC's cost estimates were extrapolated to a 150m^2 heliostat size and adjusted for inflation using the Producer's Price Index for steel (inflation for steel was 6.2%). This resulted in a pedestal cost of \$1.84 per m^2.

11.6.3 DRIVE ELECTRICAL

Drive electrical includes the cost of connecting the drive to the field wiring. Based on MDAC's estimates, this cost is \$107 per heliostat. This value was increased 30% to account for inflation based on the Consumer Price Index. This yielded a drive electrical cost of \$.93 per m^2.

11.6.4 HELIOSTAT CONTROLS

Electronic prices have been stable or decreasing in the past years and, therefore, no inflation rate was used to adjust MDAC's data for electrical controls. On this basis, heliostat controls cost \$1.84 per m^2.

11.6.5 FIELD WIRING

Field wiring was also based on MDAC's estimates and inflated per the Consumer Price Index. This resulted in a cost of \$3.76 per m^2.

11.6.6 FOUNDATION

Foundation costs are based on extrapolated data from MDAC also. Inflation adjustments are based on the assumption that half the material cost is in concrete and half is in steel. Each of these costs were inflated per their producer's Price Index value to yield a foundation cost of \$6.38 per m^2 (inflation of concrete was 14.1%).

11.6.7 FIELD ASSEMBLY AND CHECKOUT

MDAC's estimate for field assembly and checkout include costs for mounting the drive on the pedestal and mounting the reflector assemblies to drive. Both of these costs have previously been included in as SMH installation; therefore, only one fourth of MDAC's field assembly and checkout costs are included under BOH costs. This value is adjusted upward for inflation based on the Consumer Price Index. The resulting field assembly and checkout cost is \$1.21 per m^2.

11.6.8 BALANCE OF HELIOSTAT SUMMARY

The BOH cost amounted to $26.98 per m^2. This is summarized in Table 11.5.

11.7 COST SUMMARY

For cost comparison, the costs have been organized in three separate formats: by components of required revenue, by cost breakdown structure, and by location.

11.7.1 COST BY COMPONENTS OF REQUIRED REVENUE

Table 11.6 presents a summary of the costs as presented in the previous sections.

11.7.2 COST BY COST BREAKDOWN STRUCTURE

The heliostat was divided into categories developed by Sandia as a cost breakdown structure (COS) [Ref 18]. The first category, the reflector assembly, is defined as the membranes with film, the ring and its doublers, the tensioning tube, and the focus controls. The support structure includes the trusses, hub, hinges, and all associated hardware and doublers.

Table 11.7 presents the cost in this format.

11.7.3 COSTS BY LOCATION

The cost is presented in Table 11.8 as a function of the location where it is incurred.

11.8 COST VERSUS TOTAL PRODUCTION

Costs have been presented as the expected cost for the 50,000th unit produced. Assuming a 90% learning curve, the cost will drop as shown:

Production Year	Cost ($/m2)
1	55.26
2	49.73
4	44.76
8	40.28

TABLE 11.5

BALANCE OF HELIOSTAT COSTS

	COST PER m^2*
Drive Assembly	$11.00
Pedestal	1.84
Drive Electrical	.93
Heliostat Controls	1.84
Field Wiring	3.76
Foundation	6.38
Field Assembly & Checkout	1.21
	$26.96

*Based on August 1985 Dollars.

TABLE 11.6

COST BY COMPONENTS OF REQUIRED REVENUE ($/m^2)*

	COST ($/m^2)
Direct Material	16.29
Direct Labor	1.28
Consumables	1.12
Indirects	1.09
G&A	2.37
Capital Replacement & Capitalization	2.11
Property Tax and Insurance	.09
Other	1.32
Transportation	1.00
Gross Profit	1.63
Subtotal	28.30
BOH Cost	26.96
Total	55.26

*Based on August 1985 Dollars.

TABLE 11.7

COST BY COST BREAKDOWN STRUCTURE

	COST*** ($/m^2)
Reflective Assembly CMF & Transportation	11.79*
Support Structure CMF & Transportation	7.15*
Other	5.32**
SMF	4.04
	28.30
BOH	26.96
	55.26

* Includes direct materials, direct labor, replacement allowance, and gross profit.
** Includes indirect costs, consumables, property taxes and insurance, G&A, and other.
*** Based on August 1985 dollars.

TABLE 11.8

COST BY LOCATION

	COST ($/m2)*
CMF	22.83
Transportation	1.25
SMF	4.22
	28.30
BOH	26.96
	55.26

*Based on August 1985 Dollars.

11.9 COST VERSUS PRODUCTION RATE

In order to assess the effect of a variable production rate, two additional cost estimates were done based on production rates of 50% and 135% of the planned output.

At 50% of the planned rate, the CMF would use one shift as opposed to two and site production would occur at half as many sites. At 135% of the planned rate, the CMF would work seven days a week, and each SMF would work nine hour days, six days a week. No new employees would be added at any locations.

The breakdown of the costs are shown in Table 11.9. The cost per aperture area increases 15% at 50% production and decreases by 3% at 135% production.

11.10 OPERATION AND MAINTENANCE COSTS

The operation and maintenance (O&M) cost for a field of heliostats is a strong function of the BOH design. Since the BOH was not a design concern of this contract, the O&M costs for it are based on second generation study results. The O&M cost impact of using a stressed membrane reflector assembly over the second generation assembly is assessed in each of the following sections resulting in an O&M cost estimate for a field of 3,000 heliostats.

11.10.1 OPERATION COST

MMC estimates that three operators are required per heliostat field at a cost of $114,216 per year per site [Ref 17, adjusted for inflation]. This reduces to $.25 per m^2.

11.10.2 MAINTENANCE COST

Maintenance cost is divided into three sections; labor, equipment and materials.

TABLE 11.9

COST FOR VARIABLE PRODUCTION RATES*

	50% OF PLANNED RATE	100% OF PLANNED RATE	135% OF PLANNED RATE
Direct Material	16.29	16.29	16.29
Direct Labor	1.28	1.28	1.45
Consumables	1.12	1.12	1.12
Indirects	1.73	1.09	.98
G&A	4.74	2.37	1.76
Capital Replacement	4.22	2.11	1.56
Property Tax & Insurance	.18	.09	.07
Other	2.64	1.32	.98
Transportation	1.00	1.00	1.00
Gross Profit	3.26	1.63	1.21
	36.46	28.30	26.42
BOH	26.96	26.96	26.96
	63.42	55.26	53.38

*Based on August 1985 Dollars.

11.10.2.1 MAINTENANCE LABOR

Based on MMC's results, two maintenance shifts are operated per day with two men on each shift [Ref 17]. Using their labor rates adjusted for inflation, this comes to $.36 per m^2 per year.

This is a reasonable value based on the required mirror washing time and the field reliability. Mirror washing requires one half the time of the maintenance crews (see the "Heliostat Maintenance" section of this report). This leaves an average of 16 manhours per day for other tasks. Based on the field reliability data presented in the "Heliostat Maintenance" section, the average time allotted for repair of each failure is then five hours using a two man crew. This is a reasonably conservative value.

11.10.2.2 MAINTENANCE EQUIPMENT

The cost for specialized maintenance equipment required for service of the heliostat field has been accounted for in the site retained capital cost.

11.10.2.3 MAINTENANCE MATERIALS AND CONSUMABLES

Maintenance material costs are the cost of repair or replacement of failed heliostat components. This cost is based on MMC's estimate of the BOH components and on the expected material cost of the components specific to the stressed membrane.

MMC estimated $.217 per m^2 for BOH costs. Increasing this cost for inflation will give a rough estimate of the BOH cost. The cost for the stressed membrane specific materials is estimated to be $.02 per m^2 per year. This results in a material cost of $.30 per m^2 per year.

A two month supply of spares was assumed to be stocked to decrease field down time. Cost for these spares is depreciated over the first year of operation to give an additional first year cost of $.14 per m^2.

The only consumables identified are those for mirror washing. Based on MMC's estimates [Ref 1], these costs equal $.06 per m^2 per year after inflation.

The supplier service contract for the heliostat control is also based on MMC's results. Its cost is $.07 per m^2 per year (adjusted for inflation and heliostat size).

11.10.3 OPERATION AND MAINTENANCE SUMMARY

The annual O&M cost for the 3,000 unit heliostat field is summarized in Table 11.10.

TABLE 11.10

ANNUAL FIELD OPERATION AND MAINTENANCE COSTS

	Cost ($/m2/Yr)
Operating Labor	.25
Maintenance Labor	.36
Maintenance Materials	.30
Heliostat Washing	.06
HAC Service Contract	.07
Annual Total	1.04
First Year Total	1.18

SECTION 12.0

INTRODUCTION

TO PROTOTYPE DESIGN

The following sections cover the test results obtained during Phase I, a preliminary test and evaluation plan, and the prototype design and fabrication procedures used in Phase II of the contract. Tests accomplished in Phase I were limited to items required to explore key concepts in the design, and included membrane handling techniques, weld process development, tensioning methods, focal control, and surface error measurements. The methods and results of these tests were qualitative in some instances and quantitative in others.

The fifty square meter prototype components and fabrication procedures are also discussed and illustrated in the accompanying drawings and photographs. Reductions in component size were scaled from the commercial design as closely as possible. Departures from the commercial design are noted.

SECTION 13.0

PHASE I TESTING

A limited amount of testing was completed during Phase I to verify the feasibility of key elements of the design and fabrication concept. For this purpose, several two meter scale model mirror modules were built and tested.

The membranes were made from 36 inch wide .010" 5052 H34 aluminum stock. The seams were overlapped and welded together with a series of electric resistance spot welds. Electric resistance spot welds were also used to join the membrane to the ring. The rings were made from .063" 5052 H34 aluminum and sized in rough proportion to the commercial design.

A structure was used to support the finished mirror modules at six points through hinged joints similar to the commercial heliostat design.

Various methods were used and tested to achieve membrane tension. These included pre-tension, edge crimping, and inflatable tube tensioning.

All mirror modules were fitted with variable speed fans for focal control and used to focus sunlight. These tests were used to analyze the mirror surface in a general way for improvements of the production techniques.

The major objectives of this test program were to test seam joint design, possible tensioning methods, membrane stiffening, and control concepts. Additional goals included assessment of material processing requirements and to analyze a membrane surface for error. These objectives are addressed in the following sections.

13.1 MATERIAL PROCESSING

The ring and the membrane are delicate components by themselves and can be easily damaged during production. The handling and processing of these components is a unique industrial problem and requires special consideration. For this reason, one of the test objectives during Phase I was to identify unique handling or processing requirements of the ring and membrane.

The coil width for the membrane material used for these tests was 36". Sheets of this material up to 12 feet long were handled by two men with no significant difficulty. However, after the

sheets were joined together into a membrane, handling became quite difficult. The difficulty with handling the entire membrane was due to gravitational sag between discreet supports. This sag propagates towards the membrane center, and if the sag is great, will create sharp points of inflection which result in localized, permanent creases in the material. This problem was avoided by rolling the membrane onto cylindrical mandrels for transportation. Following a move, the membrane would simply be unrolled onto a flat surface. The membrane was able to withstand a slight amount of compression without buckling, and therefore, constant tension was not required. Actually, the 2 meter membranes could be positioned on a flat surface by hand without risk of buckling or creasing. This, however, does not appear feasible for significantly larger membranes.

When individual sheets are welded together to form the membrane, any initial waviness or misalignment is made permanent by the weld. Placement and position of the sheets is therefore critical. For the tests, SKI chose to tension the sheets lengthwise to remove any slop and to position the sheets with respect to the ends. This had merit in that it did not require extensive equipment or tooling but it had three drawbacks. It was slow, difficult to obtain accurate positioning, and created an alignment problem due to gravitational sag. Tensioning and alignment were very sensitive to small variations and proved to be time consuming and difficult. The natural sag of the sheets caused misalignment with the welding head. The sheets had to be lifted at the welding point without inducing any differences between sheets. This proved to be almost unworkable.

An alternative to this method is to hold each sheet with a vacuum platen during alignment and welding. In this way, the sheets would be assured of being flat and alignment could be simplified with tooling holes and pins in the platens.

Behavior of the ring material during the rolling process was also investigated. Although roll forming is not an unusual process like membrane handling, the ability to roll thin walled sections was identified as an area of concern. Testing of various material thicknesses showed that to avoid crippling .063" thick material is needed for a 1.5" leg. This leg length was the width of the test rings. The mass production ring, however, requires a 3" leg and is expected to require .090" material thickness.

Positioning of the membrane for welding to the ring is as critical as positioning the membrane sheets for welding to each other. Two methods were used during testing. One method involved supporting the two meter membrane from thirty-six(36) spring loaded clamps located around the circumference. Tension was induced to remove any slop or sag. The most significant drawback of this process is that the tension is applied at

discreet points and induces non-uniform membrane tension from clamp to clamp.

Two additional problems are: each spring applies slightly different loads resulting in non-uniform membrane tension, and clamps and springs present interference problems with the welding apparatus. SKI used a flat vacuum platen to support the entire membrane during positioning and welding. The vacuum platen did not interfere with welding and did not induce non-uniform membrane tension. SKI, therefore, has adopted the vacuum platen method for mass production.

13.2 WELD TESTS

The method used to join the sheets of the membrane together has the potential to distort or weaken the membrane. Several joining methods were tested on membrane samples to assess their impact.

The first test determined the differences between a single row of welds and two parallel rows. With a single row of welds, all stress is transferred through the weld and the weld, therefore, moves to the center of the stressed area (center line of the membrane). See Figure 13.1. Since the membrane has very little flexural rigidity, it will flex and rotate at the weld as shown in this simplified figure. This rotation places the weld in peel which is an undesirable loading condition for resistance welds. With a double row of welds, the centroid of the two welds moves to the membrane center line. The distance of the welds from the centroid limits the rotation. In this way, there is little rotation and the welds are under only small peel loads.

Several samples of membrane material were welded with these two methods and tested to failure in tension. A series of resistance spot welds were used to simulate a seam weld with a row spacing of .25". The seams with a double row of welds proved to be 32% stronger per weld area. Although the double row of welds did prove stronger than a single row, the single row weld strength was still adequate (with a factor of safety greater than five) to sustain the tensile loads in the commercial design. Welds at the membrane to ring attachment were somewhat weaker, most likely due to the substantial difference in ring and membrane gage.

The second test determined if additional weld strength could be acquired by removing all peel stress from the welds. This was done by placing a .005" joggle in each sheet and joining them with two rows of spots (Figure 13.2). These specimens were pulled to failure but exhibited no greater strength than those joined without an offset.

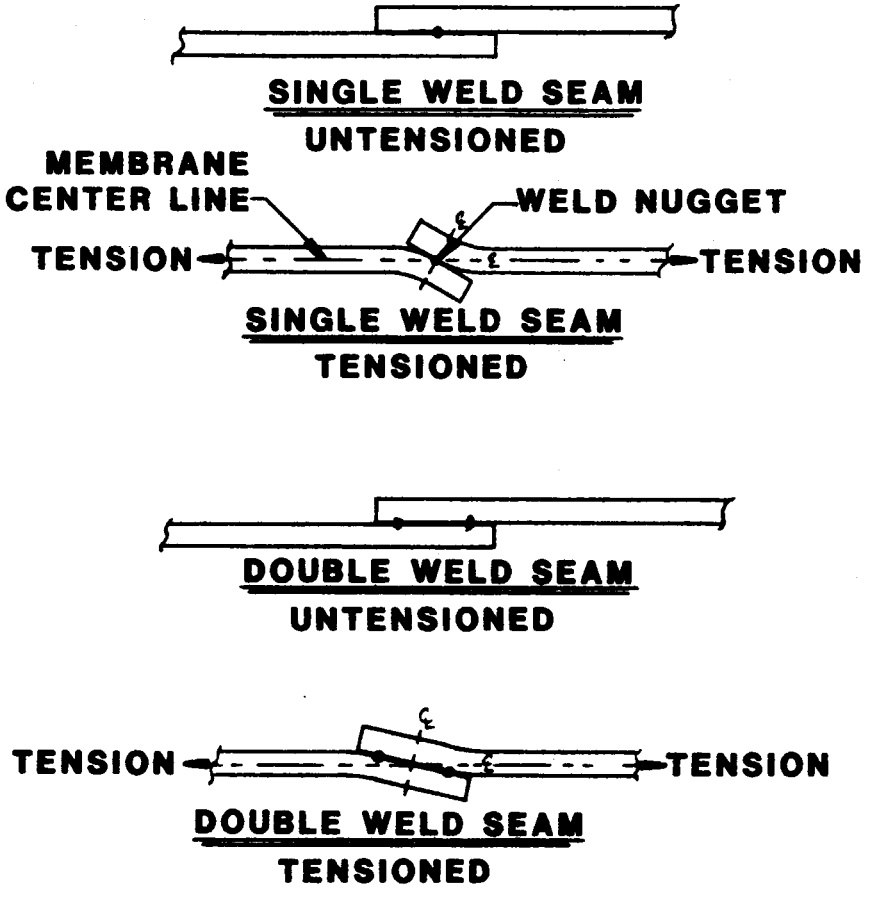

FIG. 13.1 WELD JOINT DISTORTION

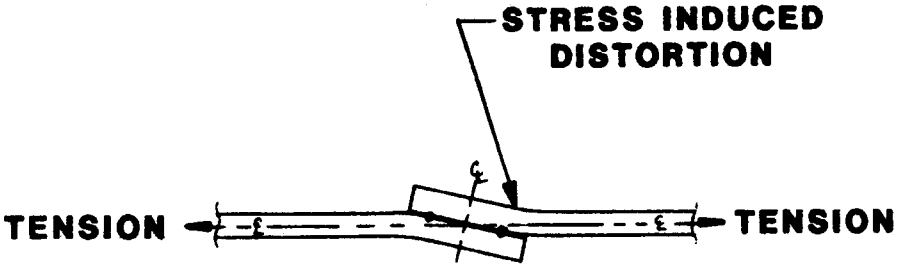

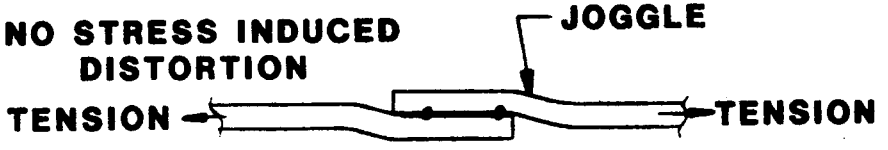

FIG. 13.2 JOINT PREPARATION

Initially, a double row of welds was selectd to provide maximum strength in the "membrane-to-membrane" and "membrane-to-ring" connection. The double weld line in the membrane was abandoned after optical testing when surface error was found to be roughly equivalent in each approach. The double row at the ring connection was maintained for strength. Offsets were abandoned as no increase in strength or optical error reduction was observed.

13.3 TENSIONING METHOD

Several different membrane tensioning methods were investigated: pre-tensioning, flange crimping, and post-assembly tube inflation.

Pre-tensioning of the membrane was tested by attaching spring loaded clamps to the membrane circumference prior to attachment to the ring. This method is similar to that described in the previous section for membrane support, but would require significantly higher tensions. In fact, pre-tensioning can only supply a portion of the final membrane tension because the pre-tensioning loads are limited by the membrane yield strength. The same problems exist for pre-tensioning as those discussed for the membrane support. That is, the loading is discreet, uneven, and the equipment creates interference with the welder. The magnitudes of the differential tensions were exaggerated over those developed by the support method.

Membrane tensioning can also be accomplished by bending the flange of the ring down after the membrane has been welded (Figure 13.3). This method was tested and found to be practical. Membrane tension is a strong function of the angle of crimp, and therefore, this angle must be accurately controlled. It is felt that with a specialized crimping tool, this would present no problem.

The third tensioning method tested during Phase I required a flexible tube between the ring and the membrane. When inflated, this tube exerted a force on the membrane that resolved into tension (Figure 13.4). The relationship between tube pressure and membrane tension was linear in the range studied (Figure 13.5). The only difficulty with this tensioning method is the membrane is lifted at an angle from the weld resulting in peel stresses in the weld nugget. Weld strength for resistance welds stressed at this peel angle, with all other conditions being ideal, was tested to be twenty-five percent less than those under pure shear. Peel of the weld joint can, however, be avoided by crimping of the flange.

The most significant advantage of tube tensioning identified during testing is the reduction in non-uniform loading in the

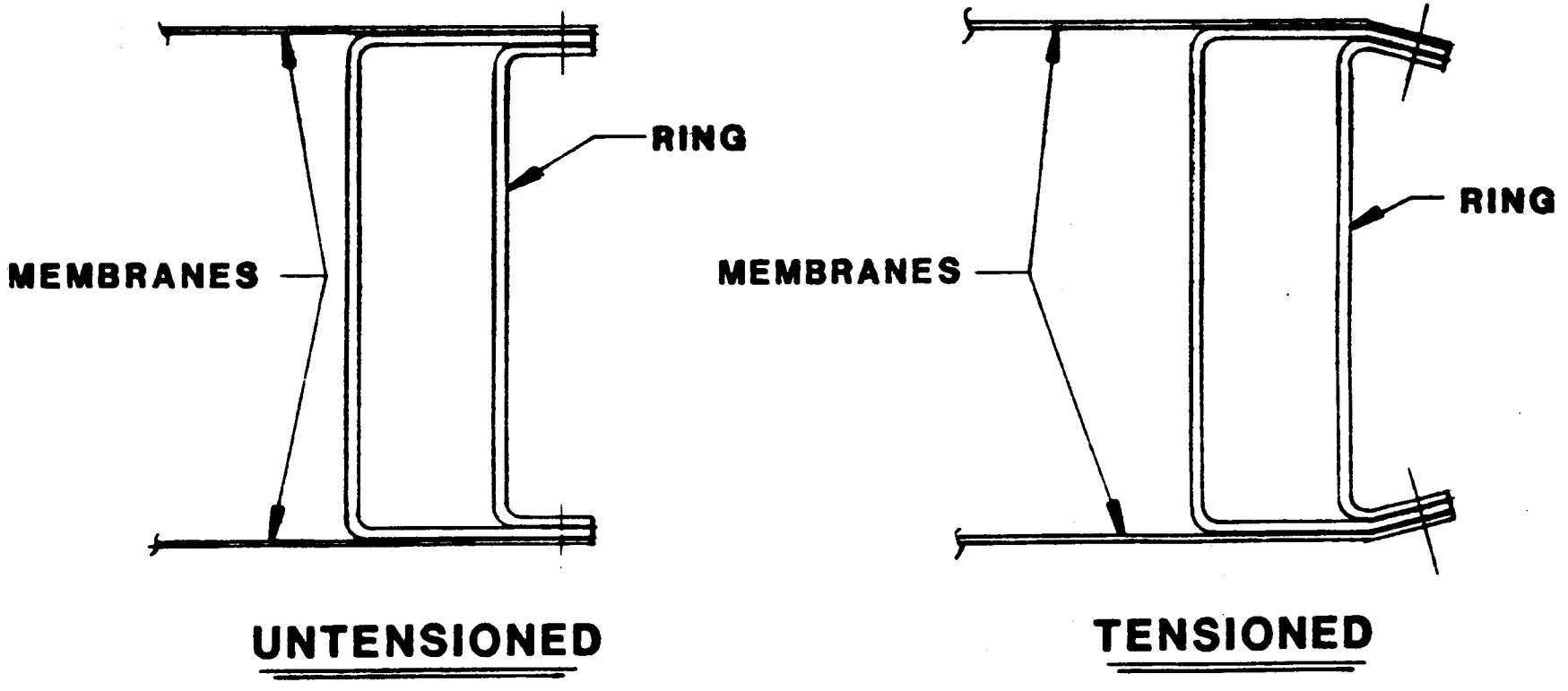

FIG. 13.3 MEMBRANE TENSIONING - EDGE ROLL

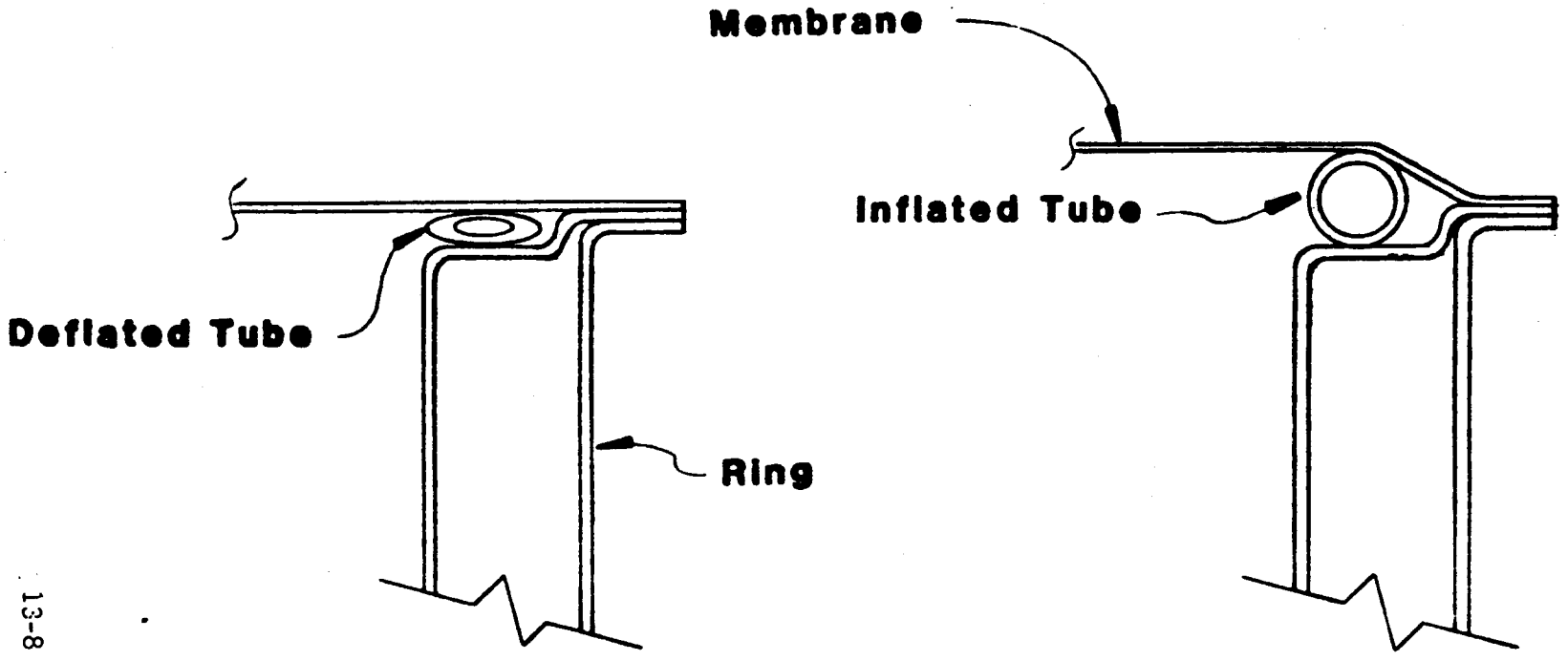

FIG. 13.4 MEMBRANE TENSIONING - INFLATABLE TUBE

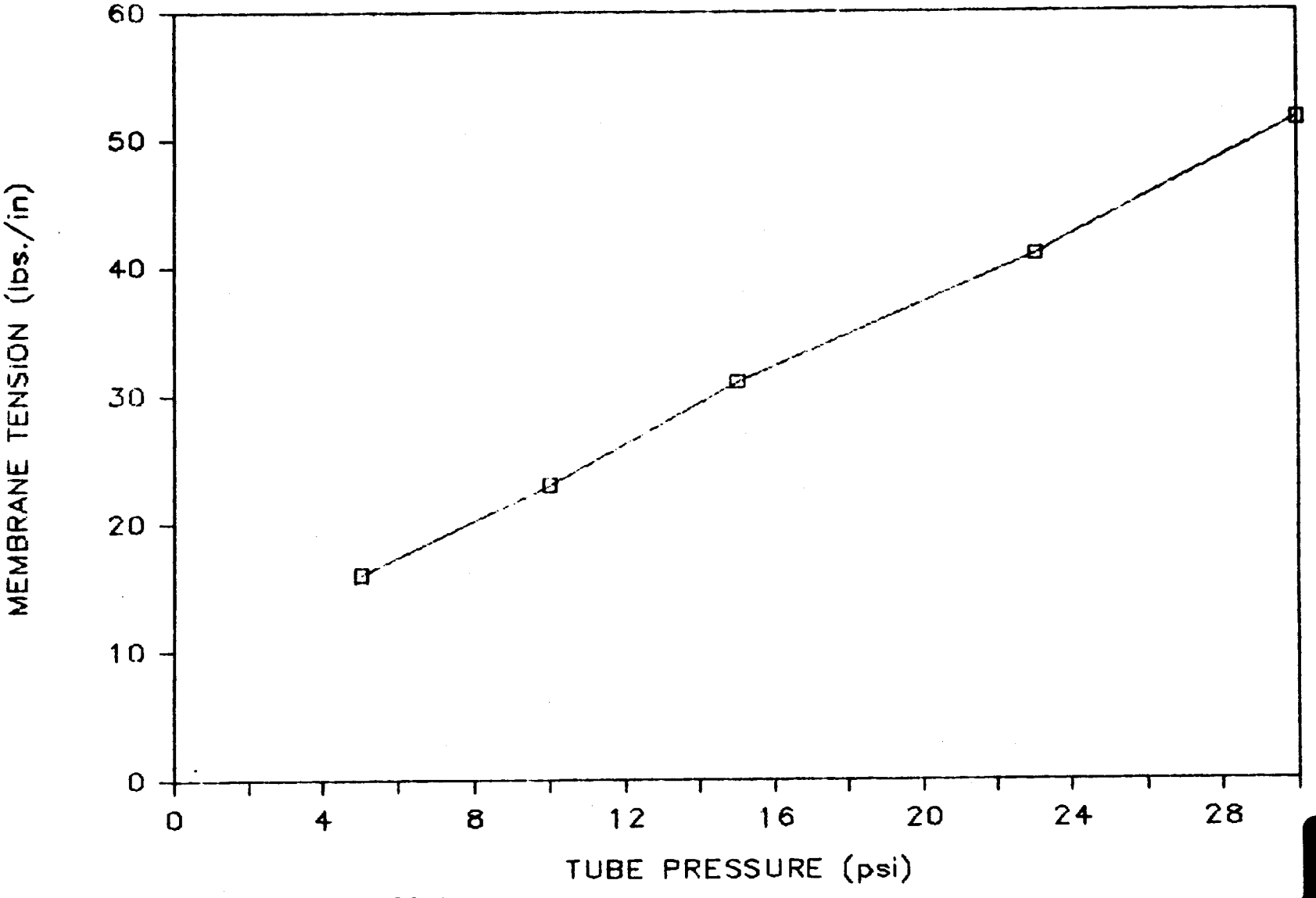

FIG. 13.5 TENSION VS. TUBE PRESSURE

membrane. Strain gage rosettes were mounted at two locations on the membrane of a two meter model. At each location, gages were mounted on both sides of the membrane. In this way, errors due to initial bending stresses in the membrane are removed and only actual membrane tension was recorded. The strain data from the two points differed by less than fifteen percent. The lack of a large difference supports the observation of uniform membrane tension.

13.4 SURFACE MEASUREMENTS

The surface of mirror module three was accurately measured to assess its optical quality. The measurements were taken by sweeping the membrane surface with a set of dial indicators mounted to a radial arm. The module was fixed to six supports and pulled into a plane at the supports. A variable speed fan was connected to the unit and stall pressure was varied to allow different focal lengths. Pressure in the inflatable tube was also varied to provide different tension valves in the membrane. The test setup is shown in Figure 13.6.

Surface height versus circumferential position of the membrane is illustrated for six different cases in Figure 13.7 through 13.12. The position of seams and supports is shown in Figure 13.13. Some surface errors which occur in the testing model are not expected to exist in the prototype. The most notable of these errors occurred at a circumferential position of 160 degrees. At this point, the tension tube was overlapped slightly to facilitate pressure connections. The error was compounded to some degree by adjusting the neutral plane of the assembly based on average membrane position. Consequently, the peak error at this position was not considered to reflect any serious problems to be dealt with in prototype construction.

Several interesting features are apparent from a review of the information presented in these figures. First, the position of the struts, at sixty degree intervals beginning at zero, is clearly shown on each of the figures. Manufacturing error due to a non-planarity in ring shape, was reduced by pulling the ring back into plane at each connection. The maximum error in height near the ring (and avoiding the 160 degree point) was 0.040 inches and periodic, though not always of the same sign. Using the model that relates deflection at the ring to surface error, the magnitude was estimated at 1.3 milliradians, rms, due to assymmetric effects.

The standard deviation of the error term was also plotted as a function of radius in Figure 13.14. This figure illustrates that error associated with asymmetric sag does decrease as distance from the ring increases.

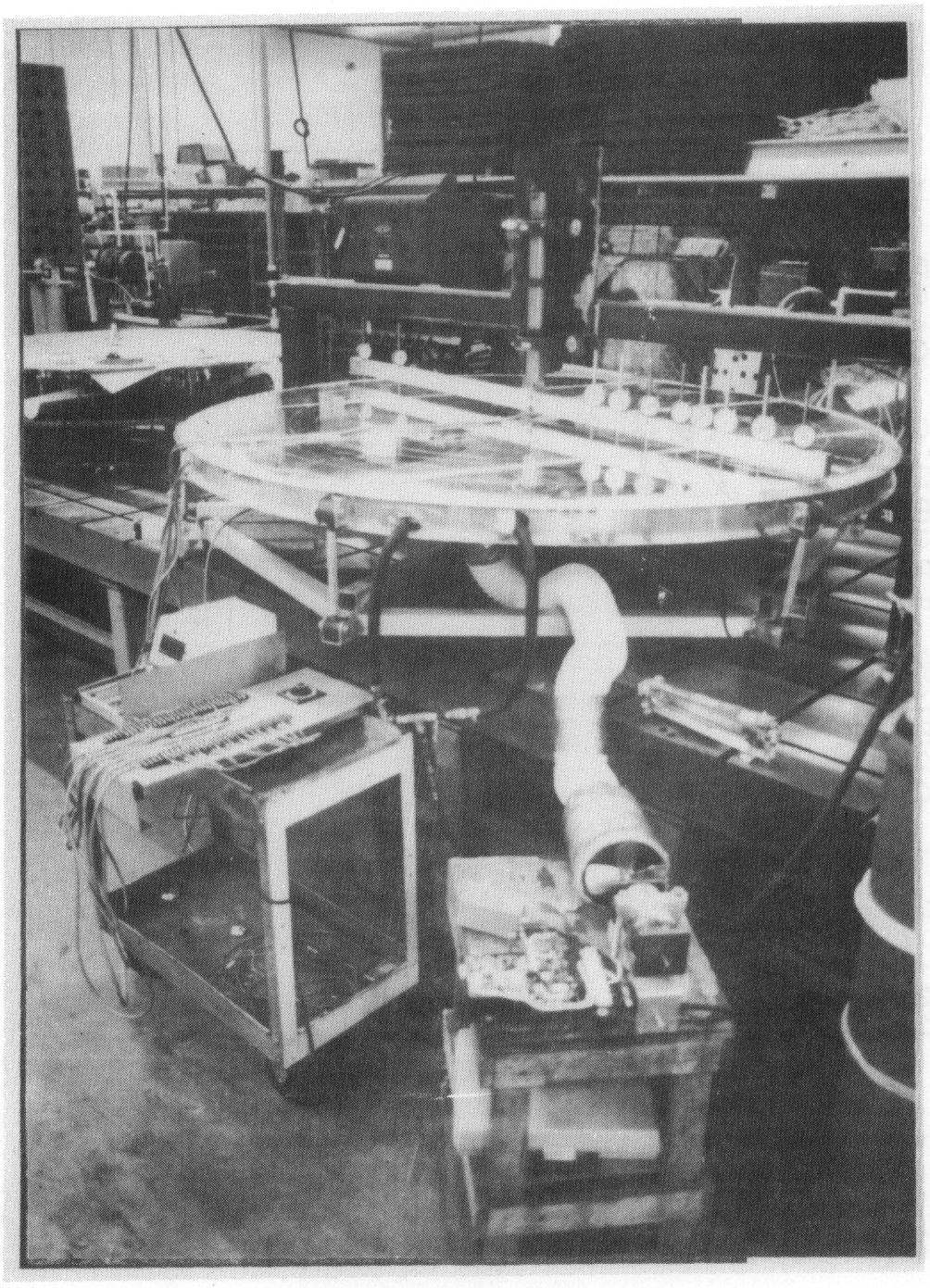

FIGURE 13.6 PHASE I TEST SET-UP

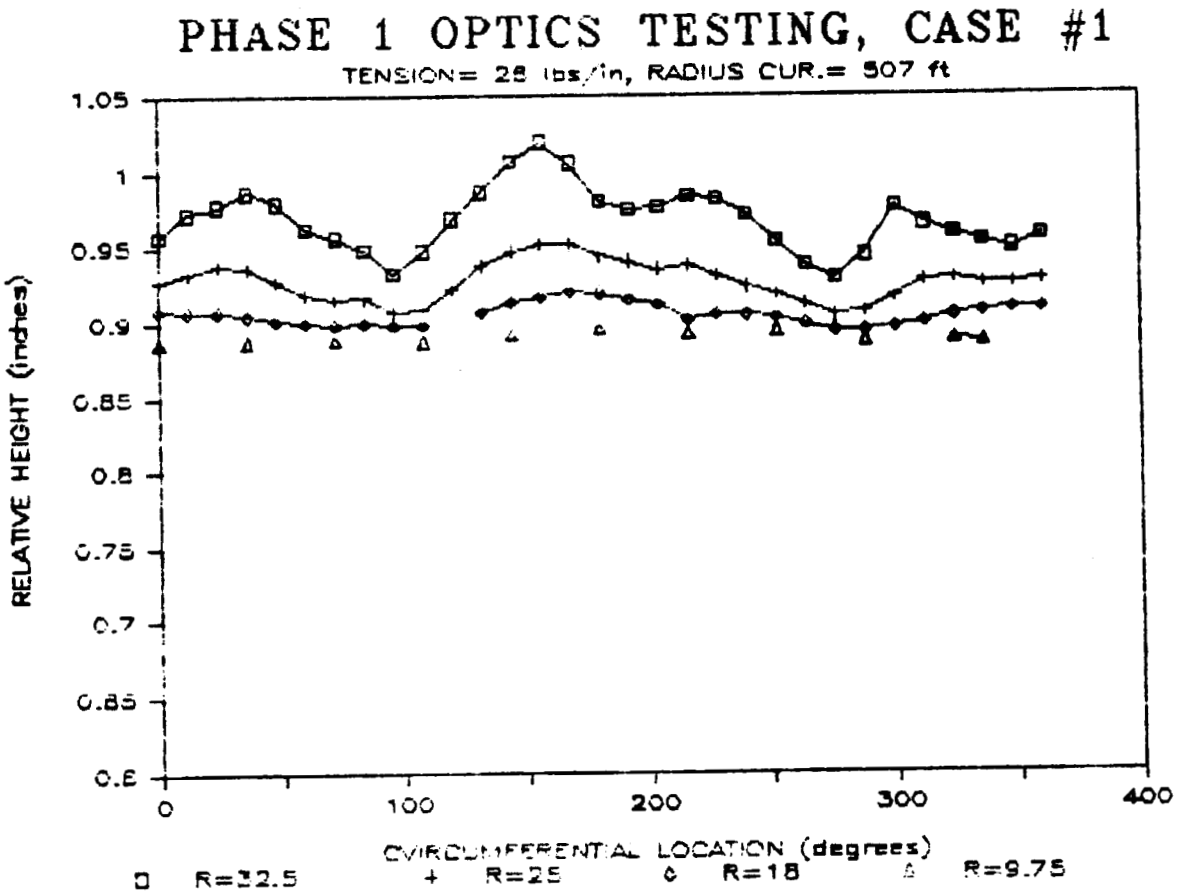

FIG. 13.7 SURFACE ERROR - CASE 1

SOLAR KINETICS INC.

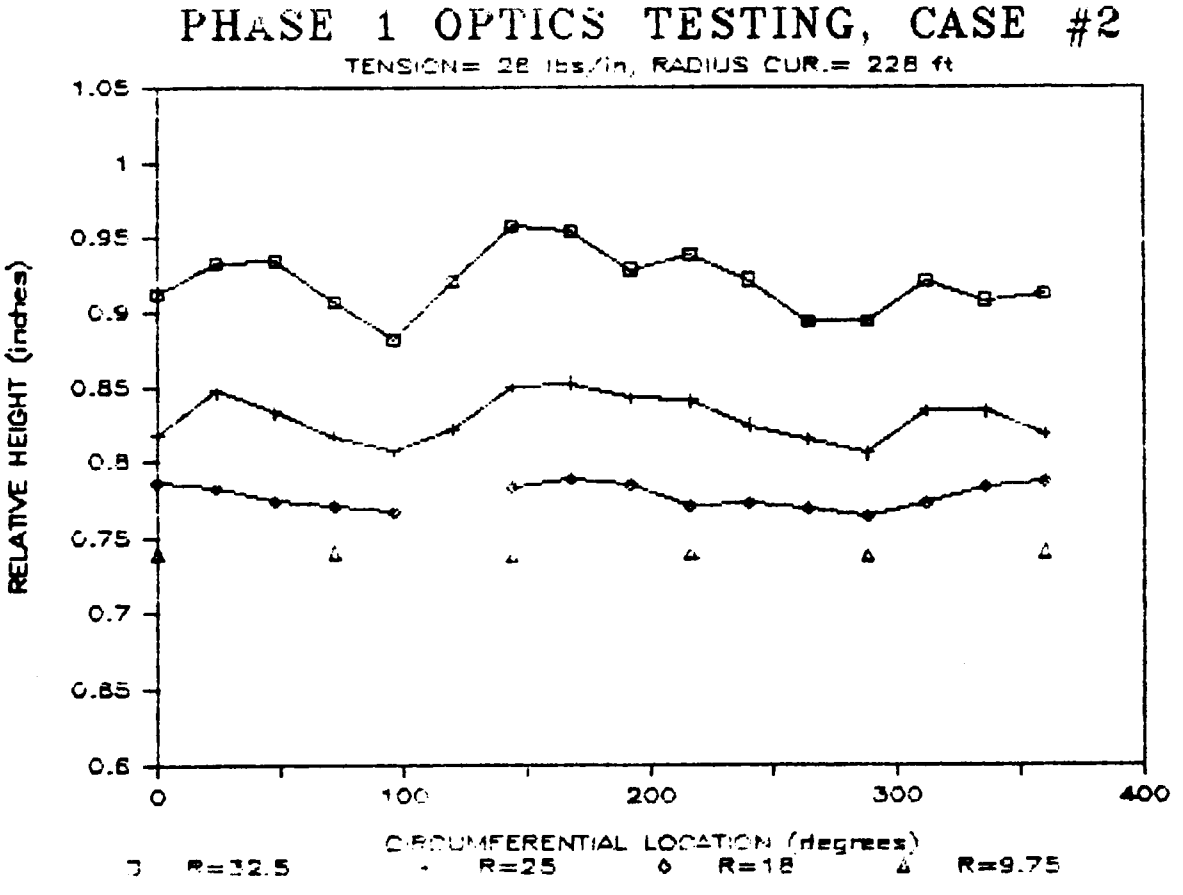

FIG. 13.8 SURFACE ERROR - CASE 2

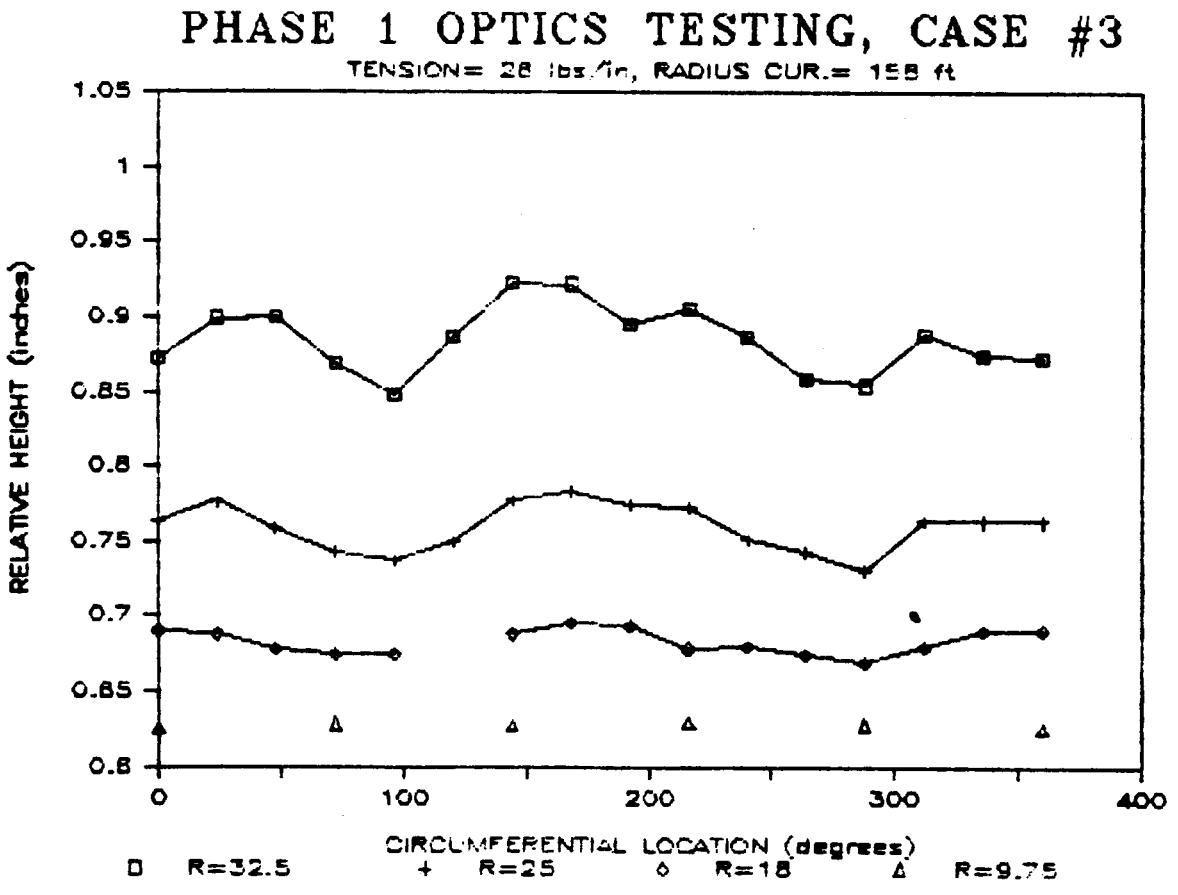

FIG. 13.9 SURFACE ERROR - CASE 3

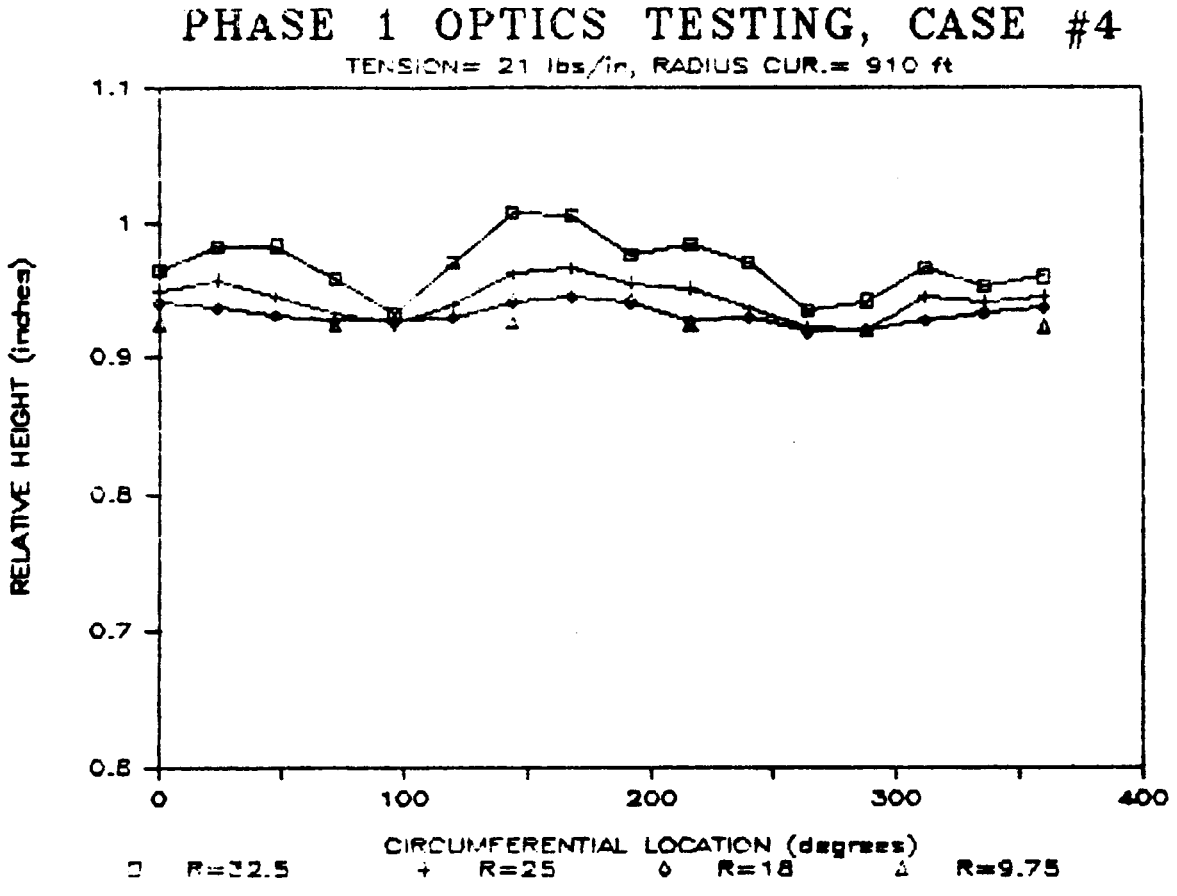

FIG. 13.10 SURFACE ERROR - CASE 4

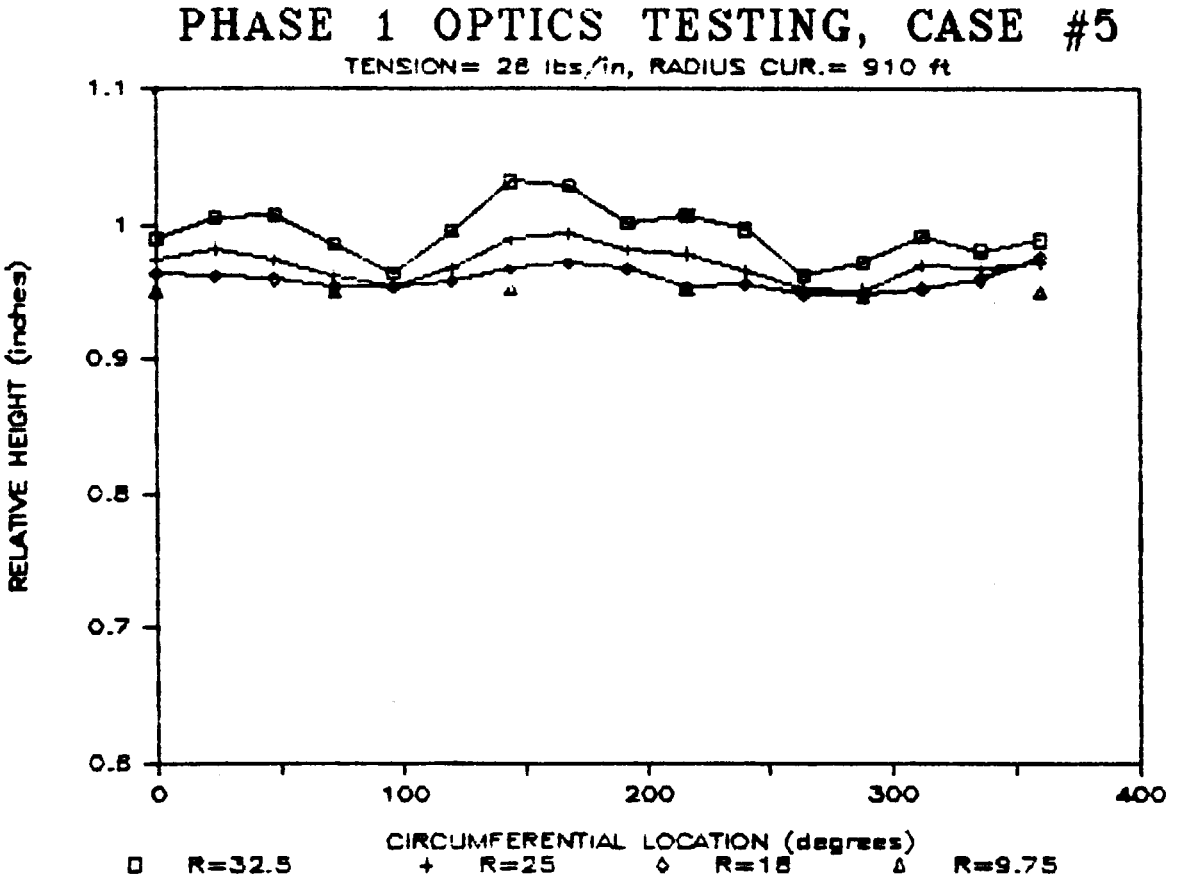

FIG. 13.11 SURFACE ERROR - CASE 5

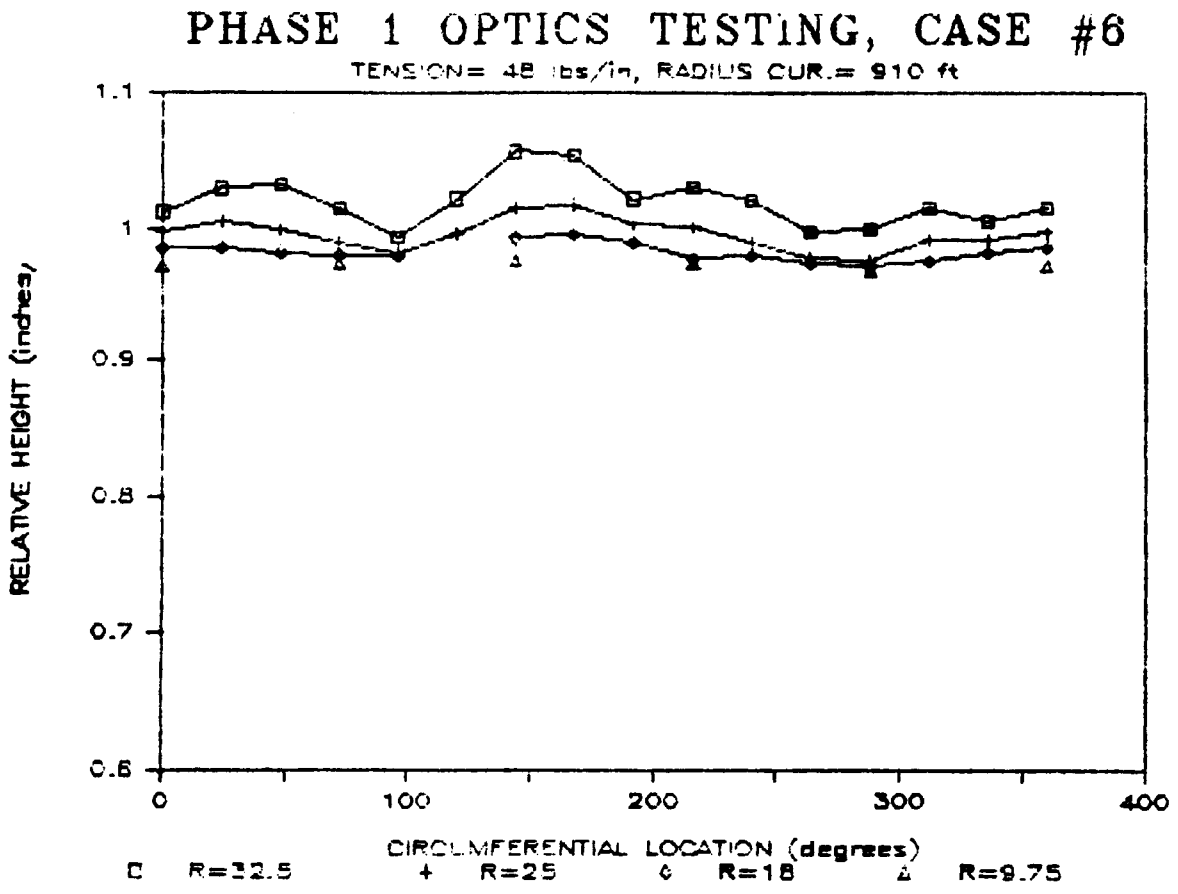

FIG. 13.12 SURFACE ERROR - CASE 6

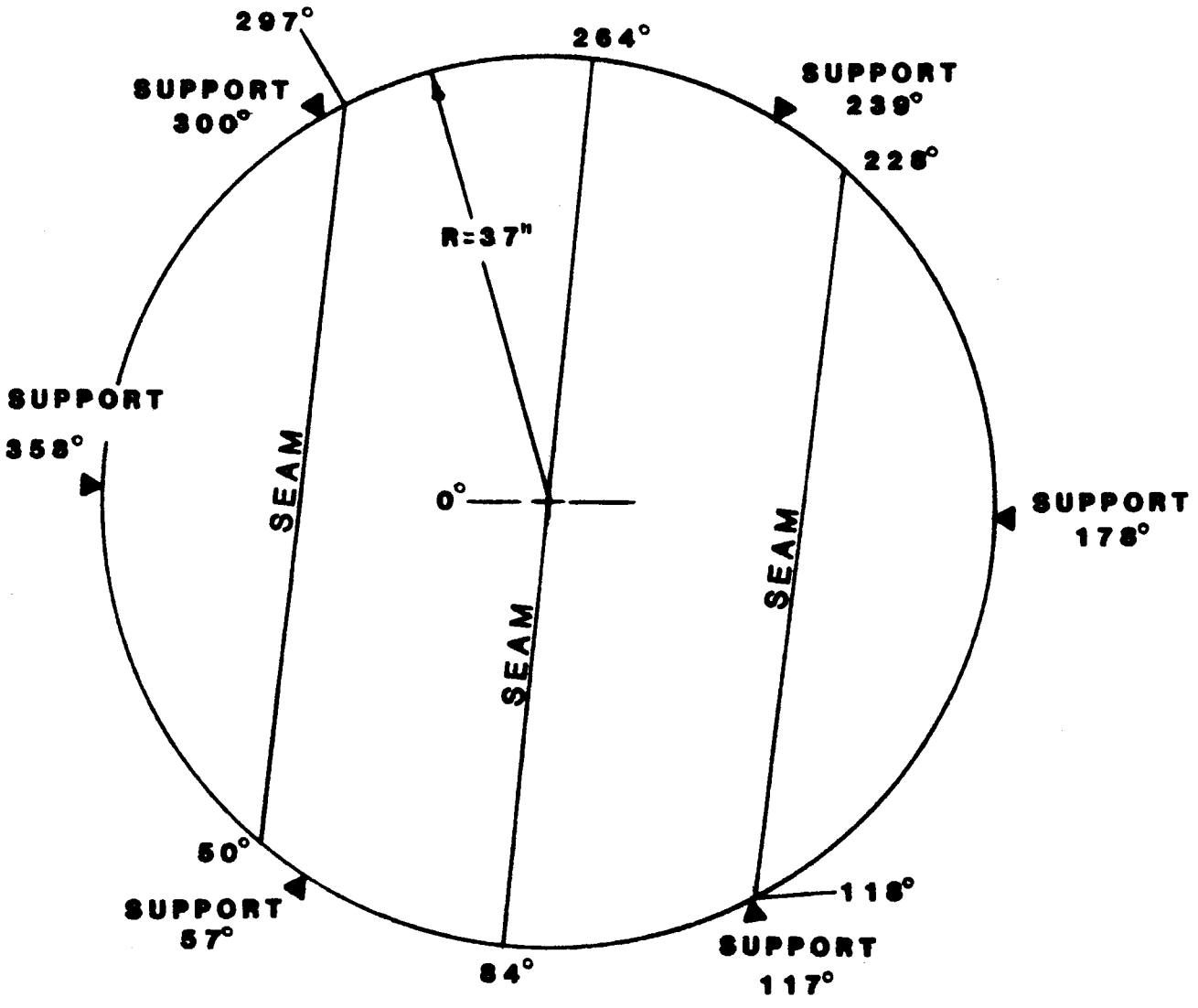

FIG. 13.13 MEMBRANE SEAM AND SUPPORT POSITIONS

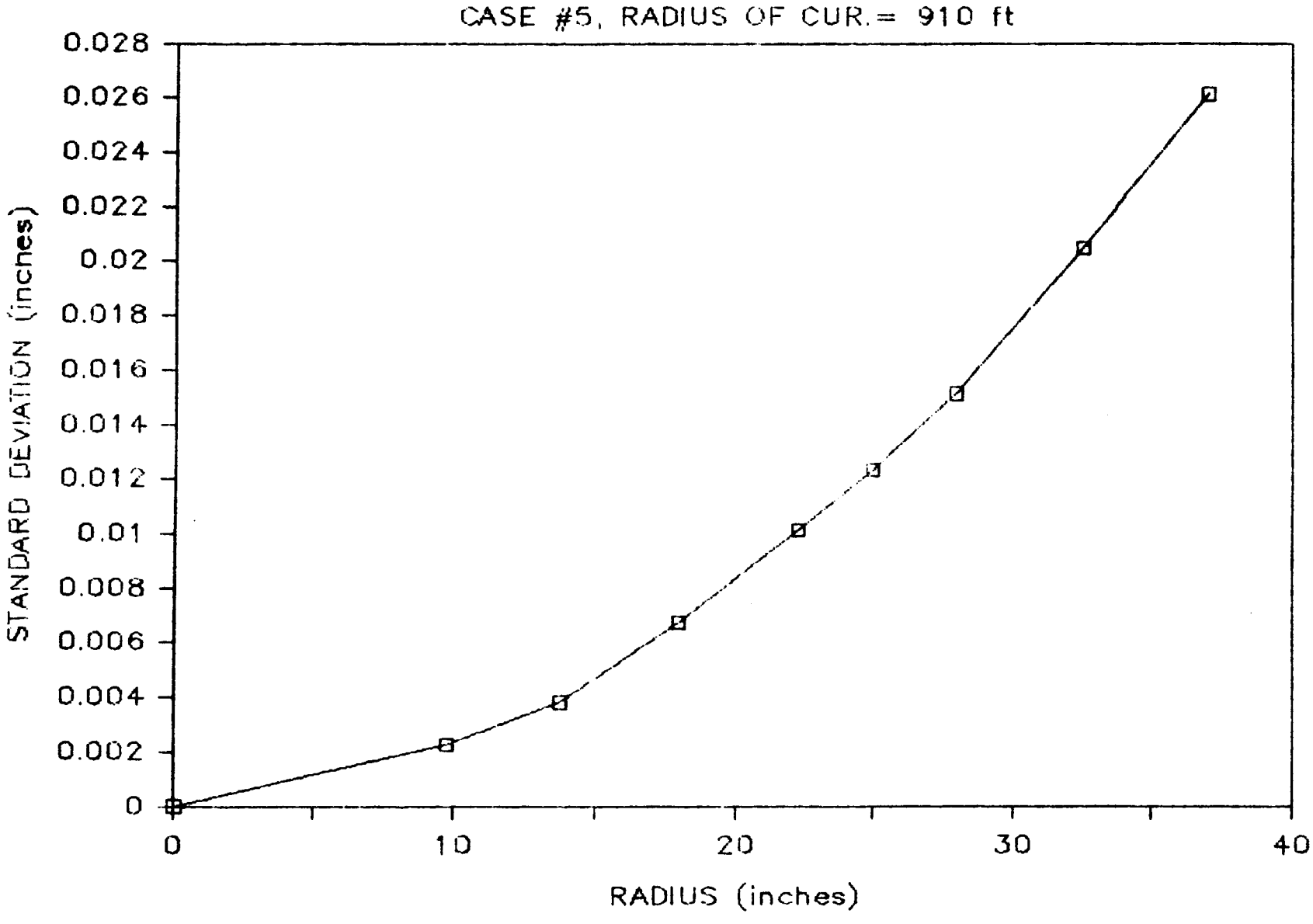

FIG. 13.14 ERROR VS. RADIUS

A second feature of membrane deflection that came from optics data was the impact of lapped, resistance welded seams on the surface. The seams do not follow radial lines and are somewhat difficult to pick out on the overall height versus circumference curves. Figure 13.15 traces membrane deflection along a radial line, and the location of seams are noted.

The most significant local change is seen along the 36 degree radius which crosses the side seam. The deflection did not increase, pass through the mean, decrease, and return to the mean as would be expected in a roll error. Instead, a constant sign error occurred indicating that the membrane did not deflect at the seam as it does away from the seam. This problem could be accounted for by weld shrinkage or additional flexural rigidity in the seam region.

The magnitude of surface slope error was difficult to identify with accuracy, and was not consistent from seam to seam or along a seam. We measured errors in vertical height of 0.003 to 0.004" at the seam and in some cases this error did not die out for six inches. Errors in the worst of these regions were estimated to be one to one and a half milliradians. This error was estimated by computing the surface normal assuming linear height changes between two points and comparing the slope to the membrane areas at similar radii but well away from a weld. Because the breadth and magnitude of error was not consistent, it is difficult to estimate the surface error average of the entire assembly due to seam error.

Finally, the impact of tension on error was looked at in Figures 13.10 through 13.12. The results indicated no changes in the asymmetric manufacturing error. A caveat should be added to this last result. The membrane tension/ring combination was not close enough to the bifurcation load to illustrate amplification effects associated with compressive loads. The commercial design is closer but still well away from the critical load and amplification is not anticipated to be a major problem.

13.5 RING BUCKLING

The load induced on the ring from membrane tension would easily buckle the ring if the membrane supplied no stiffening. The stiffening supplied by the membranes is a function of the method of attachment and can vary widely. A ring buckling test was performed to identify any unusual loads or circumstances not covered in an ideal case.

A light weight two meter ring was built for this test. The ring was formed from a single channel with a tube carrier resulting in

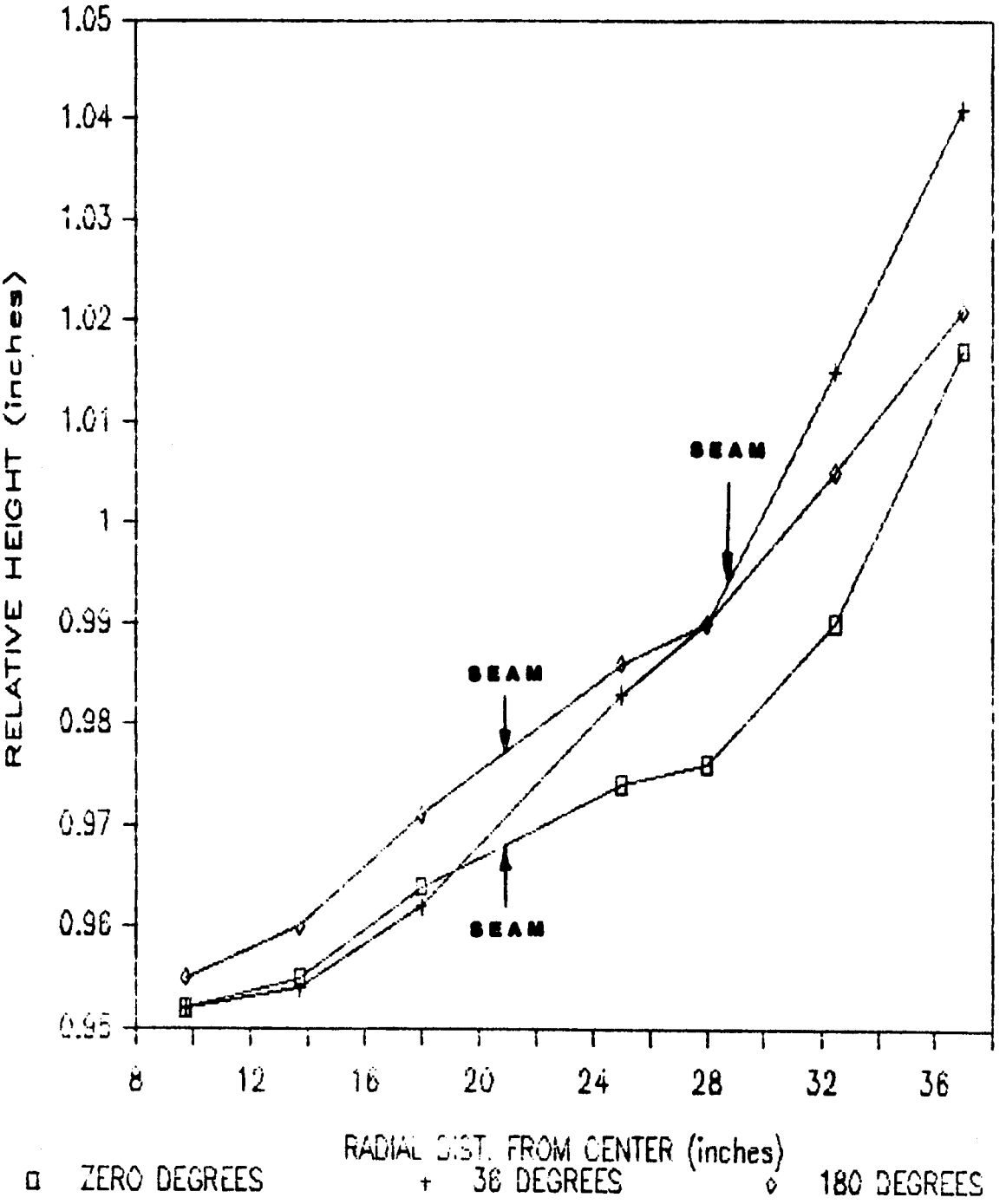

FIG. 13.15 SEAM DETAIL, CASE 5

SOLAR KINETICS INC.

a low in-plane moment of inertia. Ring-only buckling load for this structure was below ten pounds per inch.

The membranes were pre-tensioned with the spring loaded clamps and welded to the ring. Additional tension was added with the inflatable tube.

The tests indicated that radial buckling was quite sensitive to discontinuities in the ring and tube carrier. If the tube carrier was cut to bring the tube down and out of the ring, it was necessary to provide doublers in the area to locally stiffen the section. When operating above the ring only in plane buckling load, careful attention had to be paid to reduce localized reductions in the area moment.

The prototype will not suffer from localized reductions of the in-plane area moment. Radial loads induced by the struts are reduced by the hinged joint in the radial direction. Careful attention to the doublers at support connections must be given, however, to avoid inducing a low deflection mode radial buckle due to the moment of vertical loads about the ring centroid.

One interesting result of this test was the nature of buckling failure. As the radial bifurcation load was exceeded, there was no dramatic change characteristic of stability failures. Instead, a high mode gradual buckling occured and surface error began at the ring and moved towards the center, with increasing load. When tension was removed, it was obvious that buckling occured in the elastic region as the facet returned to its original shape.

13.6 CONTROL TESTING

To aid the design of the control system, characteristics of the heliostat and possible control systems were investigated. These included natural frequency tests of the two meter model of a center mounted transducer.

A fan was connected to a two meter model through a flexible duct. The fan was used to pull a vacuum on the mirror module plenum to deflect the membrane. When deflected, the fan was stopped and the membranes were allowed to oscillate. The oscillation was well damped and only two cycles were measurable. The frequency of the oscillation is plotted against membrane tension in Figure 13.16. At 50 lbs/in. of tension, the natural frequency was 1.5 Hz. It was found that the diameter and length of the flexible duct has significant impact on the natural frequency, but no testing was done to quantify this effect.

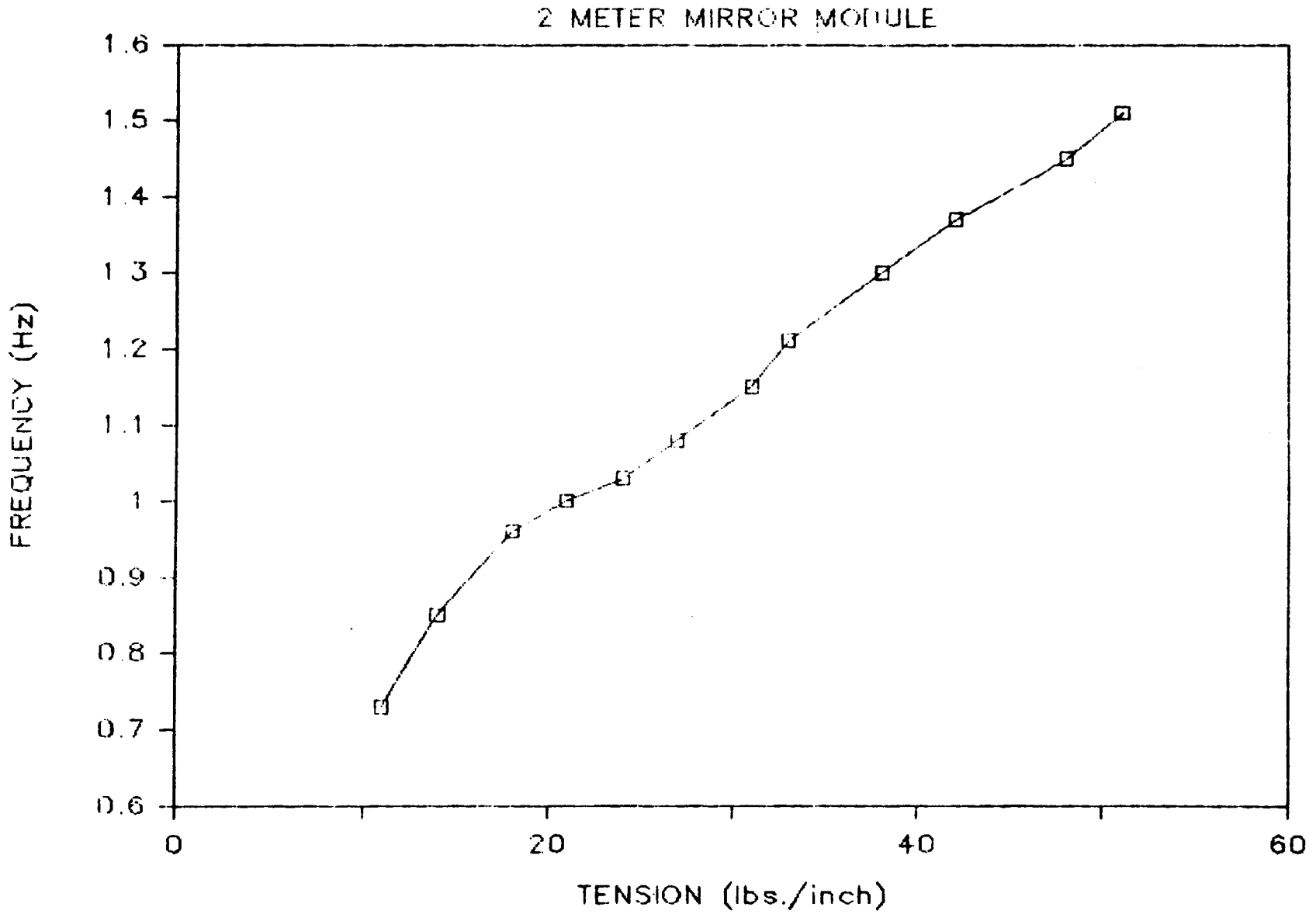

FIG. 13.16 NATURAL FREQUENCY VS. TENSION

If part of the control system is suspended in the center of the membrane by cables, it will have a pronounced natural frequency. This frequency must be much higher than the control frequency or unstable control will result. Testing was done to identify the natural frequency of such a device. A small mass approximating the mass of a transducer was attached to the center of a tightly stretched cable. Natural frequency of the cable was measured between 7 and 10 Hz at cable tensions close to yield. As larger cables are used, the natural frequency is driven by the cable mass and reductions of the mass in the center yield no substantial benefit. The natural frequency increases as the tension increases but maximum tension is limited by the cable yield strength. Based on this, no substantial increase in the natural frequency of a center mounted device is expected.

SECTION 14.0

TEST AND EVALUATION

This section details the necessary tests to evaluate performance of the stressed membrane reflective assembly. The major areas of investigation are beam quality, performance in loaded conditions, survival in loaded conditions, response to oscillatory loads, concave and convex focus controls, and anticipated life of materials. Testing and evaluation of the assembly is to be performed by Sandia.

14.1 SIMILITUDE

The stressed membrane reflector assembly is a system of components that are attached in such a fashion as to couple all deformations in response to external loads. An essential part of the concept is to imply a pre-load. This pre-load (membrane tension) lowers the ratio of survival to total loads and the absolute magnitude of the survival loads as well.

The response of the reflector assembly is inextricably tied to the radius. The numerous and complex couplings between the support structure and mirror module and elements within the mirror module itself preclude simple scaling relationships. Reference to each major scaling issue on a component by component basis is made in the following section. Some caveats are repeated here for the convenience of the reader:

a. Diaphragm tension is a significant stress component in the ring and membrane under survival conditions. Diaphragm tension is a function of size and pre-load as well as pressure differentials and material properties.

b. Out of plane deformation, and the consequent load, is also a significant stress component in the ring and support structure under survival conditions. The truss deflection and ring stiffness are closely coupled and cannot be considered apart from one another.

c. Survival loadings in non-uniform pressure loadings are sensitive to truss and ring stiffness. Stress based designs should consider non-uniform profiles and the moments about the azimuth, elevation, and optical axis of the collector.

d. Optical surface error is a function of size. Careful interpretation of deflections in the structure must be made to scale the results.

e. Optical surface error is related to roll and deflection (inherently coupled deflection modes in any ring). Loading the trusses with dead weight does not simulate wind loadings precisely and in some cases actually reverses the direction of roll deformation as well as failing to reproduce the exact magnitude of surface error.

f. Optical surface error from non-uniform loads is sensitive to both truss and ring stiffness. A development of performance that neglects any consideration of non-uniform pressure profiles will not reflect an accurate approach to support structure design.

We would recommend that an in depth, non-linear, finite element analysis of commercial and prototype designs be accomplished for operational and survival conditions. Stress and surface error scaling could be accomplished through comparison of the two results. We also recommend that those responsible for testing consider the structural work presented in references 2, 9, 12, and 20.

We would also again recommend that careful attention be paid to loading trusses with dead weight to simulate wind load. As the truss is actually connected away from the ring centroid, secondary moment loadings are introduced that can alter the magnitude of the stress and deflection, and in some cases can actually reverse the direction of roll deflection and stress. The response of a stressed membrane reflector assembly to distributed loads across the membrane does not compare precisely to point loads on the ring.

14.2 BEAM QUALITY AND SURFACE ERROR

We would recommend that the Beam Characterization System (BCS) and the Heliostat Characterization System (HCS) are obvious and existing tools to analyze beam quality and surface error. Because both of these systems are sensitive to tracking error, we would recommend that tracking orientation be checked. As this reflector assembly was modified to fit to an existing drive, the moments about the drive are substantially different due to weight, aspect ratio, and the reflective assembly centroid. The drive position may need to be offset based upon elevation angle to account for structural sag.

14.3 DYNAMIC RESPONSE

The response of the reflective assembly to a forcing function is influenced by the coupling between the ring and membrane, diaphragm tension, pressure tubes, plenum air mass, and the rear membrane orifice size. The complexity of the relationship between these factors make the exact prediction of the response of the reflective assembly to an oscillatory wind very difficult. Solar Kinetics proposes that the installed prototype be observed in gusty winds by the HCS with the focal control system providing constant and active pressure control. By this means, the required response time and pressure/volume characteristics can be determined.

14.4 FOCUS CONTROLS

We have provided outputs on the control system to indicate membrane position at the transducer. There are several problems in identifying an absolute reference plane to measure membrane deflection from, particularly in a variable load environment. Sandia may choose to measure membrane deflection with the existing transducer (this approach does have certain problems of independence between the measurement and the measured variable) or one of several other techniques. Video deformation measurements such as those developed by SERI or the HCS itself can be used as indications of surface quality/deformation.

We would recommend that arbitrary values of focus and de-focus displacement not be defined to determine the time response of a system. It is the nature of our control system to rapidly approach a set point (and in some instances, overshoot), and then make slow adjustments to the final position. Consequently, we recommend that membrane position or flux intensity be presented as a function of time.

SECTION 15.0

PROTOTYPE FABRICATION

The fifty square meter prototype fabricated by Solar Kinetics, Inc. and installed at the Central Receiver Test Facility (CRTF) at Albuquerque, New Mexico represents the culmination of many efforts in this development contract. The prototye design was influenced by several factors, dominated by an effort to fabricate a test article representative of the commercial design. Each component and final assembly are discussed in the following sections.

The most significant departures between commercial and prototye design was size. The prototype incorporates approximately fifty square meters of aperture, while the commercial design provides one-hundred and fifty square meters. As our development effort did not include drives or supports, our prototype was constrained to mount on existing second generation heliostat drives and pedestals. In particular, our reflector assembly was mounted to a Northrup pedestal/drive assembly at the CRTF. Consequently, some scaling relationships are included in our discussion of departures between commercial and prototype design.

15.1 MEMBRANES

Membrane fabrication requires several discrete steps handled in a linear, continuous flow. Production at the large volume level is summarized in Figures 7.1, 7.2, and 7.3. Design issues were discussed in section 3.0. Substantial effort was made to mimic the commercial design in the material selection and fabrication method used for the prototype membrane. A summary is presented in Table 15.1.

Membrane thickness considerations were based upon operating stress, survival stress, handling constraints, and cost per unit of aperture. The prototype membrane thickness and tension was identical to the commercial design. As such, it is representative of the operating condition, the handling problems, and costs.

Survival loadings, on the other hand, are based upon a combination of pre-load and diaphragm stress. Although pre-loads are identical in each case, diaphragm stress is a function of the ratio of center deflection to radius. In the commercial design proposed, the pre-load condition is of the same magnitude as the survival load. The prototype has an identical pre-load, but overall loads at survival conditions will be decreased by

TABLE 15.1

MEMBRANE SIMILITUDE

Item	Commercial Design	Prototype Design
Size, nominal aperture	1615 ft.^{2} (150m^2)	513 ft.^{2} (48m^2)
Membrane Structural Material	5000 series aluminum	5052-H34
Membrane Thickness	0.010 inches (0.25mm)	0.010 inches (0.25mm)
Sheet width	55 inches (1.4m)	30 inches (0.75m)
Reflective Material	Silvered polymer	3M ECP 300® silvered acrylic
Raw material format	Coiled stock	Coiled stock
Preparation	Stretcher leveled	Reverse bend
	Wash and abrade	Wash and abrade
Lamination	Continuous, on coil line	Continuous, on coil line
Cut reflective film	NC Laser	Manual, knife
Seal edge	Acrylic overcoat, spray	Acrylic tape, 3M ECP 244®
Shear	NC Laser	Sheet metal shear
Sheet positioning	Vacuum chuck table	Vacuum chuck table
Welding	Specialized seam resistance	Specialized spot resistance
Shipping	Re-coil	Re-coil
Initial load per membrane	60 lb./in. (10.6 kN/m)	60 lb./in. (10.6 kN/m)

approximately twenty percent because the prototype has a different radius. We elected to provide a test article with the same initial tension to mimic operation. Survival loads in the membrane will be somewhat lower than in a large area assembly, though it should be noted that even a full scale membrane is stressed to only fifty percent of yield at survival conditions.

Prototype fabrication did illustrate an important source of optical error relating to variations in the base stock: a variation in length across the width of the sheet. The length was greatest at the center. This problem did not appear to be substantial in the two meter bench test model, and consequently, was not anticipated in the prototype. In both cases, the sheet would not lay flat of its own accord. The vacuum platen allowed us to "sweep" the waves out and then weld. When the vacuum was released, the waves reappeared. (See Figures 15.1 and 15.2)

We anticipated that membrane tension would also serve to eliminate any waves, and it did substantially reduce the problem. Preliminary observation of the prototype surface with the HCS monitor indicated that some scallop occured between each seam reducing the available aperture by three to five percent (qualitative judgement). We attribute this edge effect to the length variation. One panel retained a small wavy area in its center, but the aperture loss due to that error is probably less than one or two percent (also a qualitative judgement).

A leveler was provided in the manufacturing scenario, and would likely correct the problem. The prototype did not benefit from leveling. Instead, only a reverse bending load was applied to remove coil curvature. We therefore, do not anticipate this edge effect to be a problem with the commercial design manufacturing scenario, even with the increase in sheet width.

Although the vacuum platen did not prove to be successful at eliminating a wave problem, it remains an essential part of the membrane fabrication for several reasons. First, even relatively constant length sheet will not lie flat due to residual stresses from temper. It is essential to maintain flatness during the welding operation. The vacuum provides an excellent chuck to hold large area sheets under uniform loads and avoid localized clamping distortions. With over 50000 pounds of clamping force, the relative position of two sheets is absolutely maintained, without motion, during the welding process.

Contractural constraints prevented Solar Kinetics from purchasing a seam resistance welder. Consequently, we modified an existing spot welder to automatically increment and weld at successive points much as a seam welder would perform. With the vacuum providing the enormous clamping force, there was no need to spot weld at seperated points and then fill in each area. The welding

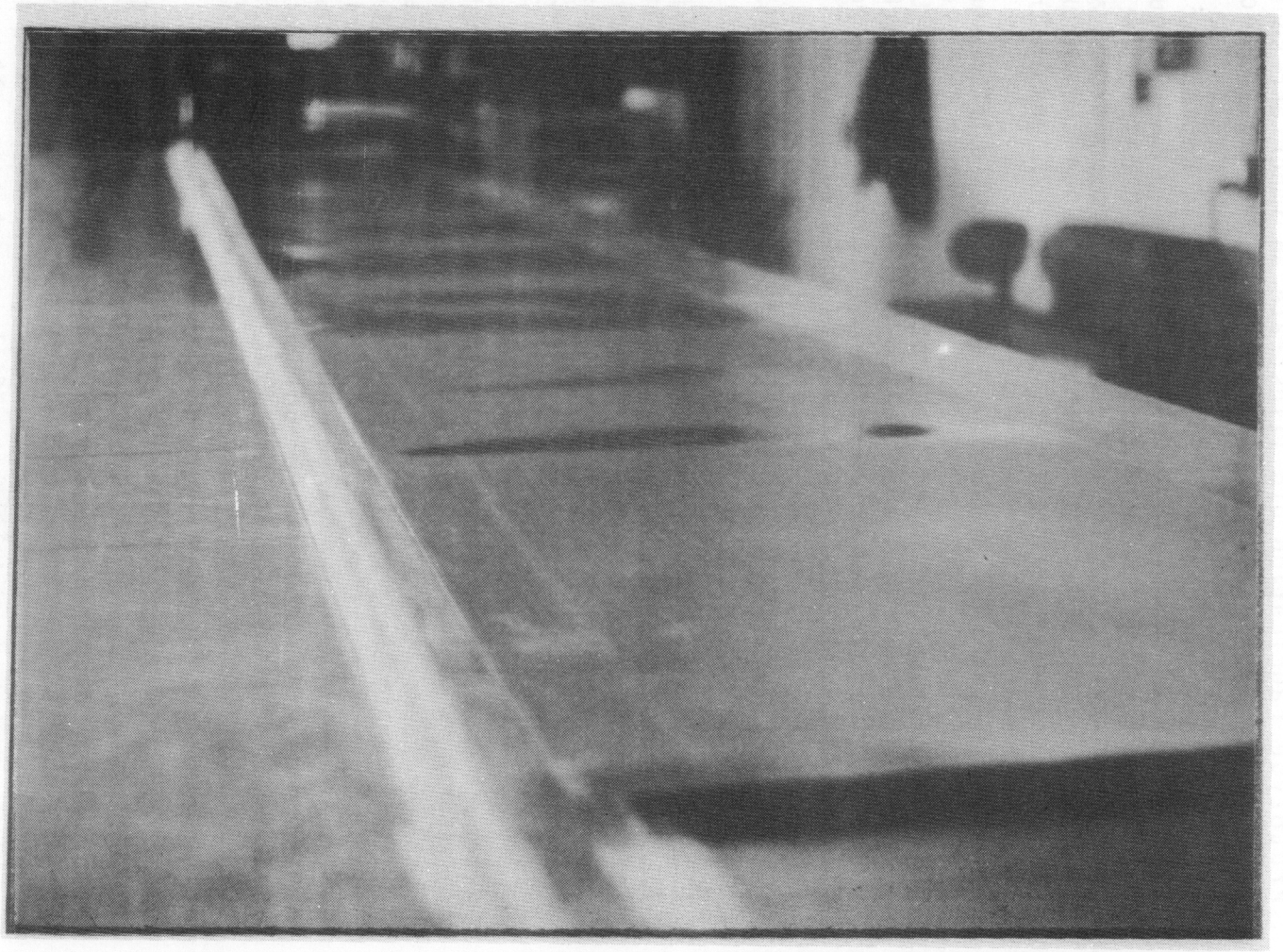

FIGURE 15.1 MEMBRANE MATERIAL AT WELD STATION, NO VACUUM

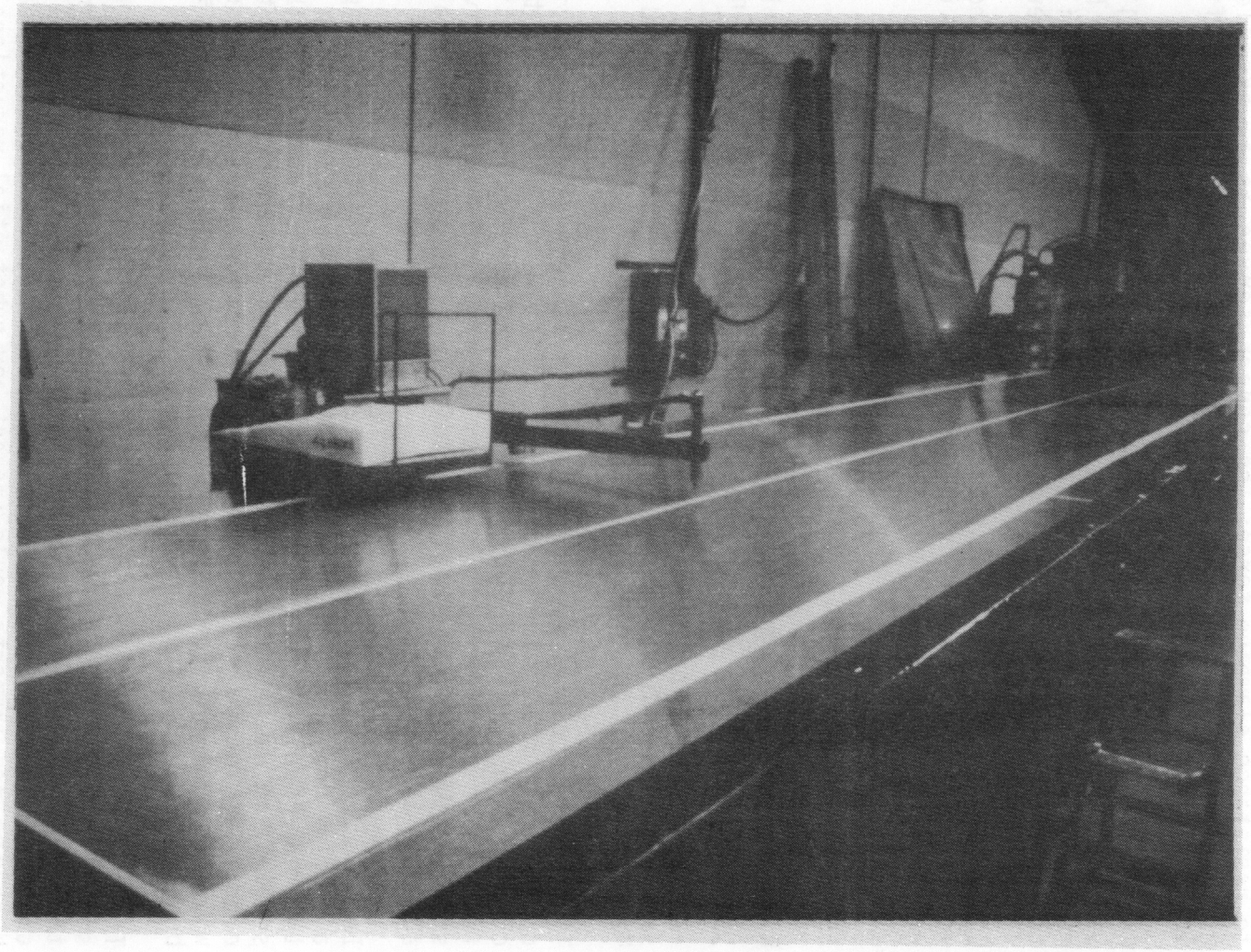

FIGURE 15.2 MEMBRANE MATERIAL UNDER VACUUM

was started at one end, progressively moving to the opposite end precisely as the production machine would perform.

A copper buss bar was also provided to serve as the lower electrode exactly as proposed in the commercial manufacturing scenario. The bar provides a solid surface at the joint, without obstructing the welding head. The buss serves two useful functions: the sheet metal is not locally deformed or dimpled due to resistance clamping force; the copper serves as an excellent heat sink to prevent temperature problems with the polymer film located only a fraction of an inch from the weld zone.

Finally, as each seam was welded, we moved the sheet laterally; each successive free edge being welded to the next sheet. The membrane was rolled as each weld was made, substantially similar to the process shown in the commercial manufacturing seam welder.

Cleaning and lamination was accomplished on a coil line as shown in the commercial manufacturing scenario. No sheet preparation was performed at the welding station.

15.2 RING

Ring production and design issues were discussed earlier (sections 3.0 and 9.0). The ring was also fabricated in a fashion similar to the commercial design and was scaled to represent anticipated response in the smaller prototype. A summary of the differences in the two developments is provided in Table 15.2.

The cross-sectional area of the ring is largely determined by the operating and survival stresses. Operating stress is the compression induced by pre-load plus the bending load resulting from out of plane deflections from gravity and wind. Survival stress results from similar loadings; diaphragm stress is also added to the pre-load.

In an effort to scale the ring to the smaller aperture prototype, a similar cross-sectional area was maintained and a reduction in the out-of-plane moment of inertia was applied. To achieve this scaling, it was necessary to increase the wall thickness of the ring. As indicated in the previous section, survival stresses will be somewhat lower in the prototype than at full scale because diaphragm tension is not linear with aperture.

The planar moment of inertia is not truly scaled to reflect the smaller aperture as angles were added to provide tube support. the commercial design incorporates tube support in the rolled cross-section. It should be noted, however, that the in-plane buckling requirements would prevent any substantial reductions in

TABLE 15.2

RING SIMILITUDE

Item	Commercial Design	Prototype Design
Radius	7m (23 ft.)	4m (13 ft.)
Ring structural material	5000 series aluminum	5052-H32
Ring thickness	2.3mm (0.090 in)	3.2mm (0.125 in)
Ring height	300mm (12 in)	150mm (6 in)
Ring width	76mm (3 in)	38mm (1 1/2 in)
In plane area moment	2.0E-6m^4 (4.9 in^4)	1.7E-6m^4 (4.0 in^4)
Out of plane area moment	1.8E-5m^4 (44 in^4)	7.1E-6m^4 (17 in^4)
Raw material format	Coil Stock	Coil Stock
Preparation	Stretcher leveled Wash and abrade	Stretcher leveled Wash and abrade
Cross-section forming	Continuous roll form	Continuous roll form
Circular forming	Pyramid roll-continuous	Pyramid roll-sectional
Final attachment	TIG weld	TIG weld
Tube support	Integral to rolled shape	Angles added
Shipping	Made at site	Prefab, shipped in sections

area moment as the radial loads in operation are identical, and at survival, the loads are decreased by only twenty precent. The prototype does reflect the buckling response of a commercial design.

Out-of-plane response, causing asymmetric error, is determined by the distance between supports, roll enhanced stiffness from the membranes, and the out-of-plane moment of inertia. The area moment was reduced in scale as indicated. The distance between supports is cut in half, however, and this cannot be reflected in the prototype if the basic quantity of trusses remains unaltered. The moment arm against which roll occurs is reduced and this will counter the the shorter span to some extent. We estimate, however, that asymmetric error in the prototype will only be approximately sixty to seventy percent of that which would occur at full scale, and stress values at survival will be approximately the same ratio.

The only apparent difference in ring manufacture is that the ring was pre-fabricated in sections, shipped, and butt welded at the site. In the commercial design, the ring is fabricated in a continuous section and butt-welded at one point only. We anticipate that the prototype fabrication is actually somewhat worse than the commercial procedure because of the difficulty in alignment of three separate pieces into a single plane and the additional heat input from the welds.

Ring planarity was a major issue, as any non-planar deformation translates as optical error. Following development of proper tooling, we found that roll bending could be controlled quite well. After roll, the planarity of any one-third section was plus or minus 0.25mm (0.010 in). When these elements were welded together, planarity was plus or minus 1.0mm (0.040in). The error was periodic between supports. Planarity was checked using dial indicators mounted on the end of a post and arm assembly (see Figure 15.3) during each phase of assembly and again at the site to assess the error contribution of each stage of fabrication. Following a final dimensional check, the ring was separated into thirds and shipped to the site.

15.3 SUPPORT

The mirror module support primarily consists of six cantilever trusses connectd to a hub. The hub provides for the tracking drive mount and houses the focus control actuation assembly. The trusses are braced with tie rods and attach to the mirror module through six hinges. Design issues are discussed in sections 3.0 and 4.0; fabrication is described in section 7.0 for the commercial design. A summary of the commercial and prototype

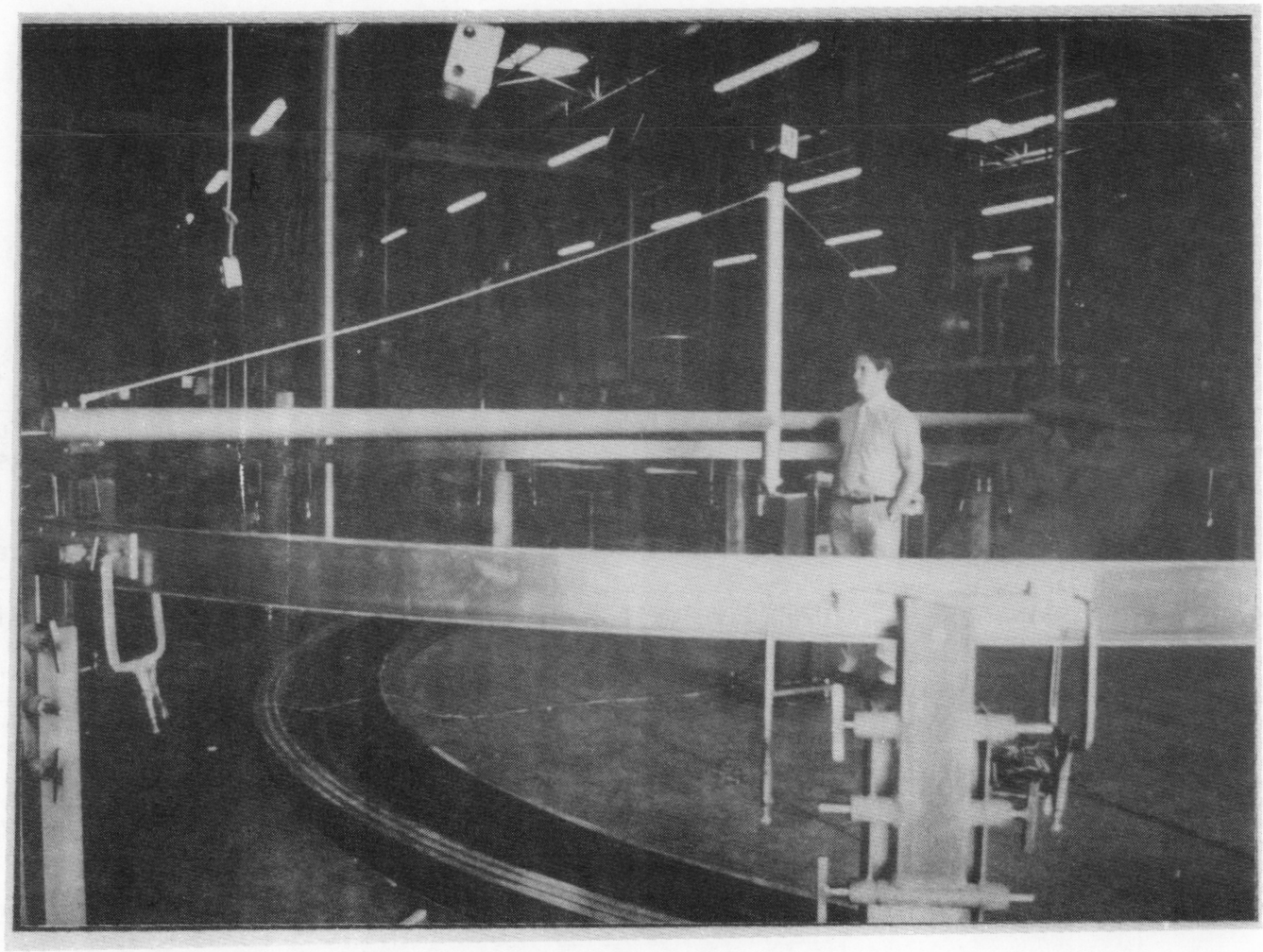

FIGURE 15.3 RING - MEASURING PLANARITY WITH DIAL INDICATORS

TABLE 15.3

SUPPORT SIMILITUDE

Item	Commercial Design	Prototype Design
Truss-size	1.4m(54") deep x 6m(236") long	0.75m(30") deep x 3.3m(132") long
Truss quantity	6	6
Hub size	1.8m(72") dia x 1.4m(54") deep	1.2m(48") dia x 0.75m(30") deep
Structural Material	Carbon Steel	A36 Carbon Steel
Raw material format	Coil stock	Coil stock
	Cold rolled bar stock	Cold rolled bar stock
	Hot rolled shapes	Hot rolled shapes
Corrosion protection	Paint	Paint
Welding	Robotic MIG	Manual MIG
Truss out of plane area moment	5.6E-4m^4 (1350 in^4)	1.7E-4m^4 (404 in^4)
Truss in plane area moment	2.8E-6m^4 (6.8 in^4)	3.7E-6m^4 (8.8 in^4)

system is provided in Table 15.3. Material selection and fabrication methods were quite similar in the two designs.

Scaling of the support structure is a more complex problem than is immediately apparent. Initially, the rear structure appears to simply present a cantilever truss, fixed on one end with a point load on the opposite end. The ratio of commercial to prototype properties in the truss are:

Area moment ratio	3.3
Length ratio	1.8
Load ratio	3

The rear structure is coupled to the mirror module and, consequently, the out of plane ring/membrane response must be considered. The two-term linear approximation for stressed membrane response was used to determine deflection versus load (ie spring constant) for the two designs. The ratio of spring constants, commercial to prototype is six.

The coupling between the rear support structure and mirror module result from their connection. As the truss tip deflects, so does the ring . If all trusses see a uniform load, the mirror module moves as a rigid body and no surface error is induced by the truss from an out of plane deflection (The hinge effectively isolates the ring from moments about its cross-section). If truss loading is non-uniform, two types of surface error are induced: secondary asymmetric error (see Figure 2.2) and tracking error.

Secondary asymmetric error is defined as the surface error that occurs due to ring sag between periodic supports due to the non-uniformity of the loads. This error is super-imposed on the primary asymmetric error resulting from the uniform wind load. Our estimate of secondary asymmetric error indicated that this term was not particularly significant in truss design.

Tracking error occurs when one side of the mirror module is loaded more heavily than the other (eg, the pressure center of the wind profile does not coincide with the optical axis) and moments about the azimuth and elevation axis occur. This type of non-uniform load occurs even in very uniform velocity profiles due to aerodynamic effects. The result is a combination of rigid body rotation of the mirror module (the optical axis is displaced) and ring deflection (each differential surface normal is displaced). Because the ring must physically deform to accommodate varying truss deflections, the spring constant of the mirror module affects overall performance.

The surface error of a reflector is not simply proportional to deflection, but can better be described in terms of the ratio of deflection to radius. In both asymmetric error and rigid body tracking error, the relationship between error and the ratio of deflection to radius is roughly linear through small angles of rotation and ring deflection.

If the supporting structure is considered without regard to the ring and membrane (ie coupling is ignored), the prototype trusses will deflect approximately twenty percent of the total value in the commercial design, and see approximately one-third of the stress. The surface error in the prototype, in response to non-uniform loadings, would be twice the deflection value.

Calculations for surface error in the prototype due to non-uniform profiles where coupling is considered were not formally conducted. We would note, however, that the mirror module stiffness was more effective at limiting error than increased truss stiffness in the commercial design. In other words, further increases in truss stiffness had diminishing impact upon tracking error. Consequently, coupling is likely to be important in attempting to scale surface error from the prototype to the commercial assembly. Prototype trusses do need to provide greater stiffness to imitate surface error than would be calculated through a simplified cantilever beam approach.

15.4 CONTROLS

The focus control of a stressed membrane reflector assembly consists of a position transducer, fan actuator, and logic circuits. Design issues are discussed in section 5.0. A summary of the commercial and prototype system is provided in Table 15.4.

The transducer used in the prototype and commercial design, an LVDT, is identical with the exception of range. The commercial design must accommodate a larger range for similar focal lengths. The mount is also somewhat different. The LVDT arm is mounted at the quarter point of the ring, but the LVDT is actually external to the heliostat. The reduction in ring height did not allow for an internal mounting arm of reasonable rigidity. Attachment to the front membrane is accomplished through a rigid link, as in the commercial design, the link is simply longer.

As the LVDT is not mounted at the center of the heliostat, some reduction or deamplification of the membrane deflection does occur. This deamplification is similar though not identical for the two mirror modules. It should be noted that the actual deflection measured at the transducer is actually smaller in the prototype reducing the effective focal length resolution. We do

TABLE 15.4

CONTROL SIMILITUDE

Item	Commercial Design	Prototype Design
Transducer	LVDT	LVDT
Mounting Position, from membrane centerline	6m(236")	3.1m(123")
Mounting Position, with respect to supports	Quarter point	Quarter point
Mounting Position, with respect to plenum	Inside	Outside
De-amplification of center deflection	27%	35%
Deflectin at transducer for 300m(1000 ft.) focal length	10.9mm(0.43")	4.5mm(0.18")
Actuator	Propeller fan/motor	Propeller fan/motor
Blade diameter	450mm(18")	300mm(12")
Motor size	0.19 kw (0.25 Hp)	0.09 kw (0.12 Hp)
Mounting position	Centerline rear membrane	Centerline rear membrane
Pressure regulation	Speed controlled	Speed controlled
Digital logic	Dedicated microprocessor	Programmable controller
Analog logic	Dedicated analog circuit	Discrete analog circuit

not anticipate a problem in this area, however, as the LVDT has excellent accuracy and repeatability.

The fan, which provides for focus and defocus of the mirror module, is smaller and provided with less power than the commercial design. Based upon fan scaling laws and the inefficiencies of the straight inlet bell of the prototype, we estimate that the volumetric flow rate has been reduced by a factor of three to five.

The logic controller is comprised of several discrete parts available as "off-the-shelf" components. Displays are provided as are voltage outputs for the analog circuits. These outputs and displays are not typical of the commercial design, but are provided for testing purposes. The operational logic of the controller, however, is identical to the commercial design.

15.5 SITE ASSEMBLY

The assembly of materials at the site for the commercial design was discussed in section 9.0. Prototype assembly proceeded in a fashion quite similar to commercial design. Some accommodation of financial restraint was made for a single prototype unit.

Extensive use of vacuum platens as an effective method for handling light gage sheet was made. In an effort to reduce cost, only one platen, rather than the two identified in the commercial manufacturing scenario, was used. The frame assembly served as the lifting device. The ring was fabricated at the factory in three sections and butt-welded into a complete assembly at the site. Resistance spot, rather than seam welding was used to attach the membrane to the ring. Mechanical deformation of the ring flanges (crimping) was done incrementally rather than continously.

The supporting frame assembly was manufactured at the factory and site fabrication was limited to bolted assembly. Figure 15.4 shows the frame assembly at the site. This assembly was used as a lifting bar during manufacturing of the mirror module. The fan assembly was installed in the hub prior to final attachment between the ring and trusses.

Figure 15.5 shows the membrane after it was rolled out onto the platen, Figure 15.6 demonstrates the vacuum chucking ability of the table. Membrane handling does require attention but is not likely to be a significant cost issue in these gages. The vacuum platen provided an exceptionally good method for handling and fixturing large area, thin sheets.

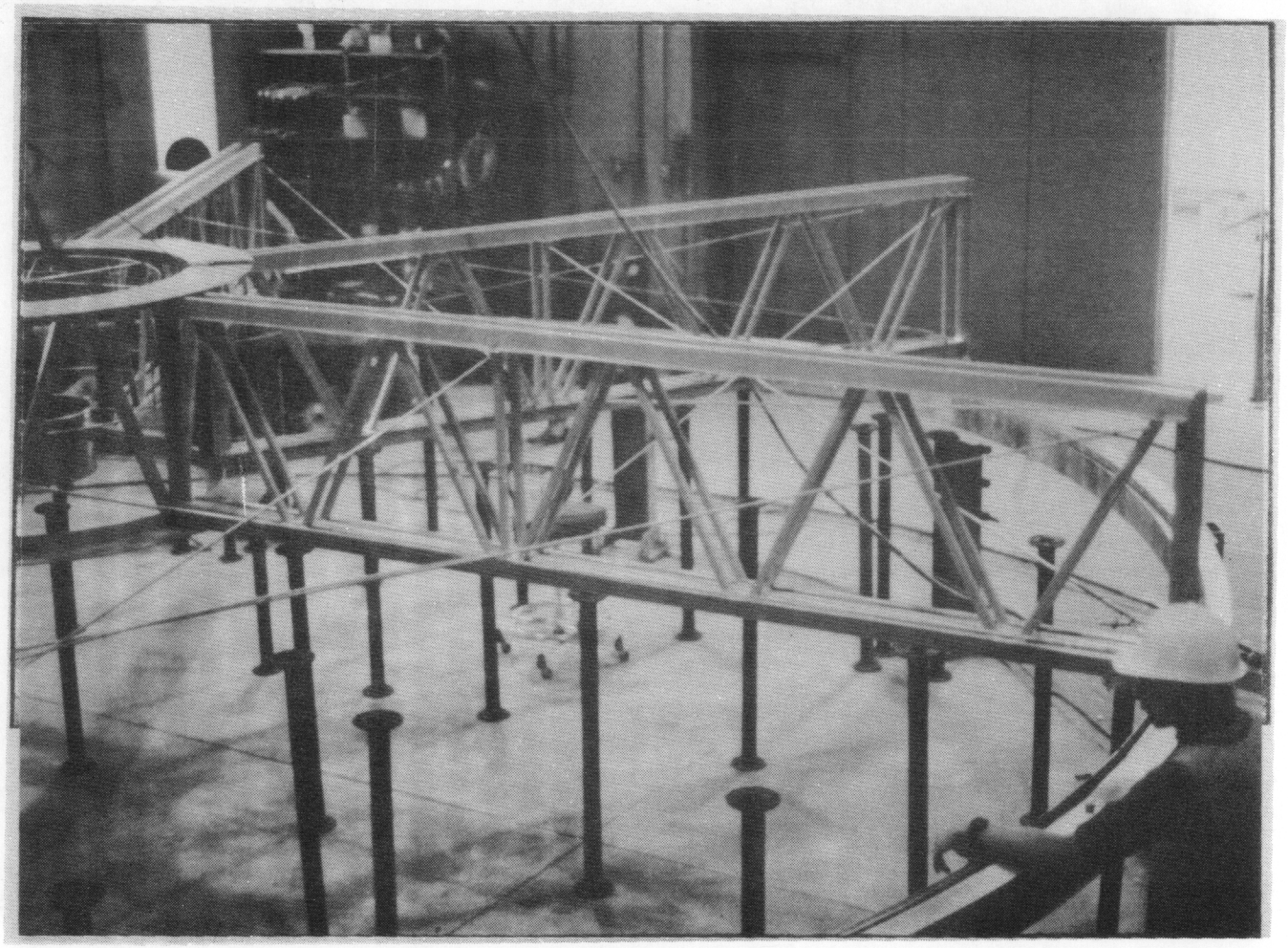

FIGURE 15.4 FRAME ASSEMBLY

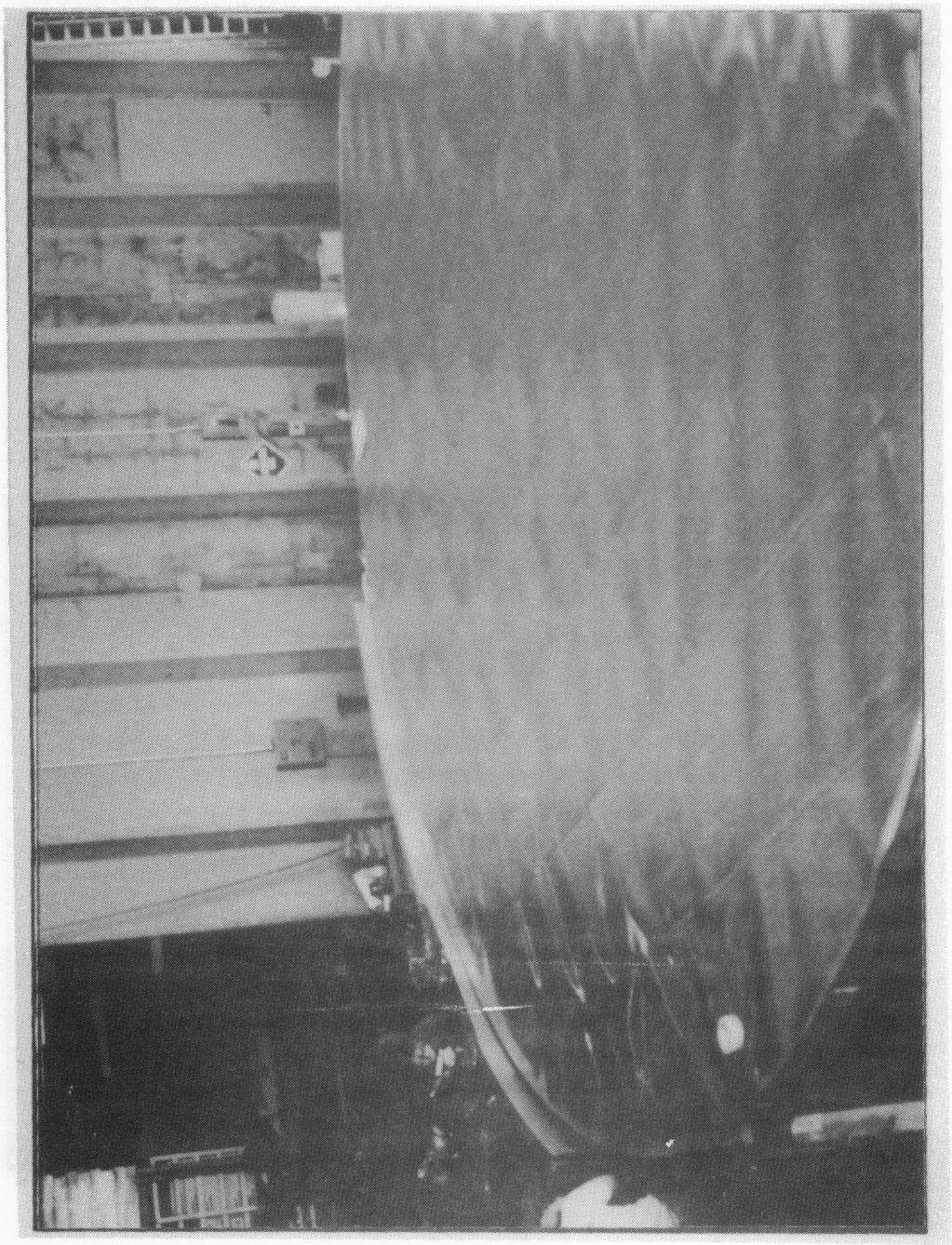

FIGURE 15.5 MEMBRANE ON ASSEMBLY PLATEN AT SITE

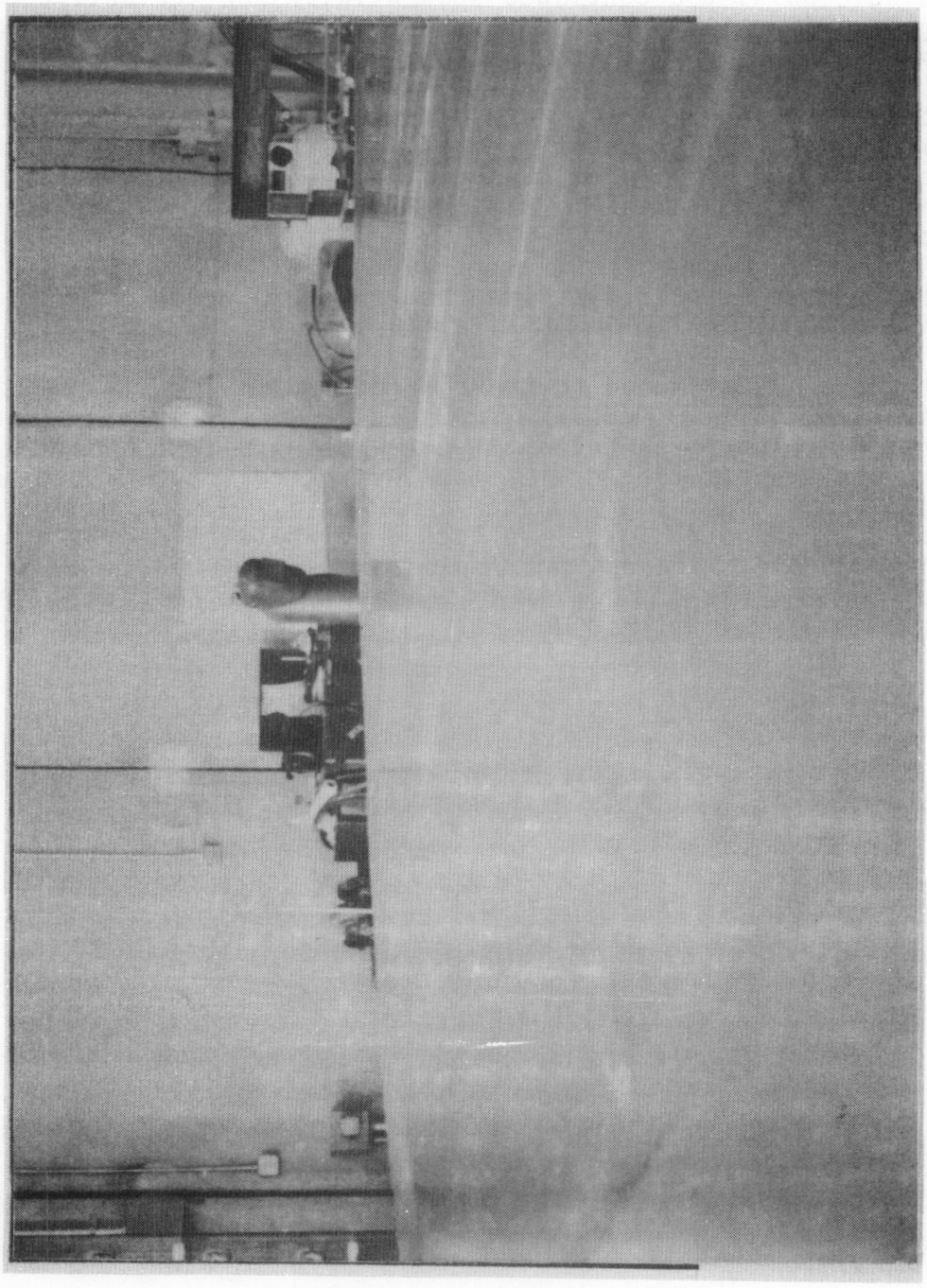

FIGURE 15.6 MEMBRANE VACUUM CHUCKED TO SURFACE

The commercial manufacturing design for membrane to ring attachment used a rolling seam resistance welder. To avoid purchase of this piece of equipment, a spot welder was mounted to a carriage that moved about a circular track. The carriage motion was automated to provide regular weld spacing. It should be noted that we did not attempt to take advantage of the incremental weld assembly fabrication technique; welding began at a single point and continued sequentially for the entire 360 degrees without intermediate positioning welds. Figure 15.7 shows a close up of the membrane to ring weld joint in process.

After welding was complete, the vacuum chuck was released and the tube was partially inflated to enhance membrane to ring coupling. Mechanical deformation of the ring flange (see Figure 15.8) also proceeded in incremental fashion. The membrane was tensioned in progressively tighter bends and on each side of a diametral line before making the next crimp approximately ninety degrees away. This approach should simulate the four head crimping machine recommended in the commercial site manufacturing facility.

The frame was attached to the completed mirror module, and the reflector assembly was transported to an existing second generation Northrup heliostat drive/pedestal. The unit was bolted to the existing drive, and the controls were wired in. Figure 15.9 shows the completed assembly in place. Figure 15.10 shows the reflected image, in focus, of the stressed membrane mirror module. The estimated spot size is three and one-half to four meters (12-13ft.) in diameter. The slant range is approximately 320 meters (1050 ft.).

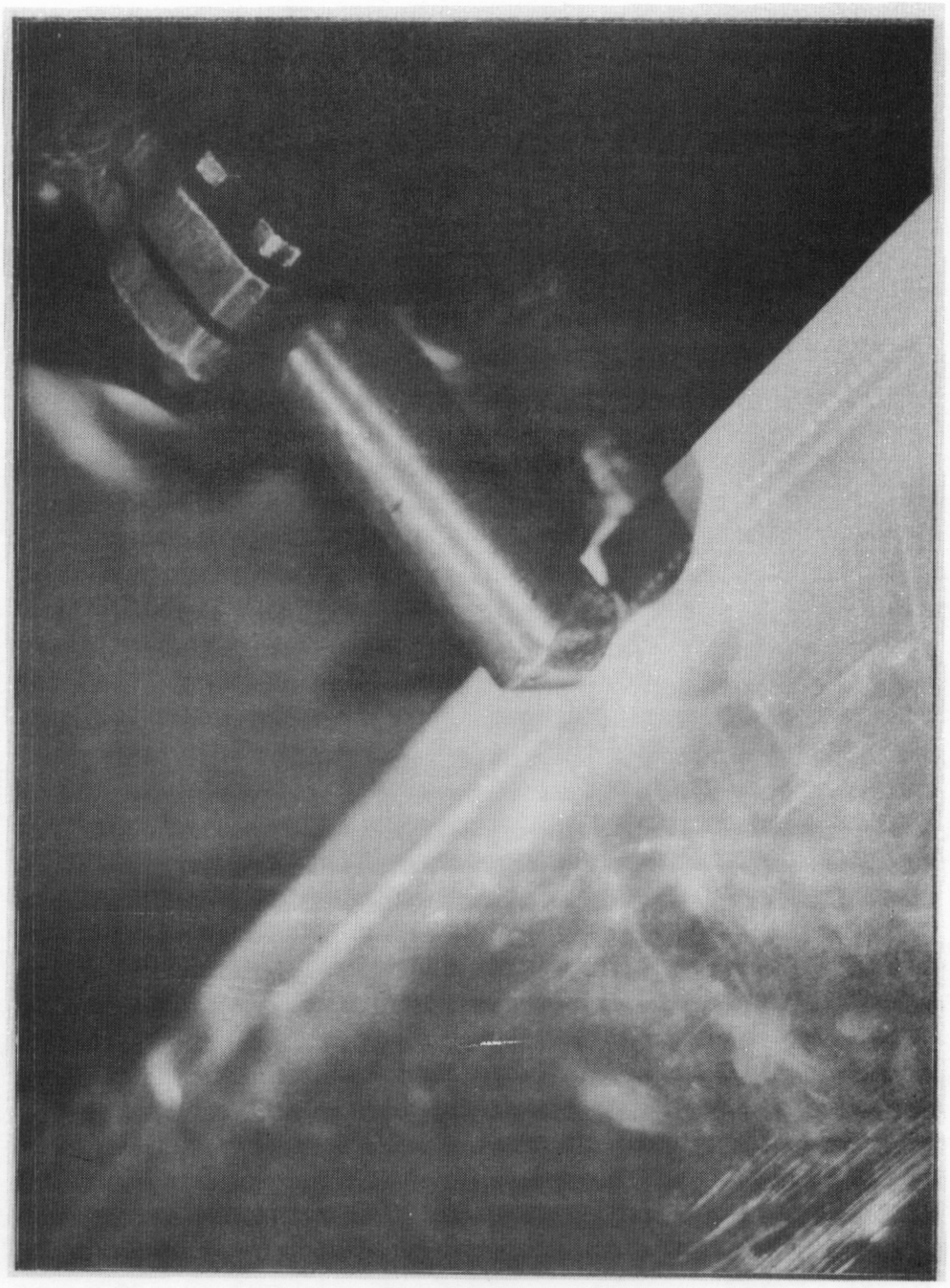

FIGURE 15.7 MEMBRANE TO RING WELD DETAIL

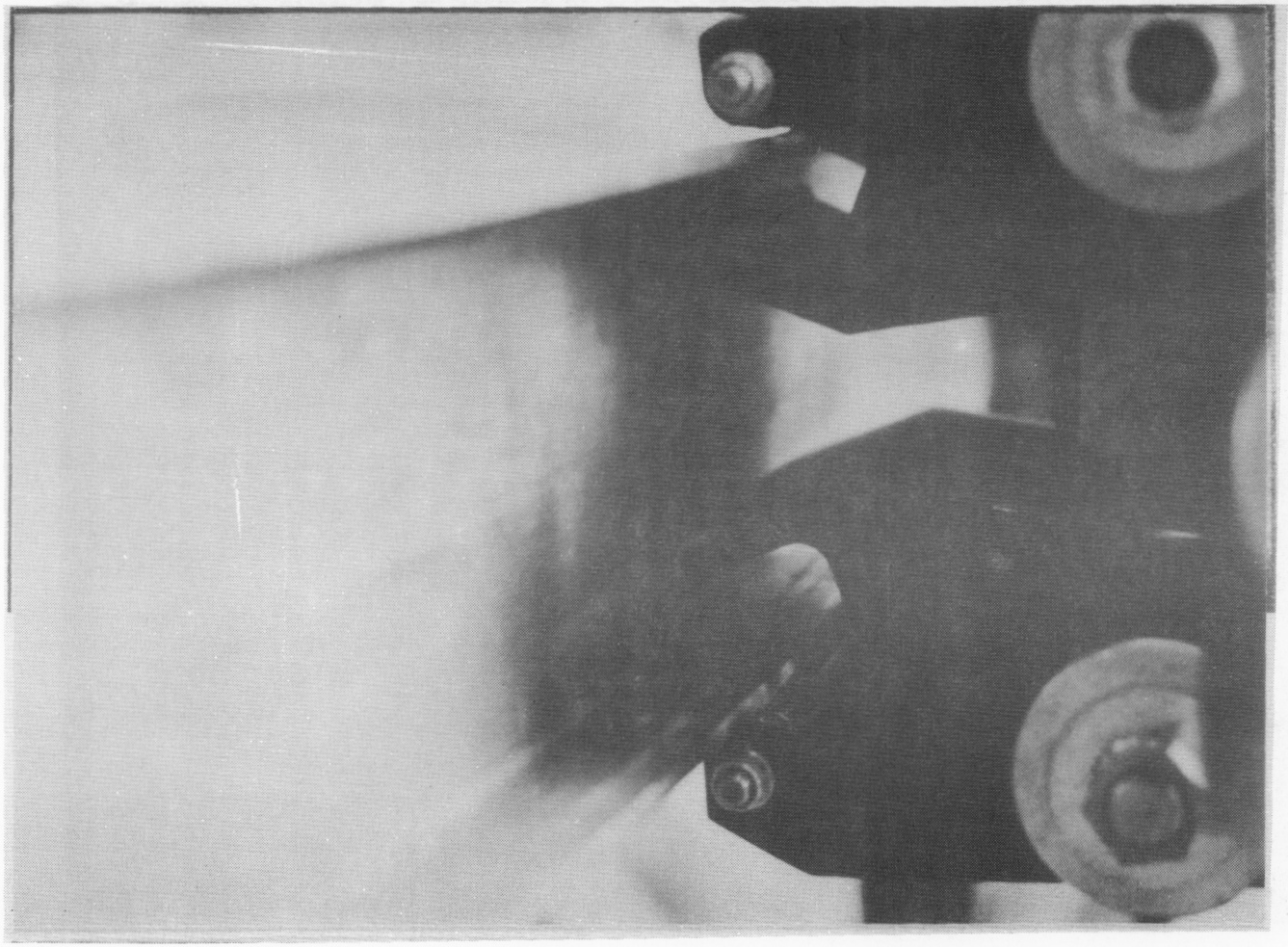

FIGURE 15.8 MECHANICAL DEFORMATION OF RING FLANGE

FIGURE 15.9 COMPLETED ASSEMBLY

FIGURE 15.10 REFLECTED IMAGE

SECTION 16.0

CONCLUSION

The stressed membrane mirror module makes extremely efficient use of material to present an optical quality surface in response to a variable load environment. This approach to concentrator design offers substantial potential for cost reduction in central receiver applications. The concept is not merely innovative as an end to itself; rather it provides for a significant reduction in material usage and is easily fabricated by continous coil line processes.

As a major departure from conventional design, the stressed membrane carries loads through tension rather than bending. A pre-load is imposed upon the mirror module; this initial tension lowers the ratio of survival to total loads as well as reducing the magnitude of the survival load itself. Consequently, loadings on the optical surface are less variable.

In addition to providing an efficient structure for load transfer, the membrane actively responds to changes in load. The focus is regulated by altering the pressure differential across the front surface. The pressure actuator is a simple, axial fan with speed control.

Our development effort indicates that the stressed membrane reflector assembly is a suitable structure for taking advantage of cost savings in the pedestal/drive assemblies associated with size as well as a reduction in reflector assembly costs. We estimate that first year costs of a stressed membrane reflector assembly (per square meter) would be $28.30*, the remaining assemblies $26.96, for a total of $55.26 per square meter. This compares with $71.19 for a second-generation glass-metal design optimized and increased to an identical aperture.

Our optimization work resulted in a monolithic mirror module with 150 square meters of aperture. Mirror module weight was approximately 3kg/m^2(6.7lb./m^2, 0.6lb./$ft.^2$), the total reflector assembly weight was 9.3kg/m^2(20.4lb./m^2, 1.9lb./ft^2). The ring and membrane are fabricated from aluminum, a silvered polymer provides the reflective surface, and the support structure is steel. The design is largely stress critical; that is, material requirements are determined based upon stress in high winds and not by deflection or optical quality.

* All costs expressed in 1985 dollars and based upon the 50000th unit produced in a volume of 50000 per year.

The prototype, assembled and installed at the CRTF in Albuquerque, is a reasonably accurate representation of the commercial design. Our experience with this prototype and glass-to-metal heliostat facets would suggest that the stressed membrane concept would be less expensive to fabricate in even moderate volume.

The stressed membrane is an important and successful vehicle to reduction in concentrator costs for central receiver technology.

REFERENCES

1. "Stressed Membrane Heliostat," T.D. Brumleve, et al., SNLL, from "A Description and Assessment of Solar Central Receiver Systems Technology," SAND 82-8023.

2. "Technical and Cost Benefits of Lightweight, Stretched Membrane Heliostats," L.M. Murphy, SERI/TR-253-1818.

3. "Second Generation Heliostat," McDonnell Douglas, SAND 81-8177.

4. "Optimization of the Second Generation Heliostat Design and Specification," McDonnell Douglas, SAND 82-8181.

5. "System Performance and Cost Sensitivity Comparisons of Stretched Membrane Heliostat Reflectors...," L.M. Murphy, et al, SERI/TR-253-2694 Draft.

6. Sandia specification A10772, attachment III to RFQ 91-8808, SNLL.

7. "Wind Loading on Solar Collectors...," E.J. Roschke, JPL-1060-66.

8. "Second Generation Heliostat Development for Solar Central Receiver Systems," Vol. II, Appendix E-System Studies, Northrup, Inc., SAND 79-8194.

9. "Analytical Modeling and Structural Response of a Stretched Membrane Reflective Module," L.M. Murphy, et al., SERI/TR-253-2101.

10. "Wind Loading on Solar Collectors," S. Bhaduri, L.M. Murphy, ASME/84-WA/Sol-16.

11. "Structural Design Considerations for Stretched Membrane Heliostat Reflector Modules with Stability and Initial Imperfection Considerations," L.M. Murphy, SERI/TR-253-2338, Draft.

12. "A Variational Approach for Predicting the Load Deformation Response of a Double Stretched Membrane Reflector Module," L.M. Murphy, SERI/TR-253-2626, Draft.

13. "CSIRO Radio Telescopes," Jeffrey, Annals New York Academy of Sciences.

14. "Second Generation Heliostat Detail Design Report," McDonnell Douglas, SAND 78-8192.

15. "Metals Handbook, Welding and Brazing," American Society for Metals, 8th edition.

16. "Wind Forces and Pressures," Cohen, et al., Annals New York Academy of Sciences.

17. "Second Generation Heliostat Development," Final Report, Martin Marietta Corporation, April 1981, SAND 81-8176.

18. "Manufacturing and Cost Analyses of Heliostats Based on the Second Generation Heliostat Development Study," H.F. Morris, Jr., and S.S. White, Sandia National Laboratories, Dec. 1982, SAND 82-8007.

19. "Second Generation Heliostat Development for Solar Central Receiver Systems," Northrup, Inc. (ARCO Power Systems), March 1981, SAND 81-8178.

20. "Moderate to Large Axisymmetric Membrane Deformations of Optical Membrane Surfaces," L.M. Murphy, SERI/TR-253 Draft.

APRIL 1, 1987
UNLIMITED RELEASE
INITIAL DISTRIBUTION

U.S. Department of Energy (5)
Forrestal Building
Code CE-314
1000 Independence Avenue, S.W.
Washington, D.C. 20585
Attn: H. Coleman
S. Gronich
F. Morse
M. Scheve
R. Shivers

U.S. Department of Energy
Forrestal Building, Room 5H021C
Code CE-33
1000 Independence Avenue, S.W.
Washington, D.C. 20585
Attn: C. Carwile

U.S. Department of Energy
Albuquerque Operations Office
P.O. Box 5400
Albuquerque, NM 87115
Attn: D. Graves

U.S. Department of Energy
San Francisco Operations Office
1333 Broadway
Oakland, CA 94612
Attn: R. Hughey

University of California
Environmental Science and Engineering
Los Angeles, CA 90024
Attn: R. G. Lindberg

University of Houston (2)
Solar Energy Laboratory
4800 Calhoun
Houston, TX 77704
Attn: A. F. Hildebrandt
L. Vant-Hull

Analysis Review & Critique
6503 81st Street
Cabin John, MD 20818
Attn: C. LaPorta

Arizona Public Service Company
P.O. Box 21666
Phoenix, AZ 85036
Attn: E. Weber

Babcock and Wilcox
91 Stirling Avenue
Barberton, OH 44203
Attn: D. Young

Bechtel Group, Inc.
P.O. Box 3965
San Francisco, CA 94119
Attn: P. DeLaquil
S. Fleming

Black & Veatch Consulting Engineers (2)
P.O. Box 8405
Kansas City, MO 64114
Attn: J. C. Grosskreutz
J. E. Harder

Boeing Aerospace
Mailstop JA-83
P.O. Box 1470
Huntsville, AL 35807
Attn: W. D. Beverly

California Energy Commission
1516 Ninth St., M/S 40
Sacramento, CA 95814
Attn: A. Jenkins

California Public Utilities Com.
Resource Branch, Room 5198
455 Golden Gate Ave.
San Francisco, CA 94102
Attn: T. Thompson

Centro Investigations Energetica
Medroansental Technologie (CIEMAT)
Avda. Complutense, 22
28040 Madrid
Spain
Attn: F. Sanchez
M. Alvarez

DFVLR RF-ET
Linder Hohe
D - 5000 Koln 90
West Germany
Attn: Dr. Manfred Becker

El Paso Electric Company
P.O. Box 982
El Paso, TX 79946
Attn: J. E. Brown

Electric Power Research Institute (2)
P.O. Box 10412
Palo Alto, CA 94303
Attn: J. Bigger
E. DeMeo

Foster Wheeler Solar Development Corp.
12 Peach Tree Hill Road
Livingston, NJ 07039
Attn: S. F. Wu

Georgia Institute of Technology
GTRI/EMSL Solar Site
Atlanta, GA 30332

D. Gorman
5031 W. Red Rock Drive
Larkspur, CO 80118

Jet Propulsion Laboratory
4800 Oak Grove Drive
Pasadena, CA 91103
Attn: M. Alper

Los Angeles Department of Water and Power
Alternate Energy Systems
Room 661A
111 North Hope St.
Los Angeles, CA 90012
Attn: Hung Ben Chu

Martin Marietta Aerospace
P.O. Box 179, MS L0450
Denver, CO 80201
Attn: H. Wroton

McDonnell Douglas (2)
MS 49-2
5301 Bolsa Avenue
Huntington Beach, CA 92647
Attn: R. L. Gervais
J. E. Raetz

Meridian Corporation
5113 Leesburg Pike
Falls Church, VA 22041
Attn: D. Kumar

Public Service Company of New Mexico
M/S 0160
Alvarado Square
Albuquerque, NM 87158
Attn: T. Ussery
A. Martinez

Olin Chemicals Group (2)
120 Long Ridge Road
Stamford, CT 06904
Attn: J. Floyd
D. A. Csejka

Pacific Gas and Electric Company
77 Beale Street
San Francisco, CA 94106
Attn: J. Laszlo

Pacific Gas and Electric Company (4)
3400 Crow Canyon Road
San Ramon, CA 94526
Attn: G. Braun
T. Hillesland, Jr.
B. Norris
C. Weinberg

Public Service Company of Colorado
System Planning
5909 E. 38th Avenue
Denver, CO 80207
Attn: D. Smith

Rockwell International
Rocketdyne Division
6633 Canoga Avenue
Canoga Park, CA 91304
Attn: J. Friefeld

Sandia Solar One Office
P.O. Box 366
Daggett, CA 92327
Attn: A. Snedeker

Science Applications International Corp.
10401 Roselle Street
San Diego, CA 92121
Attn: B. Butler

Solar Energy Research Institute (3)
1617 Cole Boulevard
Golden, CO 80401
Attn: B. Gupta
D. Hawkins
L. M. Murphy

Solar Kinetics Inc.
P.O. Box 47045
Dallas, TX 75247
Attn: J. A. Hutchison

Southern California Edison
P.O. Box 325
Daggett, CA 92327
Attn: C. Lopez

Stearns Catalytic Corp.
P.O. Box 5888
Denver, CO 80217
Attn: T. E. Olson

Stone and Webster Engineering Corporation
P.O. Box 1214
Boston, MA 02107
Attn: R. W. Kuhr

6000 D. L. Hartley; Attn: V. L. Dugan, 6200
6220 D. G. Schueler
6222 J. V. Otts
6226 J. T. Holmes (10)
8000 R. S. Claassen; Attn: R. J. Detry, 8200
P. Mattern, 8300
R. C. Wayne, 8400
8100 E. E. Ives; Attn: J. B. Wright, 8150
D. J. Bohrer, 8160
R. A. Baroody, 8180
8130 J. D. Gilson
8133 C. L. Mavis
8133 L. G. Radosevich
8133 A. C. Skinrood (3)
8133 D. N. Tanner
8244 C. Hartwig
8245 R. J. Kee
8265 Publications Division for OSTI (30)
8265 Publications Division/Technical Library Processes Division, 3141
3141 Technical Library Processes Division (3)
8024 Central Technical Files (3)